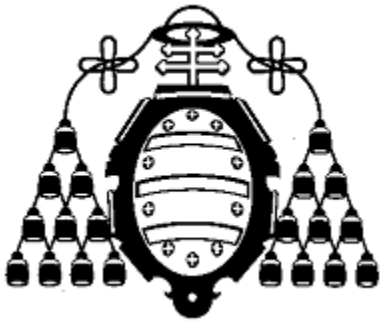

UNIVERSITY OF OVIEDO

DEPARMENT OF ELECTRICAL, ELECTRONIC, COMPUTERS AND SYSTEMS ENGINEERING

PHD THESIS

POWER ELECTRONIC SUPPLIES FOR PUBLIC LIGHTING SYSTEMS WITH DISTRIBUTED GENERATION CAPABILITY: SOLUTION PROPOSALS FOR POWER AND CONTROL STAGES, CHARACTERIZATION AND MINIMIZATION OF THE IMPACT IN GRID QUALITY

by

PABLO JOSÉ QUINTANA BARCIA

Gijón, November 2015

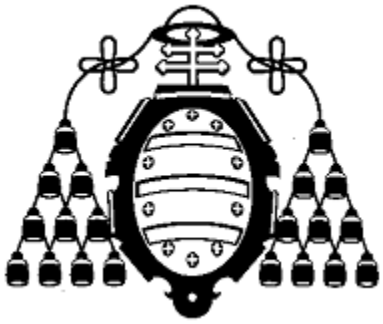

UNIVERSIDAD DE OVIEDO

DEPARTAMENTO DE INGENIERÍA ELÉCTRICA, ELECTRÓNICA, DE COMPUTADORES Y SISTEMAS

TESIS DOCTORAL

EQUIPOS ELECTRÓNICOS DE ALIMENTACIÓN EN SISTEMAS DE ALUMBRADO PÚBLICO CON CAPACIDAD DE MICROGENERACIÓN DISTRIBUIDA: PROPUESTA DE SOLUCIONES PARA ETAPAS DE POTENCIA Y CONTROL, CARACTERIZACIÓN Y MINIMIZACIÓN DEL IMPACTO EN LA RED ELÉCTRICA

por

PABLO JOSÉ QUINTANA BARCIA

Gijón, November 2015

RESUMEN DEL CONTENIDO DE TESIS DOCTORAL

1.- Título de la Tesis	
Español/Otro Idioma: Equipos electrónicos de alimentación en sistemas de alumbrado público con capacidad de microgeneración distribuida: propuesta de soluciones para etapas de potencia y control, caracterización y minimización del impacto en la red eléctrica	Inglés: Power electronic supplies for public lighting systems with distributed generation capability: solution proposals for power and control stages, characterization and minimization of the impact in grid quality

2.- Autor	
Nombre: Pablo José Quintana Barcia	DNI/Pasaporte/NIE:
Programa de Doctorado: Energía y control de procesos	
Órgano responsable: Universidad de Oviedo	

RESUMEN (en español)

Esta Tesis Doctoral titulado "Equipos Electrónicos De Alimentación En Sistemas De Alumbrado Público Con Capacidad De Microgeneración Distribuida: Propuesta De Soluciones Para Etapas De Potencia Y Control, Caracterización Y Minimización Del Impacto En La Red Eléctrica" fue desarrollada como una de las actividades principales del grupo de investigación Conversión Eficiente de Energía, Electrónica Industrial e Iluminación (CE^3I^2) del Departamento de Ingeniería Eléctrica de la Universidad de Oviedo.

Este trabajo tiene como objetivos la mejora de diferentes soluciones para aplicaciones de iluminación en términos de electrónica de potencia, aspirando a mejorar el comportamiento del sistema completo, la eficiencia energética y la fiabilidad.

Hoy en día, la eficiencia energética es un componente crucial para responder al cambio climático. Una cantidad considerable de energía es gastada de forma ineficiente en diferentes fuentes de iluminación a lo largo del mundo, incluyendo alumbrado urbano, comercial, doméstico y en oficinas. El presente trabajo se centra en dos aspectos clave que afectan severamente a la eficiencia energética en los sistemas de potencia.

- Capacidad de microgeneración de energías renovables combinado con alumbrado público urbano (con o sin capacidad de almacenamiento). El hecho de que se pueda ahorrar energía aprovechando los medios naturales como son las energías renovables para ayudar a reducir el efecto invernadero es un punto importante a considerar.
- Una cantidad importante de energía se gasta debido a las no linearidades de muchas cargas eléctricas que provocan distorsiones en la red eléctrica. Entre esas cargas no lineales, en términos de iluminación, se encuentran los balastos electromagnéticos, considerados uno de los más contaminantes hablando de polución eléctrica. Estos dispositivos están basados en una tecnología robusta y madura que se emplea para encender ciertas lámparas. A pesar de su buen comportamiento en términos de fiabilidad y durabilidad, el contenido armónico que inyectan en la red es bastante importante. Aun así, debido a problemas financieros o a amortizaciones no

recuperadas, en ciertas partes del mundo aún se siguen utilizando.

- Aunque han ido apareciendo con los años nuevas soluciones para substituir a los balastos electromagnéticos, como son los electrónicos basados en circuitería electrónica de estado sólido (resonantes, de onda cuadrada...), aún hay margen de mejora en términos de eficiencia y fiabilidad.
- Con los LED de potencia se abren nuevas posibilidades a sistemas baratos, fiables y eficientes. Hace aparición el concepto de dimming como una interesante apuesta.
- Hay pocos trabajos centrados en desarrollar equipamiento electrónico compatible con los antiguos y con los modernos sistemas de iluminación, incluyendo la integración de energías renovables en la red.

De hecho, debido a la naturaleza escolástica de las energías renovables, se necesitan estrategias de control robustas para poder integrarlas de forma fiable en la red eléctrica. Este control, si se hace de la manera correcta, implica que:

- Menores esfuerzos en los equipos de potencia
- Amplio ancho de banda, y por lo tanto, la respuesta a perturbaciones y fallos sea más rápida.
- Se pueden incluir lámparas tipo LED con condensadores no electrolíticos que permitan un rizado de tensión mayor pero también una vida útil más larga.

Los objetivos princípiales de este trabajo de doctorado se enumeran a continuación:

- Caracterizar el efecto de los balastos electromagnéticos en la red y estudiar estrategias para mitigar los armónicos generados.
- Estudiar diferentes soluciones para la interconexión entre la red y sistemas de alumbrado público callejero, incluyendo el diseño de topologías de potencia con o sin aislamiento galvánico y estudiar su optimización.
- Estudiar el efecto de las soluciones propuestas en redes más débiles, conocidas como microrredes, que pueden estar conectadas a su vez a redes más fuertes o estar en isla. De este modo, sería interesantes ver el efecto de incluir las farolas con capacidad de microgeneración dentro de las microrredes y observar si el convertidor es capaz de corregir la contaminación armónica.
- Estudiar topologías que soluciones los problemas de inyección de energía a la red y alimentación de las luminarias en lámparas urbanas con capacidad de microgeneración. Esto significa tener un control completo de la energía disponible y ser capaz de moverla en ambos sentidos: de la red a la lámpara y de la fuente de energía renovable a la red.
- Evaluación de sistemas de iluminación mixtos donde coexisten balastos de baja frecuencia y lámparas de HPS con modernas farolas formadas por lámparas tipo LED con unidades de generación distribuida incluidas. La idea detrás de este estudio es la de reducir la contaminación armónica en la red provocada por los balastos electromagnéticos por medio de los balastos electrónicos que controlan las lámparas LED. Estos convertidores electrónicos deberían ser capaces de alimentar a la lámpara que les corresponda y de inyectar la corriente que proporcionan las energías renovables con la forma de onda necesaria para contrarrestar la corriente

distorsionada demandada por los balastos electromagnéticos.

Palabras clave: alumbrado público, balastos electromagnéticos, convertidor bidireccional, convertidores conectados a la red, convertidores en MCD, Corrección del Factor de Potencia de dinámica rápida, electrónica de potencia, etapas bidireccionales de interconexión con la red, filtro activo, generación distribuida, microrredes monofásicas, modelado de convertidores, sistemas multifuncionales.

RESUMEN (en Inglés)

This PhD Thesis entitled "Power Electronic Supplies For Public Lighting Systems With Distributed Generation Capability: Solution Proposals For Power And Control Stages, Characterization And Minimization Of The Impact In Grid Quality" was developed as one of the core research activities of the Efficient Energy Conversion, Industrial Electronics and Lighting Engineering group (CE^3I^2), from the Electrical Engineering Department of University of Oviedo.

This work targets the enhancement of power electronic solutions for lighting applications, aiming to increase the system performance, the energy efficiency as well as the reliability.

The system performance is studied from the power and control stages, in order to optimize the final design upon given technical and economic constraints.

Nowadays, energy efficiency is a crucial component of the multidisciplinary response to climate change. A remarkable amount of energy is wasted through inefficient lighting from many sources across the world, including public street/road lighting, commercial, industrial, domestic, and office lighting systems. The present work focuses on some key aspects that severely affect energy efficiency in power systems:

- Renewable energy microgeneration capability combined with street lighting systems (with or without energy storage). The fact that any kind of energy saving by taking advantage of the renewable energies helps to prevent the greenhouse effect is a point to be considered.
- A considerable amount of energy is wasted in terms of losses due to non linearities of many electric loads that generate distortions in the AC mains. Between those no lineal loads, in terms of illumination, electromagnetic ballasts are considered one of the most polluting. These devices are based on a robust and mature technology employed to control some lamps ignition. Despite their good behaviour in terms of reliability and durability, the harmonic content they inject in the grid is truly disturbing. However, due to financial and amortization issues, the electromagnetic ones are still in use in some areas.
- Although new solutions have appeared these last years to substitute the electromagnetic ballasts like the electronic ones based on solid-state electronic circuitry (resonant, square-wave...), there is still room for reliability and efficiency improvement.
- With the power LED, new windows to cheap, reliable and efficient systems are opened. Dimming possibility is also a quite interesting performance.
- There are only a few works focused on an electronic design compatible with former

and new lighting systems, including the integration of renewable energy sources into the grid.

As a matter of fact, due to the scholastic nature of the renewable energy sources, robust control strategies need to be present in order to reliably integrate them in the utility grid. This control, whether it is done properly, implies:

- Lower efforts in the power equipments.
- High bandwidth and thus, faster response to disturbances and failures.
- Allowance of the LED lamps with non-electrolytic capacitors and a high ripple and hence, longer life span.

The main objectives of this PhD work are listed below:

- Characterization of the effect of electromagnetic ballasts in the grid and study of harmonic mitigation strategies.
- Study of different solutions for the interconnection between the grid and street lighting systems, including the design of power topologies with or without galvanic isolation and its optimization.
- Study of the effect of the proposed solutions in smaller grids, known as microgrids that can be connected to stronger grids or being in island. Trying to correct the harmonic pollution in these special grids is still a hot topic for the researchers.
- Study of topologies to solve problems of grid power injection and luminaires feeding in street lampposts with microgeneration capability. This means fully control of the energy in both directions: from the grid to the lamp or from the renewable energy source to the grid.
- Evaluation of mixed lighting systems were low-frequency ballasts and HPS lamps coexist with new street lights formed by LED lamps and distributed generation units. The idea behind this study is to reduce the harmonic pollution of the grid generated by the electromagnetic ballasts by means of the electronic ballasts that drive the LED lamps. Theses electronic converters should be able to feed the lamp and inject the available power from the renewable energy sources into the grid with the proper waveform in order to counteract the distorted current demanded by the electromagnetic ballasts.

Key words: active filter, bidirectional converters, bidirectional grid interface stages, converter modelling, DCM converters, distributed power generation, electromagnetic ballasts, fast dynamics PFC, grid-tie inverter, multifunctional systems, power electronics, Power Factor Correction, single phase microgrid, street lighting.

SR. DIRECTOR DE DEPARTAMENTO DE_____/
SR. PRESIDENTE DE LA COMISIÓN ACADÉMICA DEL PROGRAMA DE DOCTORADO EN _____

PhD Thesis

POWER ELECTRONIC SUPPLIES FOR PUBLIC LIGHTING SYSTEMS WITH DISTRIBUTED GENERATION CAPABILITY: SOLUTION PROPOSALS FOR POWER AND CONTROL STAGES, CHARACTERIZATION AND MINIMIZATION OF THE IMPACT IN GRID QUALITY

EQUIPOS ELECTRÓNICOS DE ALIMENTACIÓN EN SISTEMAS DE ALUMBRADO PÚBLICO CON CAPACIDAD DE MICROGENERACIÓN DISTRIBUIDA: PROPUESTA DE SOLUCIONES PARA ETAPAS DE POTENCIA Y CONTROL, CARACTERIZACIÓN Y MINIMIZACIÓN DEL IMPACTO EN LA RED ELÉCTRICA

By

Pablo José Quintana Barcia

Public defence held at the

DEPARMENT OF ELECTRICAL, ELECTRONIC, COMPUTERS AND SYSTEMS ENGINEERING

of

UNIVERSITY OF OVIEDO

In partial fulfilment of the requirements for the

Degree of European Doctor of Philosophy

PhD Thesis

POWER ELECTRONIC SUPPLIES FOR PUBLIC LIGHTING SYSTEMS WITH DISTRIBUTED GENERATION CAPABILITY: SOLUTION PROPOSALS FOR POWER AND CONTROL STAGES, CHARACTERIZATION AND MINIMIZATION OF THE IMPACT IN GRID QUALITY

EQUIPOS ELECTRÓNICOS DE ALIMENTACIÓN EN SISTEMAS DE ALUMBRADO PÚBLICO CON CAPACIDAD DE MICROGENERACIÓN DISTRIBUIDA: PROPUESTA DE SOLUCIONES PARA ETAPAS DE POTENCIA Y CONTROL, CARACTERIZACIÓN Y MINIMIZACIÓN DEL IMPACTO EN LA RED ELÉCTRICA

PhD student: **Eng. Pablo José Quintana Barcia**

Advisors: **Prof. Jorge García García, University of Oviedo**

Prof. Emilio Ramón López Corominas

ASSESSMENT COMITTE:

President: **Prof. Manuel Rico Secades, University of Oviedo, Spain**

Secretary: **Prof. Marina Mendes Sargento Domingues Perdigão, Polythecnic Institute of Coimbra, Portugal**

Board Member: **Prof. Christian Brañas Reyes, University of Cantabria, Spain**

EXTERNAL REVIEWERS:

Prof. Henrique A. Carvalho Braga. Federal University of Juiz de Fora, Brazil

Prof. Ray-Lee Lin. National Cheng Kung University, Taiwan

A mis padres, Fini y José Luis,

a mi hermana, Cova,

y a mis amigos y compañeros

por haberme apoyado, animado y aguantado todo este tiempo.

AGRADECIMIENTOS

Me gustaría mencionar en primer lugar a las dos personas que hicieron posible que este trabajo haya salido adelante, los profesores Jorge García García y Emilio López Corominas. Desde que entré a hacer el proyecto fin de carrera allá por el 2010-2011, me han guiado, enseñado y formado para poder acabar entregando una tesis doctoral en electrónica de potencia, algo que jamás hubiera imaginado cuando suspendí por primera vez Teoría de circuitos.

También quiero agradecer a los profesores que de una u otra manera me han ayudado a lo largo de mi etapa doctoral: Antonio J. Calleja, Pablo García, Pablo Arboleya, Marcos Alonso, Manuel Rico, Jesús Cardesín y Javier Ribas.

No puedo olvidarme tampoco de aquellos que me acogieron en sus grupos de trabajo cuando ni siquiera sabían de mi existencia. Tanto los profesores, Josep M. Guerrero y Juan Carlos Vasquez, como los colegas Tomi, Lexuan (Lucas), Nelson, Chendan, Dan, Qobad y Fen me recibieron en Dinamarca y en su departamento como si fuera uno más. Por ello estaré agradecido eternamente. Debo mencionar también a los miembros del grupo GEDRE, en Brasil, que también me ayudaron muchísimo para poder hacer este trabajo: doy las gracias a los profesores Marco Dalla Costa, Rafael Pinto, Ricardo Nederson do Prado, Marcelo Freitas y todo el grupo de alumnos a su cargo, en especial a Maicol, Vitor, Deco, Cose y demás. Son tantos que llenaría esta página solo con sus nombres.

Gracias a mis amigos aquí en España, tanto de laboratorio como de cervezas, que me habéis aguantado hasta el final. Siempre viene bien tener un punto de apoyo así y yo tuve la suerte de tenerlos en abundancia.

Y por último, y no por ello menos importante, muchísimas gracias a mi familia, pero en especial a mis padres y a mi hermana. Me han dado consejos y me han apoyado siempre, sin excepción, y me han ayudado mucho más de lo que ellos creen. Dicen que la familia te viene elegida y tienes que quererlos solo por eso, pero en mi caso es imposible que sea de otra manera. No he conocido a mejores personas que ellos en mi vida: sinceros, amables, entregados y solidarios.

ABSTRACT

This PhD Thesis, entitled "Power Electronic Supplies For Public Lighting Systems With Distributed Generation Capability: Solution Proposals For Power And Control Stages, Characterization And Minimization Of The Impact In Grid Quality", has been developed as one of the core research activities of the Efficient Energy Conversion, Industrial Electronics and Lighting Engineering group (CE^3I^2), from the Electrical Engineering Department (DIEECS) of the University of Oviedo.

This work targets the enhancement of power electronic solutions for lighting applications, aiming to increase the system performance, the energy efficiency as well as the reliability. The system performance is studied in a top-down approach, focusing on the power and control stages in the lighting system, in order to optimize the final design upon given technical and economic constraints.

Nowadays, energy efficiency is a crucial component of the multidisciplinary response to climate change. In this context, a remarkable amount of energy is wasted through inefficient lighting from many sources across the world, including public street/road lighting, commercial, industrial, domestic and office lighting systems. In order to propose solutions to solve this issue, the present work focuses on the following key aspects that severely affect energy efficiency in power systems: renewable energy microgeneration capability combined with street lighting systems (with or without energy storage). The fact that any kind of energy saving by taking advantage of the renewable energies helps to prevent the greenhouse effect is a point to be considered.

- The study and discussion of the combination of renewable energy distributed microgeneration systems, public street lighting systems and energy storage systems. As in any other applications, lighting systems would benefit of any kind of energy saving, particularly considering renewable energies and storage systems helps in preventing the greenhouse effect.
- A considerable amount of energy is wasted in terms of losses due to non-linearities of many electric loads that generate distortions in the AC mains. In lighting applications, low frequency (LF) electromagnetic ballasts for discharge lamps are considered as one of the most important sources of line parameters distortion. These devices are based on a robust and mature technology employed to control the discharge lamps operation. Despite their good behaviour in terms of reliability and durability, the harmonic content they inject in the grid is truly disturbing. However, due to financial and amortization issues, these electromagnetic ballasts are still in use in some areas.
- Although new solutions have appeared during the last years, aiming to substitute these LF electromagnetic ballasts there is still room for reliability and efficiency improvement. These solutions include HF electronic ballasts based on solid-state electronic circuitry for discharge lamps (based on resonant or square-wave inverters, for instance), High-Brightness LEDs drivers, etc.
- The recent developments in solid-state lighting and the commercialization of power LEDs, allow to consider new features for the design of cheap, versatile, reliable and efficient lighting systems. One of the most remarkable among these features is the possibility of dimming.
- Currently, there are few works focused on an electronic design that is compatible with conventional and new lighting systems, including the integration of renewable energy sources into the grid.

As a matter of fact, due to the stochastic nature of the renewable energy sources, robust control strategies need to be present in order to reliably integrate them in the utility grid. This control, whether it is done properly, implies:

- Lower efforts in the power equipments.
- High bandwidth and thus, faster response to disturbances and failures.
- Allowance of the LED lamps with non-electrolytic capacitors and a high ripple and hence, longer life span.

The main objectives of this PhD work are listed below:

- Characterization of the effect of electromagnetic ballasts in the grid and study of harmonic mitigation strategies.
- Study of different solutions for the interconnection between the grid and street lighting systems, including the design of power topologies with or without galvanic isolation and its optimization.
- Study of the effect of the proposed solutions in smaller grids, known as microgrids that can be connected to stronger grids or being in island. Trying to correct the harmonic pollution in these special grids is still a hot topic for the researchers.
- Study of topologies to solve problems of grid power injection and luminaires supplying in street lampposts with microgeneration capability. This means fully control of the energy in both directions: from the grid to the lamp or from the renewable energy source to the grid.
- Evaluation of mixed lighting systems were low-frequency ballasts and HPS lamps coexist with new street lights formed by LED lamps and distributed generation units. The idea behind this study is to reduce the harmonic pollution of the grid generated by the electromagnetic ballasts by means of the electronic ballasts that drive the LED lamps. These electronic converters should be able to feed the lamp and inject the available power from the renewable energy sources into the grid with the proper waveform in order to counteract the distorted current demanded by the electromagnetic ballasts.

This PhD work is structured as detailed below:

In **Chapter 1**, a brief introduction to artificial lighting is outlined. Afterwards, the most common light sources are listed and reviewed. Light-Emitting Diodes are then introduced and thoroughly described. Afterwards, the most important issues about LED lighting will be discussed, paying special attention to their characteristics as power loads. It will be shown how this characteristic greatly differs from LEDs to incandescent or gas-discharge lamps.

In **Chapter 2**, the performance of Discontinuous Conduction Mode converters is deeply studied regarding IEC 61000-3-2 Class C regulations compliance. Thus, Power Factor Correction is firstly introduced with the Class C harmonic-content requirements, and then, passive and active techniques for harmonic content reduction and/or Power Factor Correction are listed and described.

Chapter 3 shall deal with a kind of non-linear loads, particularly electromagnetic ballasts which cause a great distortion in the grid. Real ballasts will be studied and their models will be obtained in order to perform simulations. Afterwards, different control techniques will be considered in order to compensate the effect of these loads.

Then, **Chapter 4** is intended to check the effect of non-linear loads in single-phase microgrids and minigrids, mostly operating in island mode. Two control schemes shall be proposed in order to correct the effect of the harmonics into these grids. They will be compared in terms of efficiency, complexity or computational cost.

In **Chapter 5**, a brief introduction to renewable energy sources compatible with street lamppost shall be discussed and the most common ways of interconnection with the AC grid.

Chapter 6 will show a brief state of the art about power factor correctors: most known topologies, most common control techniques, operation modes and different architectures.

In **Chapter 7** it will be studied a new control methodology for power factor correctors. A brief background about the bidirectional Flyback can be found in this chapter, together with the mathematical development of the model and a full description of the control scheme. Finally, experimental results will be shown.

Chapter 8 will deal with a unification switching of the bidirectional Flyback semiconductors technique, useful either in rectifier (when the energy is sent from the grid to the loads) and inverter (when the energy is sent from the renewable energy source to the utility mains) mode. A mapping should be done and a common point between both operation modes shall be found. Then, experimental results will be shown.

Key words: active filter, bidirectional converters, bidirectional grid interface stages, converter modelling, DCM converters, distributed power generation, electromagnetic ballasts, fast dynamics PFC, grid-tie inverter, multifunctional systems, power electronics, Power Factor Correction, single phase microgrid, street lighting.

RESUMEN

Esta Tesis Doctoral titulada “Equipos Electrónicos De Alimentación En Sistemas De Alumbrado Público Con Capacidad De Microgeneración Distribuida: Propuesta De Soluciones Para Etapas De Potencia Y Control, Caracterización Y Minimización Del Impacto En La Red Eléctrica” fue desarrollada como una de las actividades principales del grupo de investigación Conversión Eficiente de Energía, Electrónica Industrial e Iluminación (CE^3I^2) del Departamento de Ingeniería Eléctrica de la Universidad de Oviedo.

Este trabajo tiene como objetivos la mejora de diferentes soluciones para aplicaciones de iluminación en términos de electrónica de potencia, aspirando a mejorar el comportamiento del sistema completo, la eficiencia energética y la fiabilidad.

Hoy en día, la eficiencia energética es un componente crucial para responder al cambio climático. Una cantidad considerable de energía es gastada de forma ineficiente en diferentes fuentes de iluminación a lo largo del mundo, incluyendo alumbrado urbano, comercial, doméstico y en oficinas. El presente trabajo se centra en dos aspectos clave que afectan severamente a la eficiencia energética en los sistemas de potencia.

- Capacidad de microgeneración de energías renovables combinado con alumbrado público urbano (con o sin capacidad de almacenamiento). El hecho de que se pueda ahorrar energía aprovechando los medios naturales como son las energías renovables para ayudar a reducir el efecto invernadero es un punto importante a considerar.
- Una cantidad importante de energía se gasta debido a las no linearidades de muchas cargas eléctricas que provocan distorsiones en la red eléctrica. Entre esas cargas no lineales, en términos de iluminación, se encuentran los balastos electromagnéticos, considerados uno de los más contaminantes hablando de polución eléctrica. Estos dispositivos están basados en una tecnología robusta y madura que se emplea para encender ciertas lámparas. A pesar de su buen comportamiento en términos de fiabilidad y durabilidad, el contenido armónico que inyectan en la red es bastante importante. Aun así, debido a problemas financieros o a amortizaciones no recuperadas, en ciertas partes del mundo aún se siguen utilizando.
- Aunque han ido apareciendo con los años nuevas soluciones para substituir a los balastos electromagnéticos, como son los electrónicos basados en circuitería electrónica de estado sólido (resonantes, de onda cuadrada…), aún hay margen de mejora en términos de eficiencia y fiabilidad.
- Con los LED de potencia se abren nuevas posibilidades a sistemas baratos, fiables y eficientes. Hace aparición el concepto de dimming como una interesante apuesta.
- Hay pocos trabajos centrados en desarrollar equipamiento electrónico compatible con los antiguos y con los modernos sistemas de iluminación, incluyendo la integración de energías renovables en la red.

De hecho, debido a la naturaleza estocástica de las energías renovables, se necesitan estrategias de control robustas para poder integrarlas de forma fiable en la red eléctrica. Este control, si se hace de la manera correcta, implica que:

- Menores esfuerzos en los equipos de potencia
- Amplio ancho de banda, y por lo tanto, la respuesta a perturbaciones y fallos sea más rápida.

- Se pueden incluir lámparas tipo LED con condensadores no electrolíticos que permitan un rizado de tensión mayor pero también una vida útil más larga.

Los objetivos princípiales de este trabajo de doctorado se enumeran a continuación:

- Caracterizar el efecto de los balastos electromagnéticos en la red y estudiar estrategias para mitigar los armónicos generados.
- Estudiar diferentes soluciones para la interconexión entre la red y sistemas de alumbrado público callejero, incluyendo el diseño de topologías de potencia con o sin aislamiento galvánico y estudiar su optimización.
- Estudiar el efecto de las soluciones propuestas en redes más débiles, conocidas como microrredes, que pueden estar conectadas a su vez a redes más fuertes o estar en isla. De este modo, sería interesantes ver el efecto de incluir las farolas con capacidad de microgeneración dentro de las microrredes y observar si el convertidor es capaz de corregir la contaminación armónica.
- Estudiar topologías que solucionen los problemas de inyección de energía a la red y alimentación de las luminarias en lámparas urbanas con capacidad de microgeneración. Esto significa tener un control completo de la energía disponible y ser capaz de moverla en ambos sentidos: de la red a la lámpara y de la fuente de energía renovable a la red.
- Evaluación de sistemas de iluminación mixtos donde coexisten balastos de baja frecuencia y lámparas de HPS con modernas farolas formadas por lámparas tipo LED con unidades de generación distribuida incluidas. La idea detrás de este estudio es la de reducir la contaminación armónica en la red provocada por los balastos electromagnéticos por medio de los balastos electrónicos que controlan las lámparas LED. Estos convertidores electrónicos deberían ser capaces de alimentar a la lámpara que les corresponda y de inyectar la corriente que proporcionan las energías renovables con la forma de onda necesaria para contrarrestar la corriente distorsionada demandada por los balastos electromagnéticos.

Esta tesis se estructurará de la siguiente manera:

En el **Capítulo 1** se dará una pequeña introducción al campo de la iluminación. Después se explicarán de forma breve los tipos de fuentes de luz más comunes. Se hablará de los diodos emisores de luz (LED) y serán descritos. Los aspectos más importantes de los LED se discutirán, prestando especial atención a sus características de potencia, que difieren totalmente de las lámparas de potencia o de descarga de gas.

En el **Capítulo 2** se hablará del Modo de Conducción Discontinua (MCD, en inglés DCM), estudiando en detalle la norma IEC 6100-3-2 Clase C. Después se hablará de los correctores de factor de potencia que tienen que cumplir la norma anterior, siendo pasivos o activos.

En el **Capítulo 3** se tratará sobre un tipo de cargas no lineales, en particular, los balastos electromagnéticos, que provocan una gran distorsión en la red. Se estudiarán modelos reales y se obtendrán sus características para poder crear modelos para simulación. Después de estudiarán diversas técnicas para tratar de compensar el efecto nocivo de estas cargas.

El **Capítulo 4** será dedicado a comprobar el efecto de las cargas no lineales en las microrredes y minirredes eléctricas monofásicas, sobre todo las que trabajan en isla. Se propondrán diferentes esquemas de control para corregir los armónicos generados por las cargas no lineales. Se tratarán temas como el empleo de la transformada rápida de Fourier para extraer los armónicos de una señal y corregirla con un esquema de control determinado o el emplear modelos más complejos para controlar los armónicos pero evitando las transformadas de Fourier.

En el **Capítulo 5** se investigará el efecto de la inclusión de energías renovables en la red eléctrica, los métodos más convencionales y cómo se puede conseguir que la generación distribuida sea compatible con las farolas en términos de qué tipo de energía renovable es viable a la hora de ser instalada en ellas.

El **Capítulo 6** será un pequeño estudio sobre el estado del arte sobre correctores de factor de potencia: topologías más conocidas, técnicas de control más comunes, modos de operación y diferentes tipos de arquitecturas empleadas.

En el **Capítulo 7** se propondrá un nuevo método para controlar los correctores de factor de potencia de manera rápida y eficaz. Se explicará primero de dónde salió esta idea y los orígenes del convertidor a emplear. Después se realizará el modelo en pequeña señal y se desarrollará matemáticamente el esquema de control, para después compararlo con el método clásico y obtener resultados experimentales.

El **Capítulo 8** tratará sobre una técnica de unificación del disparo de los semiconductores de un Flyback bidireccional que es útil tanto en modo rectificador (cuando se envía la energía desde la red a la carga) como en modo inversor (cuando la energía va desde la fuente de energía renovable a la red). Se deberá hacer un mapeo y buscar un punto común entre ambos modos de operación. Finalmente, se mostrarán los resultados experimentales.

Palabras clave: alumbrado público, balastos electromagnéticos, convertidor bidireccional, convertidores conectados a la red, convertidores en MCD, Corrección del Factor de Potencia de dinámica rápida, electrónica de potencia, etapas bidireccionales de interconexión con la red, filtro activo, generación distribuida, microrredes monofásicas, modelado de convertidores, sistemas multifuncionales.

TABLE OF CONTENTS

LIST OF FIGURES

LIST OF TABLES

LIST OF ACRONYMS

AC	Alternative current
ADC	Analog-to-digital converter
AF	Active filter
AM	Amplitude modulation
BCM	Boundary conduction mode
BPF	Band-pass filter
CCM	Continuous conduction mode
CCT	Correlated colour temperature
CIE	Comission Internationale de l´Éclairage
CM-VSI	Current mode-voltage source inverter
CRI	Colour rendering index
CT	Colour temperature
DC	Direct current
DCM	Discontinuous conduction mode
DG	Distributed generation (unit)
DSP	Digital signal processor
DT	Distortion factor
EMI	Electromagnetic interferences
EMR	Electromagnetic radiation
ESS	Energy storage system
FFT	Fast Fourier transformation
HAWT	Horizontal axis wind turbine
HID	High-intensity discharge (lamp)
HPM-HME	High-pressure mercury vapour (lamp)
HPS-SON	High-pressure sodium (lamp)
IR	Infrared
LED	Light-emitting diode
LPS	Low-pressure sodium (lamp)
LTI	Linear and time invariant
MH	Metal-halide (lamp)
MPP	Maximum power point
MPPT	Maximum power point tracker

PCC	Point of common coupling
PF	Power factor
PFC	Power factor corrector
PFP	Power factor preregulator
PI	Proportional integrator (controller)
PID	Proportional integrator differentiator (controller)
PLL	Phase-locked loop
PR	Proportional-resonant
PV	Photovoltaic
PWM	Pulse-width modulation
RES	Renewable energy source
RGB	Red, green, blue colours used for white light generation
SiC	Silicon carbide
SoC	State of charge
SOGI	Second-order generalised integrator
SPWM	Sinusoidal pulse width modulation
THD	Total harmonic distortion
UPS	Uninterrupted power supply
UV	Ultraviolet
VAWT	Vertical axis wind turbine
VSI	Voltage source inverter
WT	Wind turbine
WTG	Wind turbine generator

LIST OF SYMBOLS

Chapter 1

E_a	Band gap energy
k	Boltzmann constant
E_c	Conduction band energy
i	Current characteristic behaviour of the modified Shockley equation
$\vec{E}$	Electric field
q	Electron charge
E	Energy of the particle
R_{LED}	Equivalent resistance in LED model
D_{LED}	Ideal diode in LED model
n	Ideality factor
$\vec{B}$	Magnetic field
h	Planck constant
c	Propagation speed of the particle in the vacuum
I_S	Reverse current of a LED diode
T	Temperature in Kelvin
E_v	Valence band energy
V_{LED}	Voltage drop in LED model
v	Voltage drop in the diode
λ	Wavelength of the particle associated electromagnetic wave

Chapter 2

P_{avg}	Average active power
I_1	Fundamental harmonic of the current
$v(t)$	Grid period
I_n	Input current nth harmonic
THD_i	Input current total harmonic distortion
P	Instantaneous active power
S	Instantaneous apparent power

$i(t)$	Instantaneous current
$v(t)$	Instantaneous voltage
θ	Phase shift between voltage and current
I_{rms}	Root mean square current
V_{rms}	Root mean square voltage

Chapter 3

i_{CONV}	Converter current reference
$C_{ballast}$	Equivalent capacitance of the LF electromagnetic ballast
$L_{ballast}$	Equivalent inductance of the LF electromagnetic ballast
$R_{ballast}$	Equivalent resistance of the LF electromagnetic ballast
$\varepsilon_{V_{PCC}}$	Error of the voltage at the PCC
X_{y1}	Fundamental component of variable X_y
k_1	Gain of the controller of the converter
V_G	Grid voltage
L_G	Grid wire inductance
R_G	Grid wire resistance
X_{yHF}	High frequency components of variable X_y
s	Laplace domain variable
i_{LINE}	Line current of the lighting system
i_{LOAD}	Load current
Z_{LOAD}	Load impedance
P_{LOAD}	Load power demand
V_{PCC}	Point of common coupling voltage

Chapter 4

α	Alpha component of the stationary reference frame
θ	Angle between *d* and α
β	Beta component of the stationary reference frame
d	*d* component of the synchronous reference frame
I_d	*d* current component
I_d^*	*d* current reference component

ω	Line frequency
$I_{q\,n}$	n^{th} component of the q current
$i_{\alpha\,n}$	n^{th} component of the α current
$i_{\beta\,n}$	n^{th} component of the β current
$I_{d\,n}$	n^{th} component of the d current
k_p	Proportional gain of the PR controller
d	q component of the synchronous reference frame
I_q	q current component
I_q^*	q current reference component
k_{res}	Resonant gain of the PR controller
i_α	α current component
i_β	β current component

Chapter 6

P_{DC}	Average output power
C_B	DC bus capacitor
i_g	Input grid current
V_i	Input grid voltage
$P(t)$	Instantaneous output power
R_L	Load resistance
C_o	Output capacitor

Chapter 7

$\langle P_i \rangle$	Average input power
$\langle i_D \rangle$	Average output current of the Flyback in the DC side
$\langle P_o \rangle$	Average output power
Bw	Bandwidth
i_C	Capacitor current
C_o	DC bus capacitor
L_{s1}, L_{s2}	DC bus side inductors
N_2	DC bus side number of turns

S_A, S_B, S_R	DC bus side switches
U_o	DC bus voltage
d_x	Duty ratio (*x* represents the numbers 1, 2 or 3)
U_L	Flyback inductor voltage
i_g	Grid current
$\langle i_{LP} \rangle$	Grid side average inductor current
$\langle i_L \rangle$	Grid side average magnetising inductor current
L	Grid side inductor
i_{LP}	Grid side inductor current
i_L	Grid side magnetising inductor current
N_1	Grid side number of turns
S_1, S_2	Grid side switches
U_g	Grid voltage
T_{iu}	Integral gain of PI controller
i_R	Load current
R	Load resistance
C_o	Output capacitor
i_D	Output current of the Flyback in the DC side
$U_{g\ pk}$	Peak grid voltage
k_p	Proportional gain of PI controller
$\hat{x}$	Small-signal perturbation of variable *x*
T	Switching period

Chapter 8

i_C	Capacitor current
C_o	DC bus capacitor
L_{s1}, L_{s2}	DC bus side inductors
N_2	DC bus side number of turns
S_A, S_B, S_R	DC bus side switches
U_o	DC bus voltage
d_x	Duty ratio (*x* represents the numbers 1, 2 or 3)
U_L	Flyback inductor voltage
i_g	Grid current

$\langle i_{LP} \rangle$	Grid side average inductor current
$\langle i_L \rangle$	Grid side average magnetising inductor current
L	Grid side inductor
i_{LP}	Grid side inductor current
i_L	Grid side magnetising inductor current
N_1	Grid side number of turns
S_1, S_2	Grid side switches
U_g	Grid voltage
i_R	Load current
R	Load resistance
C_o	Output capacitor
i_D	Output current of the Flyback in the DC side
$U_{g\ pk}$	Peak grid voltage
T	Switching period

Chapter 1:

Introduction to electronic lighting

In this chapter, a brief introduction to electronic lighting is provided in order to allow for a better and deeper understanding of the concepts involved in lighting.

Firstly, the main theoretical concepts in general lighting, such as the magnitudes, e.g. luminous flux or intensity, and the physical background will be introduced and explained. Secondly, the main mechanisms of luminous emission will be covered. Then, the most usually employed lamps will be listed, as well as their most important features and applications. Afterwards, a comparison among the most common artificial light sources, in terms of luminous efficacy, life span, typical rated power, etc. will be carried out. Finally, Light Emitting Diodes (LEDs) will be dealt with since they are considered the future in the illumination field.

1.1 Introduction

Lighting systems are one the actual worldwide research hot topics: overall performance features, system reliability, energy savings, energy efficiency, grid pollution reductions strategies and so on are key points of these topics [1], [2], [3]. Due to its increasingly importance, many studies are being continuously carried out in order to discover new lighting sources, new topologies and costs reduction on lighting systems. For instance, in the particular case of Spain, street lighting accounts for a consumption of about 2900 GWh/year, which means an emission to the atmosphere of around 1.740.000 Tons of CO_2 every year [4]. The most interesting issue is therefore the huge capability to save energy in this sector. An average potential savings of 10% are usually estimated wheter energy efficiency technologies, regulation to optimal illumination levels and more efficient lamps were employed [4], [5].

Before going deeper with the different types of lamps available in the market or the most common ones employed in street/road illumination, it is important to evaluate the basic concepts in lighting.

1.2 Key concepts in lighting

This section will cover the main concepts of lighting that will be of help in order to face the design of a basic lighting research project.

1.2.1 Electromagnetic radiation

Electromagnetic radiation (EMR) is the radiant energy released by certain electromagnetic processes. There are many types of radiation, being the visible light, radio waves, infrared light and X rays the most known.

Generally, EMR consists of electromagnetic waves that can be characterised by either its frequency or wavelength, which are synchronised oscillations of electric and magnetic fields that propagate at the speed of light through the vacuum. They can be depicted as self-propagating transverse oscillating waves of electric and magnetic fields. The electric field is in the vertical plane whilst the magnetic field in the horizontal one. The electric and magnetic fields in EMR waves are always in phase and at 90 degrees to each other (see Fig. 1.1).

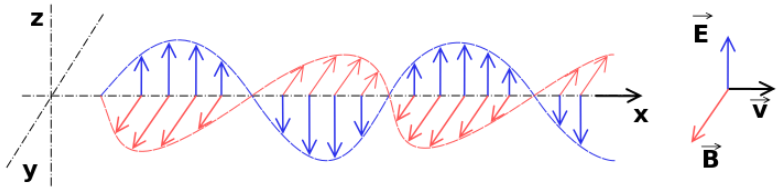

Fig. 1.1. Plane linearly polarized EMR wave propagating from left to right (figure under GNU Free Documentation License)

In the quantum theory of electromagnetism, EMR consists of photons, the elementary particles responsible for all electromagnetic interactions. Quantum effects provide additional sources of EMR, such as the transition of electrons to lower energy levels in an atom and black-body radiation.

The relationship between the energy of the particle (the photon) and the wavelength of the associated electromagnetic wave, is given by Planck's equation:

$$E = h \cdot \frac{c}{\lambda} = hv \qquad (1.1)$$

where *h* is the Planck constant, *c* is the propagation speed of the particle in vacuum, *v* is propagation speed in a medium, and λ, the wavelength of its associated electromagnetic wave.

1.2.2 Electromagnetic spectrum

The classification of the different electromagnetic radiations in terms of their wavelength into radio, microwave, infrared, visible, ultraviolet, X-rays and gamma rays constitutes the electromagnetic spectrum, as it can be seen in Fig. 1.2. The behaviour of electromagnetic radiation depends on its frequency. Lower frequencies have longer wavelengths, and higher frequencies have shorter wavelengths, and they are associated with photons of higher energy.

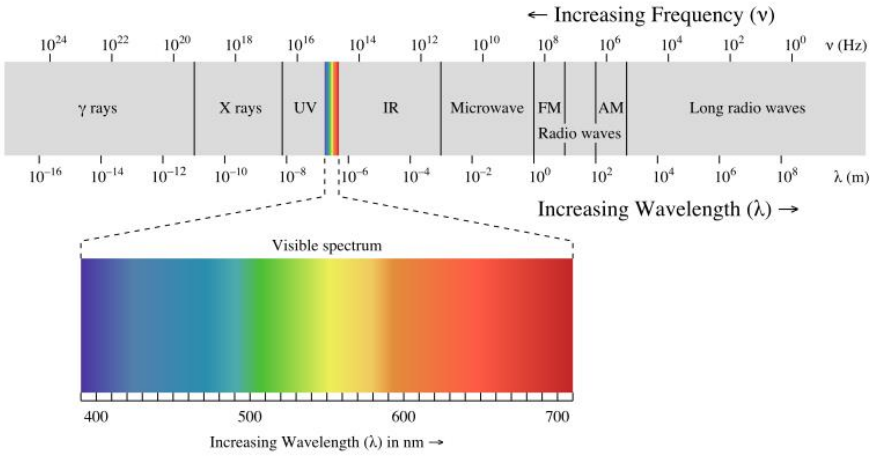

Fig. 1.2. Electromagnetic spectrum (image under the Creative Commons Attribution-Share Alike 3.0 license)

1.2.3 Light

The human retina is sensitive to a narrow band of wavelengths, which is the visible spectrum. Therefore, light can be defined as the electromagnetic radiation as seen by the human eye. Fig. 1.3 shows this visible spectrum and the colours detected by the human eye. However, the human eye sensitivity is not constant for the entire visible spectrum. Indeed, it varies with the wavelength and the amount of light available.

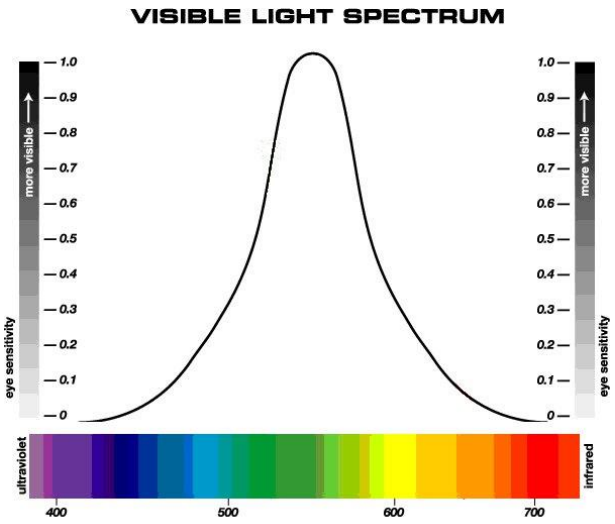

Fig. 1.3. Visible spectrum and sensitivity of the human eye (image under the Creative Commons Attribution-Share Alike 3.0 license)

1.2.4 Light emission mechanisms

The different light emission mechanisms can be classified according to the way in which the electrons are excited. There are two main mechanisms: thermal radiation (or incandescence), and luminescence.

- **Thermal radiation:** thermal radiation could be defined as the emission of electromagnetic radiation due to the thermal motion of electrons caused by the material temperature. If this electromagnetic energy emission falls into the visible spectrum, then it is called incandescence. The interaction between the electrons in an emitter increases with the temperature. The higher the body temperature is, the higher amount of energy is emitted within the visible spectrum, as it can be seen in Fig. 1.4.
- **Luminescence**: essentially, luminescence is the emission of electromagnetic energy radiated from a body due to electron excitation produced by a foreign agent. According to the excitation source, luminescence could be categorised into the following types:
    - Electroluminescence: generated by the action of an electric field inside a substance. Examples of lamps that generate light by electroluminescence are some discharge lamps, light emitting diodes (LEDs), etc.
    - Photoluminescence: generated by the absorption of photons radiated with different wavelength, this can in turn be divided into the following sub-categories: fluorescence, phosphorescence, LASER, etc.
    - Chemiluminescence: generated by chemical reactions.
    - Bioluminescence: produced by living organisms.
    - Triboluminescence: generated by a mechanical action on a body.
    - Etc.

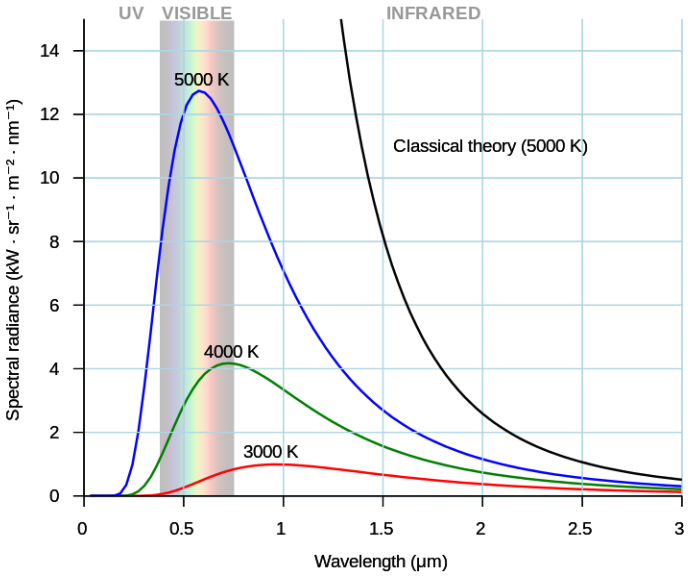

Fig. 1.4. Black body radiation curves (Planck curves) and the visible spectrum (image allowed to be shown to the public domain)

1.2.5 Colour Temperature (CT) and Correlated Colour Temperature (CCT)

The human eye has three types of colour sensors which answer to different ranges of wavelengths, thus, all visible colours would produce a three-dimensional chart. Nevertheless, the concept of colour can be split into two parts: brightness and chromaticity. There are different colour spaces but one of the most relevant is the CIE XYZ, that was specifically designed so that the *Y* parameter was a measure of the brightness of a colour. On the other hand, the chromaticity of a colour was derived in two parameters, *x* and *y* that are functions for all three tristimulus values *X*, *Y* and *Z*. This two chromatic coordinates form the diagram of Fig. 1.5.

The Colour Temperature (CT) of a light source represents its thermal appearance in Kelvin (K). Every material, when heated up to a certain temperature, begins to emit a reddish light. As long as the temperature increases, the light turns to white. This phenomenon sets up a relation between the temperature of the light source and its colour appearance.

Therefore, the CT of a light source is determined by comparison with a pattern. This pattern is based on a lamp that behaves the closest to the black body in terms of emitting properties. The different temperatures of the black body generates the Planck Locus inside the Comission Internationale de l´Éclairage (CIE) chromaticity diagram, as depicted in Fig. 1.5.

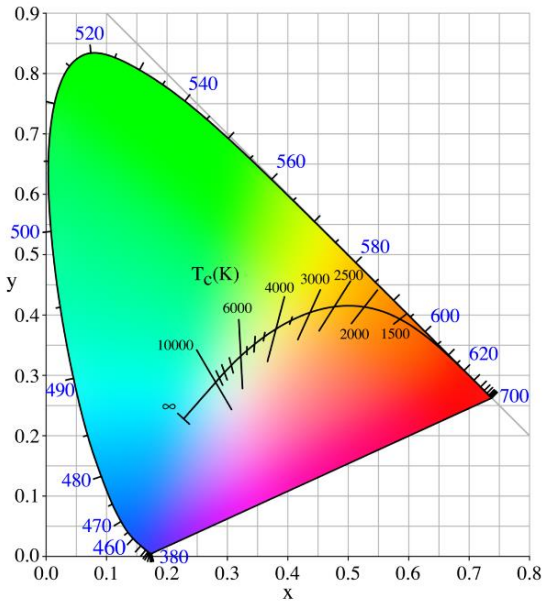

Fig. 1.5. CIE 1931 Chromaticity Diagram, Planck Locus and Correlated Colour Temperature lines (image allowed to be shown into the public domain)

For those light sources not emitting in a continuous spectrum, their colour is outside the Planck Locus, and the concept of Colour Temperature is no longer valid. In these cases, the applicable concept is the Correlated Colour Temperature, which shows the colour of the light as if it was emitted as a continuous spectrum, but gives no information about the spectral composition.

1.2.6 Colour Rendering Index (CRI)

The Colour Rendering Index (sometimes known as Colour Rendition Index) shows the ability of a given light source to reproduce colours faithfully as compared to a black-body pattern light source with the same CT. The CRI values are comprised between 0 and 100, being the higher the better reproduction of colours.

1.2.7 Luminous flux

The luminous flux is the measure of the perceived power of a luminous source. It is calculated by weighting the power for each wavelength with the luminosity function, which represents the eye's response to different wavelengths. In the SI, the employed unit is the lumen (lm). One lumen is defined as the luminous flux of light produced by a light source that emits one candela of luminous intensity (whose meaning will be explained ahead) over a solid angle of one steradian (or square radian, used in three-dimensional space). A solid angle is the two-dimensional angle in three-dimensional space that an object subtends at a point.

The luminous flux (in lumen) is a measure of the total luminous power emitted by a lamp in all directions.

1.2.8 Luminous intensity

Luminous intensity, in photometry, is defined as the amount of luminous flux emitted by a light source per unit of solid angle. Its unit in the SI is the candela (cd). It should be not confused with the luminous flux: if a lamp has a 1 lm bulb and the optics provide a 1 steradian beam, then the luminous intensity of the beam would be 1 cd. However, if the optics change to concentrate the beam into half a steradian, then the luminous intensity would change to 2 cd. The luminous intensity (in candela) differs from the luminous flux in that the first one is measured in a particular direction.

1.2.9 Luminance

Luminance is a photometric measure of the luminous intensity per unit area of light travelling in a given direction. It describes the amount of light that passes through, is emitted or reflected from a particular area, and falls within a given solid angle. The SI unit for luminance is candela per square metre (cd/m^2).

1.2.10 Luminous irradiance

The science of the measurement of electromagnetic radiation, radiometry, defines the luminous irradiance as the radiant flux received by a surface per unit area. The SI unit is the watt per square metre (W/m^2).

1.2.11 Luminous efficacy

The luminous efficiency defines how well a light source produces visible light, which is basically the ratio between luminous flux and power consumed by the lamp. This concept is important since not all wavelengths of light are equally visible, or equally effective at stimulating human vision. The luminous efficiency takes into account how the light source converts energy to electromagnetic radiation and how well this radiation is detected by the human eye.

1.3 LED lamps predecessors

Since this work is focused on solid-state street and general lighting with white LEDs, more information will be provided in depth in subsequent sections. However, before LED made its appearance, street lighting systems made use of other kind of lamps. In this section, the main types of lamps commercially available will be briefly introduced, as classified by its light emission mechanism: thermal radiation and luminescence.

1.3.1 Incandescent lamps

Incandescent lamps generate light by thermal radiation as a consequence of the flow of a current mainly through a wolfram filament. It generates energy in the visible region, actually in the IR range. Hence, these lamps lack of efficacy (between 8 and 20 lm/W). Featuring a continuous emission spectrum, the CT of the emitted light is determined by the temperature of the wolfram filament. Fig. 1.6 shows the emission spectra of an incandescent lamp at different filament temperatures. The CT of incandescent lamps corresponds to warm white (as much as 3000 K), the CRI is 100, and their life span ranges 1000 – 2000 hours [1].

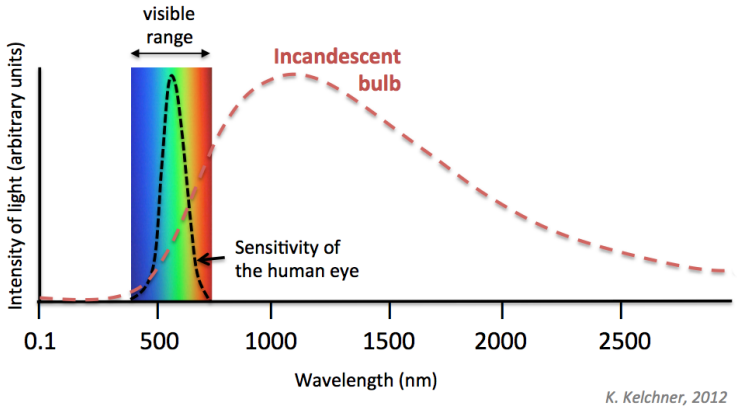

Fig. 1.6. Emission spectrum of an incandescent bulb (red dashed line) and human eye sensitivity (black dashed line) versus wavelength in nanometers (nm) [1]

1.3.2 Halogen incandescent lamps

These lamps are, basically, incandescent lamps with a halogen-based additive in the filling gas: iodine or bromine, usually. This additive allows the halogen cycle to occur and perform a regenerative effect that avoids the wolfram to fall over the bulb and allows the filament to work at higher temperatures, increasing its lifespan to 3000-4000 hours and the efficiency to values higher than 25 lm/W. Their CT is as high as 4200 K in some automotive applications [1].

1.3.3 Low-pressure gas discharge lamps

Gas discharge lamps emit light produced by the luminescence mechanism. In this kind of lamps, a plasma takes place when an electric field induces the excitation of the plasma atoms. Low-pressure gas discharge lamps are formed by a gas confined into a bulb at around 1 Pa. At each side of the bulb there are two or more electrodes responsible of generate the electric field (although there are electrodeless lamps available) [6].

This electric field causes the ionisation of the gas until the disruptive discharge is reached. At this point, the current through the gas rises very quickly, so a current-limiting ballast is used in order to limit the lamp current.

The most common low-pressure lamps are:

- **Low-pressure mercury lamps (fluorescent lamps):** wide range of CCT depending on the phosphor that covers the inner suface of the bulb, which varies between 2600 and 8000 K. The efficacy of these lamps can reach values of 100 lm/W.
- **Low-pressure sodium lamps (LPS):** known as the most efficient of all light sources with efficiencies rounding 180 lm/W; these lamps have a highly monochromatic light and a rendering index rather poor, which means they are not suitable for places where it is important to distinguish colours.

1.3.4 High-pressure gas discharge lamps (HID lamps)

They are a type of electrical gas-discharge lamp which produces light by means of an electric arc between wolfram electrodes placed inside a tube filled with both gas and metal salts. Initial arc's strike is facilitated by the filling gas and once the arc is started, it heats and evaporates the metal salts, thus increasing the intensity of the light produced by the arc and reducing its power consumption. With respect to low-pressure lamps, the CRI is improved. However, as a consequence of the higher pressure, greater temperatures are reached, hence the efficacy is also reduced due to the fact that a fraction of the energy is transformed into heat. As it happened with low-pressure lamps, high-pressure ones need a ballast to control and limit the current [7], [8].

The most common HID lamps are:

- **High-pressure mercury vapour lamps (HPM-HME):** these lamps were the first high-pressure lamps commercially available, and were the most common choice in street lighting for a long time. Nevertheless, due to their low efficacy (about 50 lm/W) they have being replaced by better options [9].
- **High-pressure sodium lamps (HPS-SON):** these lamps use sodium in an excited state to produce light. They feature a CCT around 2000 K with a CRI around 40 and a luminous efficacy around 120 lm/W or slightly higher [10]. They are widely used in street illumination.
- **Metal-halide lamps (MH):** these lamps come from HPM lamps with the addition of metallic halides and rare earth salts that radiate within the visible spectrum in order to improve both the quality of the light and the efficacy. The CCT of such lamps usually ranges between 3000 and 5500 K, depending on the additives used, the CRI is as good as 95, and its efficacy surpasses 100 lm/W in some devices [11].

1.4 Light-Emitting Diodes

Electroluminescence is the phenomena whereby a material emits light when a current goes through it. Henry Joseph Round reported it for the first time in 1907. He noticed a yellowed light emission when a voltage was applied to silicon carbide crystal (SiC) [12]. Light Emitting Diodes or LEDs are semiconductors that appear as a practical electronic component in 1962 working as a low-intensity infrared (IR) light device [13].

The first LED destined to be an indicator was developed by Nick Holonyak Jr. with an efficacy approximately of 0.11 lm/W [12]. This fact settled the first step towards a great development in the field of signalling. LEDs are basic today in electronic equipment, information panels and other devices. LEDs have experimented an impressive improvement in several characteristics such as efficacy, thermal resistance and light maintenance. Other advantages of LEDs are the absence of IR and UV radiation in the radiating output. However, LEDs still feature some drawbacks such as the loss of efficacy at high temperature, which is worsened by the fact that most of the heat generated in the *p-n* junction is dissipated by conduction.

There is a wide range of CRI, CCT and luminous efficiency values. Regarding the CRI, the most usual are around 75 up to 95. The CCT goes from 3000 K to 8000 K or even higher for some cool white devices, and the luminous efficiency has surpassed the 100 lm/W for cool white devices [1], [14], [15]. Nevertheless, LED technology compensates more than enough these drawbacks by having a long service life, high energy efficiency, quite constant CT, easy dimming capability and a compact construction that allows new designs.

High brightness LED would eventually come up trying to substitute the classic lamps in traffic lights, electronic panels, interior lighting, flashlights and street lighting [1].

1.4.1 Solid-state lighting

In this section, solid-state lighting will be briefly introduced: LED operational principles and most important issues to supply LED lamps will be addressed.

LED technology has seen an impressive improvement in some of its characteristics as thermal resistance or efficacy. Nevertheless, some drawbacks are still quite a challenge such as the loss of efficiency at high temperatures due to the fact that a great amount of heat is dissipated in the *p-n* junction.

1.4.2 Operational principles of LEDs

Luminescence injection is the light emission mechanism in LEDs. This takes place by the recombination of a hole-electron pair through the band gap of the semiconductor when the *p-n* junction is excited by an external electric field.

Electrons and "holes" are the two different charge carriers in a semiconductor lattice. Under an external electric field or under thermal excitation, electrons in the valence band are able to "jump" to free energy levels in the conduction band if they gain enough energy. This process creates a hole in the valence band. Fig. 1.7 depicts the bands diagram and the semiconductor energy levels. A recombination process is illustrated, where the electron reaches the conduction band after getting a certain amount of energy, E_a, greater than E_c-E_v, where E_c is the minimum energy level at the conduction band and E_v is the maximum energy level at the valence band.

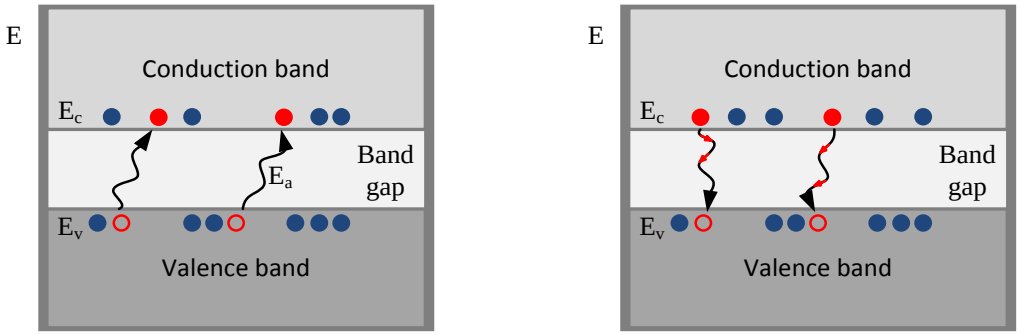

Fig. 1.7. Energy bands in an intrinsic semiconductor. Vertical axis: electrons energy, in eV. Electrons jump to the conduction band and leave a hole (left) and vice versa (right)

As a consequence of the external electric field applied, electrons gain an amount of energy that it is progressively transformed to kinetic energy due to the fact that electrons are in constant motion. As a result, they are able to reach the lower energy levels in the conduction band, and when this happens, recombination is the only solution to keep losing energy since there are no possible energy states in the band-gap. In this process, the electron descends to the valence band and occupies a hole, that is, one of the vacant energy states. This descent is possible thanks to the electron energy loss equal or bigger to the band gap energy. This released energy can be produced either by a non-radiative recombination, a phonon, that yields to heat losses or by a radiative recombination, the

emission of a photon, which is electro-magnetic radiation. If such radiation falls into the visible part of the spectrum, it yields to light. The wavelength of the obtained electromagnetic radiation is determined by the energy jump in the recombination, i.e. by the band gap of the semiconductor.

1.4.3 Constructive and lighting characteristics

The light of an LED is basically a monochromatic radiation, that means it is related to a single wavelength, which in turn is connected to the material employed in the semiconductor. The silicon crystal may be doped with different elements, e.g. gallium, aluminium, arsenic, phosphor, indium or nitrogen. The combination of these elements allows the emission of light with a wider band in the radiation spectrum (see Fig. 1.6) [13], [16], [17], [18].

1.4.4 White LED technology

However, in the field of lighting a particular kind of white light is used. Depending on time of day, season and weather, the human eye is quite sensitive to small changes in the spectral content of illumination sources. In addition, white light cannot be obtained by a monochromatic radiation.

In [19], [20], [21] are exposed three general ways to generate white light from LEDs. The first method is quite straightforward because it is based on mixing light from three or more monochromatic sources: red, green and blue, to produce a white light to the human eye. The second option employs a blue LED to pump one or more visible light-emitting phosphors integrated into the phosphor-converted LED package. This modified LED is designed to leak some of the blue light beyond the phosphor to generate the blue portion of the spectrum, while phosphor converts the remainder of the blue light into the red and green portions of the spectrum. Finally, the third method uses an ultraviolet (UV) LED to pump a combination of red, green and blue phosphors in such a way that none of the pump LED light is allowed to escape. Fig. 1.8 depicts both typical colour-filter transmission RGB and white LED spectrums. It can be seen the three peaks for red, green and blue for an RGB LED in Fig. 1.8a while Fig. 1.8b shows the dominant peak at 450 nm and a lower peak from 500 nm to 600 nm for a typical white LED.

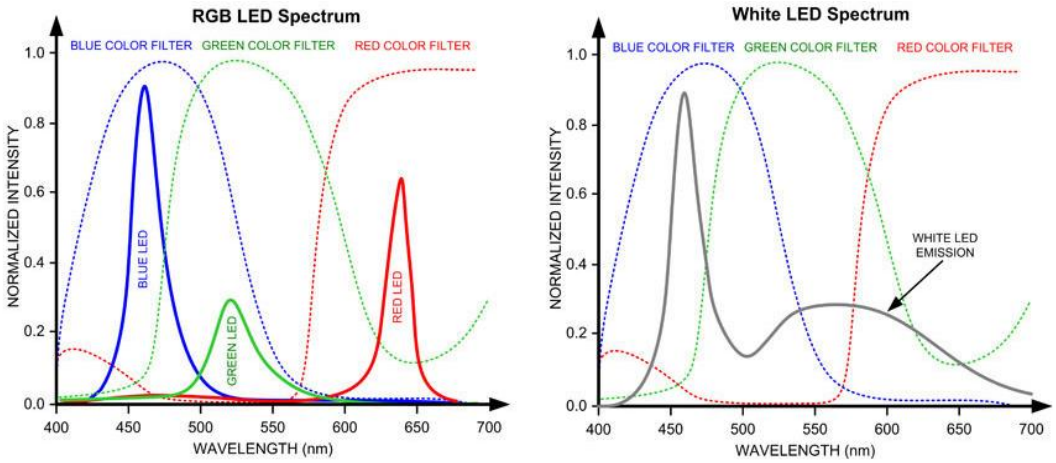

Fig. 1.8. Typical colour-filter transmission spectrums: (a) RGB LED (b) White LED [13]

1.4.5 Electrical equivalent model of an LED

LEDs are diodes. Therefore, its voltage to current characteristic behaviour follows the modified Shockley equation [12], as shown in (1.2):

$$i = I_S \cdot \left(e^{\frac{v}{\frac{n k T}{q}}} - 1 \right) \qquad (1.2)$$

where I_S is the reverse current, also known as "scale current", v is the voltage drop across diode terminals, n is the ideality factor, k is the Boltzmann constant, T is the temperature in Kelvin and q is the electron charge.

By means of (1.2), the characteristic curve V-I of an LED can be obtained. However, manufacturers usually give this data in order to ease the users modelling their LED. For example, Luxeon K2 forward current vs. forward voltage can be seen in Fig. 1.9.

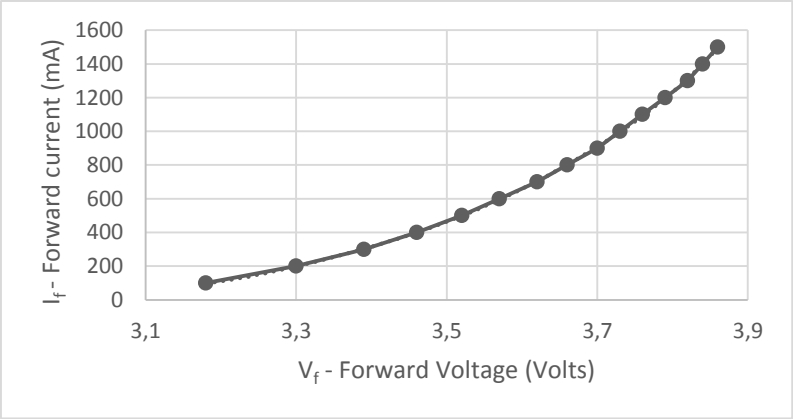

Fig. 1.9. Forward current vs. Forward voltage for white, green, cyan, blue and royal blue (Luxeon K2)

This behaviour can be modelled as a resistor in series with a voltage source and an ideal diode, as shown in Fig. 1.10 [1], [13].

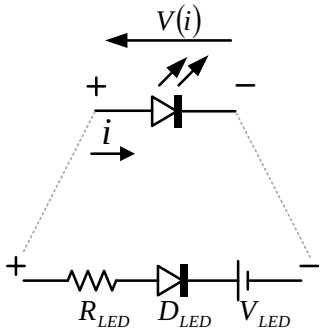

Fig. 1.10. Simplified electrical model for a power LED

There are more complex techniques to model LEDs, like several comprehensive small-signal models that analyse the parasitic effect of the parasitic inductances in the wires and leads of the package,

the skin effect, the junction capacitance and so [1], [22]. In this work, the simplified model will be enough in order to perform optimal simulations.

1.5 Comparison among lamps

In this section, most common lamps for general purpose will be briefly compared: CRI, CCT, luminous efficacy and life span will be the items to value, taking into account that these values may change from different manufacturers. TABLE 1.I gathers some useful information in order to make this comparison.

TABLE 1.I.

MAIN CHARACTERSISTICS OF COMMERCIAL LAMPS (TYPICAL) [1]

Lamp	*CRI*	*CCT (K)*	*Efficacy (lm/W)*	*Life span (h)*
Incandescent	*100*	*~2700*	*~10*	*~1000*
Halogen	*100*	*~3600*	*<25*	*<4000*
Fluorescent	*<97*	*2600-8000*	*~100*	*~20000*
LPS	*-*	*~1700*	*<180*	*~20000*
HPM-HME	*20-50*	*4000-7000*	*10-60*	*~20000*
HPS-SON	*20-85*	*2000-2800*	*50-140*	*~20000*
MH	*65-95*	*3000-5500*	*~100*	*6000-20000*
LEDs cool white	*~70*	*~5500*	*>100*	*~50000*
LEDs neutral White	*~85*	*~4000*	*~100*	*~50000*
LEDs warm white	*~95*	*~3000*	*<100*	*~50000*

1.6 Street illumination

A proper street illumination provides not only a good visual impact of the city and its nightlife but also an improvement in the quality of life. In addition, new possibilities for business and culture activities are opened since optimum luminous levels affect seriously the security of the area [23], [24].

As mentioned before, from an energetic and environmental point of view, public lighting systems can reach the 50% of the whole power consumption of a city. By implementing two-way communication (luminaires with built-in intelligence), an accurate feedback on the lamps condition can be achieved and therefore reduce the need for manual control and may plan maintenance in a cost effective way [25], [24].

However, before LEDs, other kind of lamps were used for street illumination. The first ones were incandescent lamps followed by fluorescents. Nowadays, most common lamps in street illumination still are the high-pressure lamps: HPM-HME, HPS-SON and MH [7], [10], [26].

These systems are still being used in many places, as the investment value has not yet been recovered. In fact, in some cases these systems coexist with new lighting system, giving rise to complex

situations: e.g., there are weak grids that could not bear with the traditional lighting systems, as the HPS lamps with electromagnetic ballasts, due to the harmonic content generated. However, these microgrids may be able to put up with the LED technology since the electronic ballasts use to demand very low high frequency currents. If both systems are installed in a weak grid, the electronic ballasts could be used to correct the effect of the electromagnetic ones. Actually, one of the contributions of this thesis is to deal with these possible situations and try to mitigate their negative effect in the AC mains.

High luminous efficacy and long useful life are some of the main characteristics that make LEDs suitable and appealing for lighting systems. Besides, LEDs are tougher to vibrations and mechanical bumps; they do not need any gas or filament inside nor a high voltage to light. Thus, illumination with LEDs is becoming a trending also in outside public street lighting systems [27], [28], [29], [30].

Furthermore, even though traditional lighting systems have the ability of pointing the light by means of lens, the LED technology allows this characteristic in a more easier, versatile and cheap way. Therefore, the areas to be illuminated and the areas to be not are easily chosen [31], [32]. Fig. 1.11 shows a visual comparison between LED and HPS lamps lighting a street.

Fig. 1.11. Difference between LED and traditional HPS lamps in street lighting

Thus, through the brief study of the lamps used for street illumination, it can be thought that LED technology has many advantages over older ones: less consumption, less aggressive to the environment, good illumination levels, dynamism, etc. The main drawback can be seen from the point of view of the initial investment due to the fact that LED luminaires can be still a bit more expensive than the traditional ones [28], [29], [30].

1.7 Summary and conclusions

This chapter presented an overview about general topics in lighting and solid-state lighting in particular. The fundamentals on lighting and light emission mechanisms have been covered, highlighting the various kinds of commercially available lamps assorted by their emission mechanism. Finally, a brief introduction to street illumination can be found.

LED-based systems are called to replace traditional illumination technologies. This issue implies technical challenges in different fields: electronic and electrical engineering, architecture, etc. New LED systems would change the impact in the utility grids with respect to the traditional systems. The harmonic content of the demanded current is different and this issue need to be studied.

On the other hand, a new power supply electronic system may be evaluated in order to solve the impact of having in the same grids traditional and novel illumination systems, distributed generation units, etc.

Chapter 2:

Basic concepts about input current harmonics

This chapter deals with the regulations about supplying lamps from the AC mains. Important concepts related to electromagnetic compatibility such as the total harmonic distortion or the power factor will be briefly covered according to the international standard IEC 61000-3-2: 2005 Class C.

2.1 Introduction

Power LEDs are meant to be supplied at a constant current to achieve maximum efficiency, flexibility and high-performance. Usually, electronic active drivers are designed and employed for this task [33], [34] among other features as well as dimming. However, there are some exceptions and passive LED drivers are sometimes used, consuming energy directly from the AC mains but supplying the lamp with DC current [35]. These passive drivers are just topologies based on diodes.

Line harmonic distortion and displacement between AC grid voltage and current must be kept as low as possible, maximising this way the energy delivery to the lamp and minimising the grid distortion. If high frequency harmonics coexist in the grid, several issues may appear: interferences, stability problems, unexpected disturbances, extra losses in the wiring, diminishing of life-span, increase of the failure rates and so. There is one important regulation that establish limits to both previous factors internationally: IEC 61000-3-2: 2015 Class C (EN 6100-3-2: 2014 is its Spanish equivalent) [1], [36].

2.2 Definition of power factor (PF)

IEC 61000-3-2 regulation limits the harmonic content rather than the power factor. However, as the third harmonic is defined by the power factor, and the Energy Star program requires a minimum value, this parameter needs to be properly defined. PF is the ratio between real power, *P*, and apparent power, *S*:

$$PF = \frac{P(W)}{S(VA)} = \frac{P_{avg}}{V_{rms}I_{rms}} = \frac{\frac{1}{T}\int_0^T v(t)i(t)dt}{\sqrt{\frac{1}{T}\int_0^T v(t)^2dt}\sqrt{\frac{1}{T}\int_0^T i(t)^2dt}} \quad (2.1)$$

where P_{avg} refers to the real power averaged over a period *T*, V_{rms} is the *rms* value of the input voltage, *v(t)*, and I_{rms} is the *rms* value of the input current, *i(t)*.

The classical definition of PF, applicable to pure sinusoidal waveforms accounts for the phase shift between voltage and current, Θ, and it can be written as:

$$PF = \cos(\theta) \quad (2.2)$$

Therefore, the maximum possible value for PF is 1, which is usually mentioned as unity power factor. However, PF is never perfect when electronic power supplies are involve. It can be very high but there will be always a little distortion present even if voltage and current are in phase [1]. It is called the distortion factor (DF) and it can be defined as:

$$DF = \frac{I_1}{I_{rms}} \quad (2.3)$$

where I_1 stands for the fundamental harmonic of current. Assuming that the line voltage is a pure sine wave, which is reasonable in AC power supplies with power factor correction, the DF can be expressed as a function of the input current total harmonic distortion, THD_I.

$$DF = \frac{1}{\sqrt{1 + THD_I{}^2}} \qquad (2.4)$$

2.3 IEC 61000-3-2: 2005 regulations

The IEC 61000-3-2:2005 ([36]), or its Spanish equivalent EN 61000-3-2: 2014, refers to the electromagnetic compatibility and it fixes the maximum levels for harmonic current injection back to the AC grid supply, for all electrical and electronic equipment up to 16 A per phase. This standard differentiates between four classes and the lighting equipment belongs to Class C.

According to [36], the final expression of the THD_I derived from the previous equations stays as:

$$THD_I = \frac{\sqrt{\sum_{n=2}^{40} I_n^2}}{I_1} \qquad (2.5)$$

where I_1 and I_n stand for the first and nth harmonic amplitude, respectively, being limited to the 40th order harmonics.

Therefore, an extended definition for PF, accounting for both the phase shift and the harmonic distortion present in the input current can be set as:

$$PF = \frac{\cos(\theta)}{\sqrt{1 + THD_I{}^2}} \qquad (2.6)$$

where *cos(Θ)* applies to the line-current first harmonic [37]. As it can be seen from (2.6), even if there is no phase shift, high power factor and THD can simultaneously coexist.

Depending on the lamp power, there are different harmonic content allowed levels. TABLE 2.I establishes relative limits given as a percentage of the fundamental harmonic [36].

TABLE 2.I

LIMITS FOR C CLASS EQUIPMENT

Harmonic order n	*Maximum permissible harmonic current expressed as a percentage of the input current at the fundamental frequency (P>25W)*
2	*2*
3	*30·λ**
5	*10*
7	*7*
9	*5*
11≤n≤39 (odd harmonics only)	*3*

** λ is the circuit power factor*

2.4 Summary and conclusions

In this chapter, key concepts such as PF and THD have been introduced while the existence of standards like the IEC 61000-3-2: 2005 Class C for lighting products have been briefly covered. In further chapters of this thesis, these concepts will be used to evaluate power converters and electromagnetic ballasts. Notice that we have focused on lamps with a power greater than 25 W but further information can be found in [36] about different power lamps.

Therefore, the standards imply limits in the design of the electronic ballasts that must be considered in the forthcoming chapters.

Chapter 3

Study of the grid impact of mixed lighting systems: minimisation techniques for current harmonic content

This chapter is intended to propose a methodology to improve the line current THD of a given distribution line configuration, with multiple non-linear loads such as conventional low-frequency street lighting systems mixed with electronic HF LED based ballasts. In the proposed solution, the control scheme avoids the use of current sensors, aiming for a low-cost implementation of the algorithm. The implementation of these active filters has been considered for a case of study of correction of the harmonic content generated by a given number of 150W HPS lamps.

Thus, the objectives of this chapter are:

- *Build a complete model in Matlab/Simulink of a conventional public lighting system.*
- *Develop a control algorithm for compensation of the line current harmonics of the system.*
- *Integrate both the original lighting system and the active filtering system to attain current harmonics compensation*
- *Establishing the limits for the current compensation as a function of the system constraint*

3.1 Introduction

As mentioned before, lighting accounts considerably for the total power consumption in residential and commercial buildings. Thus, energy efficiency in this field is a big deal if greenhouse emissions wanted to be reduced.

In order to drive discharge or LED lamps, high frequency electronic ballasts are widely used. Nevertheless, electromagnetic ballasts are still in use in many undeveloped street lighting systems [8], [10], [11], [38]. The use of these devices implies a great generation of current harmonics and current distortion in the AC mains.

Electromagnetic ballasts are formed by an inductor in series with the lamp plus a bulky capacitor for improving power factor. However, the current drawn by those conventional ballasts is made up of many odd harmonics and it has a high THD. Moreover, the lower frequencies (3^{rd}, 5^{th}, 7^{th}...) contain a considerable amount of energy. Thus, potential problems such as excessive heating of conductors, voltage distortion, overheating of transformers can appear [39].

There are several methods to reduce current harmonics content in the grids. Some examples can be found in the bibliography:

- Selective harmonics compensation: this is one of the most common control technique. Although there are different algorithms, the basics are the same for all the works: detect the harmonics and compensate them individually [40], [41], [42], [43], [44].
- Predictive algorithms: the accuracy of these algorithms strongly depends on precise information about future samples of equivalent electromotive force of the grid, which is in general distorted and unbalanced [45].
- Sliding-mode control: it is easy to implement and provides a good behaviour of the power converter. Besides its simplicity, it is not a very common technique [46].

Then, many other different papers mentioned several strategies, like using 5^{th} tuned passive filters ([47]), injecting the opposite current of the input one ([48]), measuring only the voltage at the point of common coupling (PCC) ([49]), cancelling undesirable excessive harmonics flowing in the neutral line of a three phase four wire system ([50]), etc. There are also interesting works with different comparisons for current control techniques for active filter applications like the one shows in [51].

Power electronics and power system engineers have been working in developing dynamic and adjustable solutions to reduce this harmonic pollution in the electrical grids [43], [44], [45], [51]. Upon these solutions, Active Filters (AF) outstand as the one of the better known and most used techniques. These AF are also called active power line conditioners, instantaneous reactive power compensators, active power filters or active power quality conditioners [39].

Upon the manifold of AF topologies used to correct the current harmonics distortion, some of them are based on a standard H-bridge input stage, which provides full current control capability. In addition, these topologies need a dedicated sensor to measure the line current [43], [46], [48]. In fact, these sensors need to present good overall performance and high bandwidth, in order to obtain a proper current measurement. This usually implies a significant cost and a reduction in the reliability because the more components in the system, the more chances of failure exist. The cost is an arguable variable: for a high power converter, the cost of a sensor does not imply a great extra charge in the overall power system price. However, for a 100 W electronic ballast, the impact in the final cost of a current sensor really does have a considerable influence.

In this chapter, a system of current harmonics compensation without current sensing is proposed and tested by simulations. The electromagnetic ballast and the lamp will be considered as a block that drains a highly distorted current. The key aspect of this chapter is the correction of this distortion with electronic drivers feeding LED lamps and connected to distributed generation units instead of using classic AF. Thus, in this lighting system would coexist old and new lighting technologies together with renewable energy sources.

3.2 Lighting systems based on electromagnetic ballasts

Fig. 3.1 shows a diagram considering the case under study with the classic solution of an AF, representing the interconnections and the elements from the substation to the dedicated lighting system, which is formed by 250 ballasts and their respective 150 W HPS lamps divided in groups of 50. It must be noticed how these are non-linear loads. On the other hand, the converter topology would be an H-bridge thus active and reactive power might be fully decouple, therefore enabling for harmonic compensation.

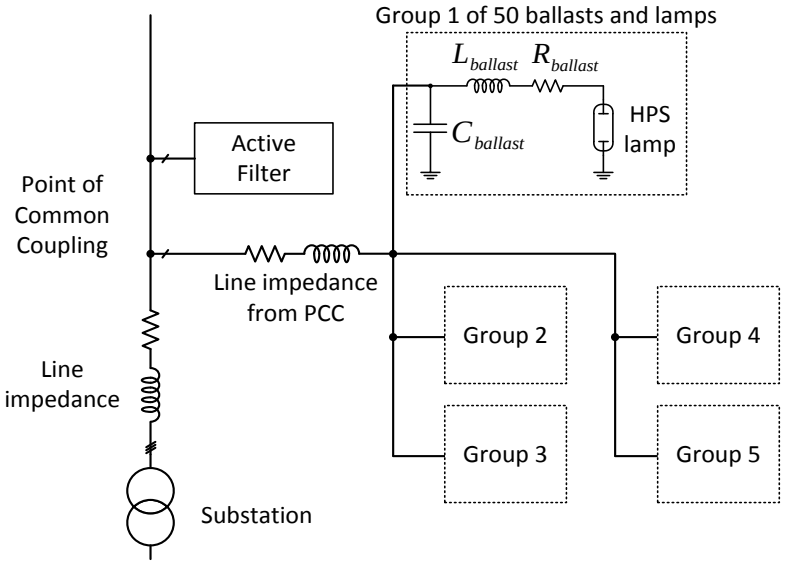

Fig. 3.1. Case of study and classic solution with AF

However, what it is proposed is a mixed lighting system as the one depicted in Fig. 3.2. The AF does not exist anymore and its function will be carried out by a group of electronic ballasts. Thus, these electronic ballasts are able to supply the LED lamps and inject the power that comes from the distributed generation units into the grid but with the proper waveform that compensates the current demanded by the electromagnetic ballasts.

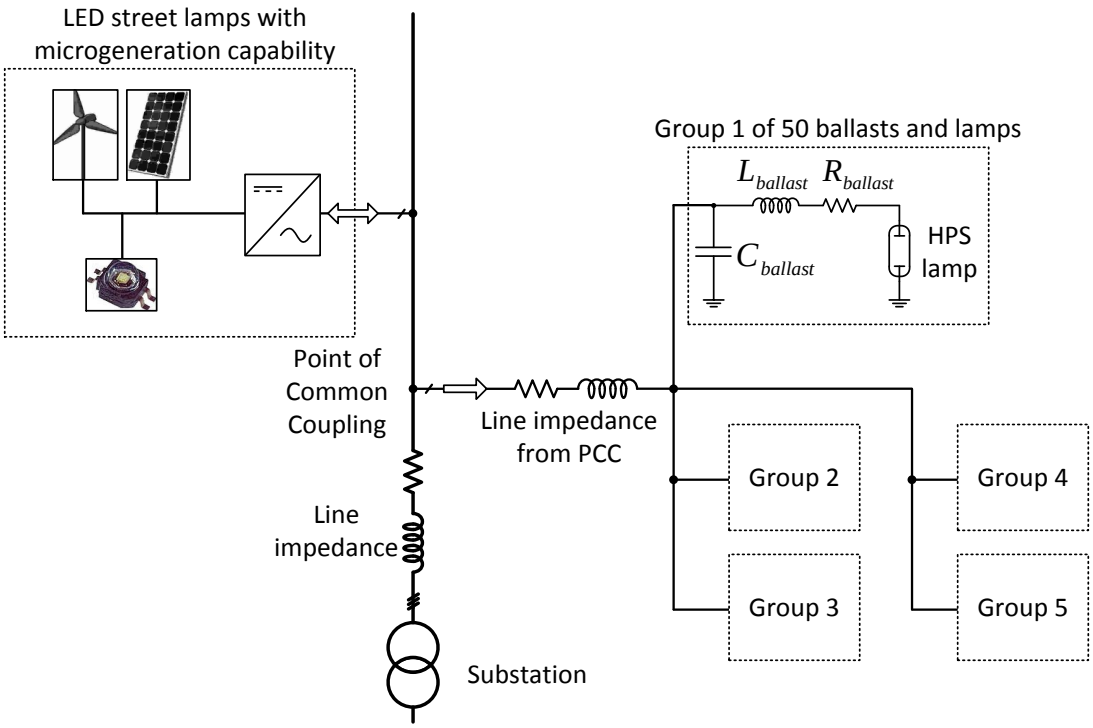

Fig. 3.2. Case of study and proposed solution in a mixed lighting system

In this chapter, one converter that will compensate the harmonic content generated by all the loads will be considered, just to simplify the problem. At this moment, only the control strategy needed to minimise the current harmonics will be dealt with. Later in the development of this work (chapters 7 and 8), possible topologies able to provide such current-shaping features will be considered.

Therefore, several steps must be taken before in order to calculate the waveform of the injected current into the grid to diminish the THD:

- Model the lighting system as a block: ballast components and HPS lamp.
- Quantify the THD that the prior model would demand.
- Develop the control strategy that would minimise this THD.
- Simulate the whole system.

3.3 Ballast and lamp models

The behaviour of the conventional low frequency electromagnetic ballast ([52]) and the 150 W HPS lamp ([53]) was taken from real devices and built in Simulink. With the obtained data, a simple, circuital model was developed. In order to simulate the line current demanded by the real loads and then study how to compensate its effect in the grid and possible solutions, the model is needed.

3.3.1 Model of the electromagnetic ballast

TABLE 3.I summarises the measured parameters of the ballast behaviour:

TABLE 3.I

REAL BALLAST AND LAMP INFORMATION

Ballast current (A)	*Ballast voltage (V)*	*Lamp current (A)*	*Lamp voltage (V)*	*R ballast (Ω)*	*L ballast (mH)*	*C ballast (μF)*
1.0	*320*	*2.7*	*108*	*5.5*	*325*	*20*

3.3.2 Model of the lamp

Much effort has been devoted to the development of sophisticated HID lamp models based on advanced diagnostic techniques in the last few decades. However, most of these models are complicated and there is a lack of practical HID lamp models that are accurate enough and yet can be easily implemented in circuit simulation software. In fact, HID lamps are extremely complex devices, which have many variables and parameters to be determined for optimum performance. Some methodologies make use of the physical laws of plasma [54] while others use non-linear models based on electrical variables [55], [56]. The choice of the best model for a given application depends on the key information needed to extract from the model, on the level of complexity that the simulation might handle, as well as the amount of data known from the real lamp and ballast system.

For the development of this Ph.D. work, a simple, circuit-based, reduced model has been proposed. This model has been used in order to ease cross-platform and multi-environment the simulations (PSpice, PSIM, Matlab-SIMULINK, dSPACE…). This model was developed in [57], where the behaviour of the lamp for LF electromagnetic, LF square wave switched electronic ballast or HF resonant electronic ones was studied and validated.

However, despite of its simplicity, the model is reliable if it is compared with real data of the lamp. The lamp model was calculated to take into account the behaviour of a 150 W HPS lamp ([53]) together with a LF lamb ballast ([52]). The simplification of is based on the voltage-source behaviour of the lamp discharge at low frequency. Two zener diodes in anti-series configuration model the basic behaviour of the discharge, being the zener voltage the arc voltage of the lamp, with a value of 95V. Two exponential curves, used to model the time constants of the re-ignition peak have also been added to this basic model. As a result, the final lamp model is presented in Fig. 3.3.

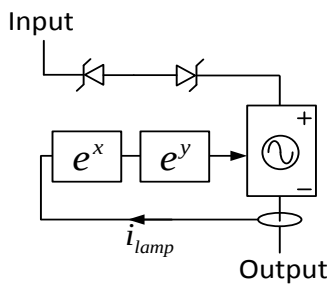

Fig. 3.3. Model of the lamp

These features are particularly interesting in applications where an accurate model is needed in LF simulations, without increasing the simulation time too much, such as analysis of current harmonics content in public lighting distribution lines, active filter design, PFC stages design, power flow analysis and so on [57].

3.3.3 Comparison between real data and the model of the lamp and the ballast

In Fig. 3.4 the data obtained from the real model and the characteristic curve current vs. voltage of the lamp are depicted. As it can be seen, the ballast current is not sinusoidal and the harmonic content is rather significant.

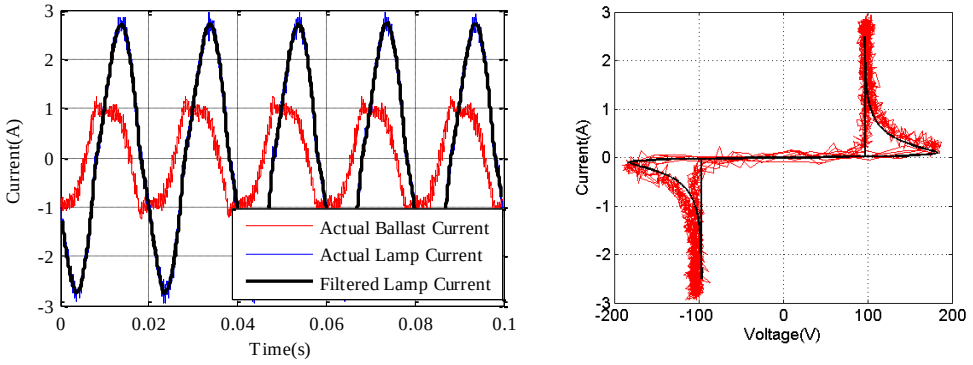

Fig. 3.4. Left: real measured ballast current; blue: real measured lamp current; black: simulated lamp current. Right: current vs. voltage characteristic curve of the real lamp (red) and the model (black)

Both the real and modelled lamp voltage and lamp current are shown in Fig. 3.5. It can be seen how the model tracks with quite accuracy the real waveforms. Hence, the developed lamp model can be used to perform the full system simulations.

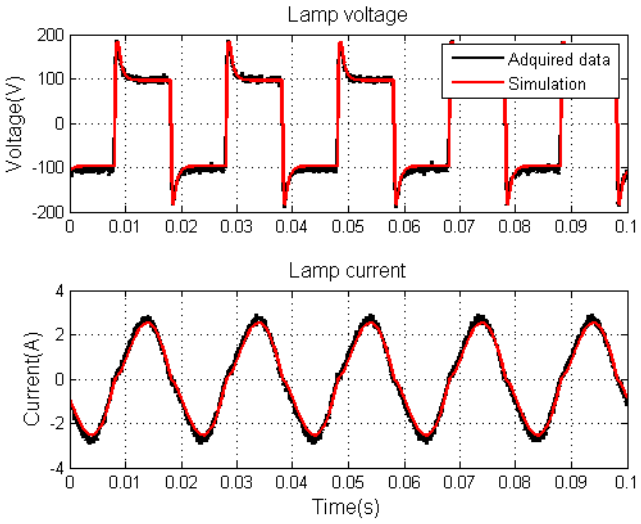

Fig. 3.5. Comparison between real data (black) and the proposed model (red)

In addition, Fig. 3.6 shows the total current demanded by the complete system formed by the lamp + LF ballast, compared with the simulated data. This current waveform is neither sinusoidal, thus yielding to large harmonic content along the power line. The THD of this current was calculated and the result was a 21.34% for the LF 50 Hz model.

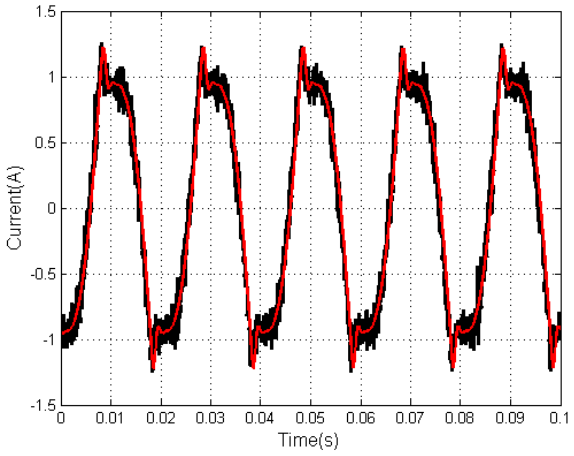

Fig. 3.6. Real (black) and simulated (red) current demanded by one ballast

3.4 Proposed control strategy

The harmonic content in distribution lines like the case under study depicted in Fig. 3.1 yields to more power losses, EMI concerns, and higher operating temperatures, which can increase the rate of failures in the system. A method aiming at mitigating these issues is, thus, proposed to enhance the system performance. The proposed method only monitors the voltage waveform at the Point of Common Coupling (PCC). Therefore, the implementation of such scheme only requires measuring the voltage at the PCC, which is also required for grid synchronization; as a consequence, it does not need a dedicated sensor for measuring the line current. The harmonic distortion of the PCC voltage is calculated, and a current proportional to this distortion is injected for generating the overall current reference of the system. The avoidance of the line current sensor will decrease in a noticeable way the cabling cost and will increase the reliability of the whole system.

In [58], a similar approach is shown. In that case, also a current sensorless method is proposed for power balancing. A STATCOM is the device used to achieve the objective in such reference, and the conclusion reached in that paper is similar to the one that will be obtained in this one. One key difference is the application of both studies. In [58], changes of 4 kVAr are applied to the load, which implies a big STATCOM in order to correct this kind of deviations. In this work, the inductive behaviour of the loads is well known and defined. Also, the cost of implement of the proposed control system in an electronic ballast is much cheaper, because the needed electronics are already present in the system, as well as the voltage sensor.

Thus, to define the operation of the converter, the reference for the instant input current on the converter must be calculated. The procedure for obtaining this reference waveform is shown ahead:

Firstly, based on Fig. 3.7, it can be stated that:

$$i_{LINE} = \frac{V_G - V_{PCC}}{s \cdot L_G + R_G} \qquad (3.1)$$

$$V_{PCC} = i_{LOAD} \cdot Z_{LOAD} \quad (3.2)$$

$$i_{LOAD} + i_{CONV} = i_{LINE} \quad (3.3)$$

where Z_{LOAD} is the impedance from the PCC to the lamps, which is not linear.

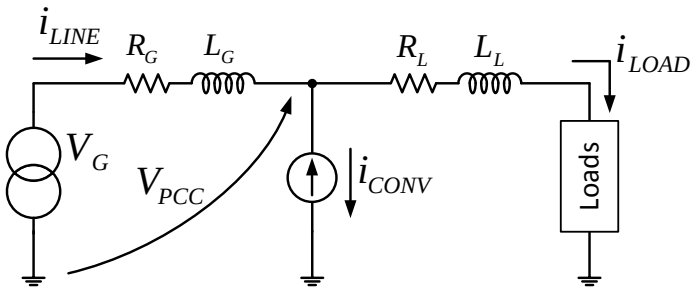

Fig. 3.7. Proposed electrical model

This mathematical proposal will separate the currents and voltages in two different components: the fundamental harmonic at 50 Hz of each variable (x_{y1}) and the rest of the harmonics, called (x_{yHF}), where '*x*' can be current or voltage and '*y*' the measurement point: load, PCC or the own converter.

Thus, if this rule is applied to the previous equations:

$$i_{LOAD} = i_{LOAD_1} + i_{LOAD_{HF}} \quad (3.4)$$

$$i_{CONV} = i_{CONV_1} + i_{CONV_{HF}} \quad (3.5)$$

$$V_{PCC} = V_{PCC_1} + V_{PCC_{HF}} \quad (3.6)$$

In order to extract the first harmonic, a resonant filter tuned at 50 Hz was used. This filter is critical since it may induce errors if sudden changes in the grid frequency would happen.

In order to calculate the current reference (i_{CONV}) and to achieve a sinusoidal line current ($\mathrm{i_{LINE}}$), (3.3), (3.4) and (3.5) can be combined:

$$\left(i_{LOAD_1} + i_{LOAD_{HF}}\right) + \left(i_{CONV_1} + i_{CONV_{HF}}\right) = \left(i_{LINE_1} + i_{LINE_{HF}}\right) \quad (3.7)$$

3.4.1 Calculation of the high frequency (above 50 Hz) current reference

In order to enhance the operation of the full system, by definition $i_{LINE\ HF}$ must be zero in (3.7). Thus, it can be stated:

$$i_{LINE_{HF}} = 0 \quad (3.8)$$

$$i_{LOAD_{HF}} = -i_{CONV_{HF}} \quad (3.9)$$

Hence, from (3.7), (3.8) and (3.9) it can be written:

$$i_{LOAD_1} + i_{CONV_1} = i_{LINE_1} \quad (3.10)$$

On the other hand, the voltage at the PCC can also be expanded by substituting (3.6) in (3.2).

$$V_{PCC_1} + V_{PCC_{HF}} = i_{LOAD} \cdot Z_{LOAD} \quad (3.11)$$

And including (3.4) in (3.11):

$$V_{PCC_1} + V_{PCC_{HF}} = i_{LOAD_1} \cdot Z_{LOAD} + i_{LOAD_{HF}} \cdot Z_{LOAD} \quad (3.12)$$

High frequency and first harmonic terms in (3.12) can be split as:

$$\begin{cases} V_{PCC_1} = i_{LOAD_1} \cdot Z_{LOAD} — \\ V_{PCC_{HF}} = i_{LOAD_{HF}} \cdot Z_{LOAD} — \end{cases} \quad (3.13)$$

where, as mentioned before, Z_{LOAD} is the impedance from the PCC to the lamps and it changes for each harmonic frequency.

Merging (3.9) and (3.13), the high frequency component of the voltage at the PCC can be written as:

$$V_{PCC_{HF}} = -i_{CONV_{HF}} \cdot Z_{LOAD} \quad (3.14)$$

And substituting (3.14) in (3.6):

$$V_{PCC} - V_{PCC_1} = V_{PCC_{HF}} = -i_{CONV_{HF}} \cdot Z_{LOAD} \Rightarrow i_{CONV_{HF}} = \frac{-1}{Z_{LOAD}}\left(V_{PCC} - V_{PCC_1}\right) \quad (3.15)$$

where $V_{PCC} - V_{PCC\,1}$ is the difference between the voltage at the PCC and the first harmonic of the same voltage and it will be considered the voltage error, $\varepsilon_{V_{PCC}}$ and $i_{CONV_{HF}}$ will be the high frequency content of the current through the converter. Up to here it has been defined the high frequency term of the current reference that would finally be:

$$i_{CONV_{HF}} = k_1 \cdot \varepsilon_{\mathrm{V_{PCC}}} \quad (3.16)$$

being k_1 the admittance of the load. However, as it was mentioned before, it depends on many factors and change with every harmonic, so it is not easy to determine its exact value.

3.4.2 Calculation of the 50 Hz current reference

According to (3.5), there are two components in the current reference of the converter and since the high frequency one was calculated in (3.16), the fundamental component will be studied ahead.

Two variables must be known in order to proceed. Firstly, the demanded power of the lighting system. On the other hand, in order to synchronise with the grid voltage, a grid synchronisation technique is needed. There are many ways to do it: a simple phase-locked loop (PLL) can be used, but in order to improve the accuracy in this work, a second-order generalised integrator (SOGI) combined with a PLL was employed [59].

Thus, the procedure to calculate the current reference will be the one of Fig. 3.8. Once the input power value is known and the PCC voltage is measured, the value of the input current for a unity power factor system can be easily calculated:

$$P_{LOADS} = V_{PCC_{1\_peak}} \cdot i_{CONV_1} \cdot \cos(\theta) \Rightarrow i_{CONV_1} = \frac{P_{LOADS}}{V_{PCC_{1\_peak}}} \quad (3.17)$$

where P_{LOADS} is the power demanded by the lighting system and the voltage at the PCC is not in *rms* values but in peak ones; on the other hand, i_{CONV_1} is the 50 Hz reference of the converter.

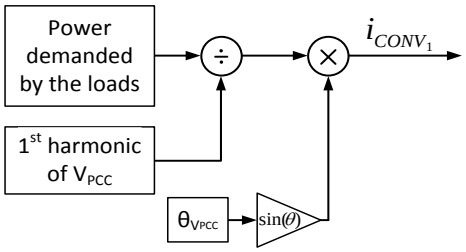

Fig. 3.8. Calculus procedure of the 50 Hz current reference

3.4.3 Final current reference expression

Hence, the final expression of the current reference of the converter will combine (3.16) and (3.17):

$$i_{CONV_{ref}} = i_{CONV_1} + i_{CONV_{HF}} = i_{CONV_1} + k_1 \cdot \varepsilon_{\mathrm{V_{PCC}}} \qquad (3.18)$$

3.5 Simulation results of the proposed strategy and the modelled lighting system

Equation (3.18) assumes a simplification that transforms the non-linear admittance into a gain. The reason is due to the difficulty of knowing its real value because this variable varies within a big range due to the effect of the different harmonics. Thus, Z_{LOAD} is changed to k_1 and then the current reference for the converter will change as k_1 does.

Consequently, (3.18) operates as a proportional regulator, which means that the more gain, the lower the error, that implies a reduction in the THD of the line current. Theoretically, (3.19) is true when a proportional regulator is involved.

$$\lim_{k_1 \to \infty} \varepsilon_{\mathrm{V_{PCC}}} = 0 \qquad (3.19)$$

However, some limitations must be mentioned:

The proposed current source converter is an electronic ballast, and therefore the overall cost will not be very high. The measurement needed is the voltage at the PCC, that will be provided in most cases by a cheap, low performance sensor, so the error between the first harmonic and the whole signal might not be zero. Therefore, even though some enhancement is obtained in the system performance, the control will not be able to completely compensate the THD, according to (3.18). Moreover, the converter cannot support the grid with infinite power in order to reduce the THD, thus k_1 is limited. The controller must provide reasonable current references to the converter.

Despite of these drawbacks, several simulations were performed in order to test the idea. Notice that the case of study is the one depicted in Fig. 3.1, where 5 groups of 50 lamps were connected to the distribution line. Each simulation was done with a different value of k_1 and all the results are gathered in TABLE 3.II. The THD value of the current through the distribution line, the values of the

harmonics of this current, the error of the voltage between the voltage at the PCC and its first harmonic are summarised in TABLE 3.II. On the other hand, TABLE 3.III shows the harmonic content of the current through the distribution line in % normalised to the first harmonic.

TABLE 3.II

THD AND HARMONICS OF THE CURRENT THROUGH THE LINE DEPENDING ON K_1, ERROR OF THE VOLTAGE AT THE PCC AND CURRENT THROUGH THE CONVERTER

k_1	*THD current*	*1st harm. (A)*	*3rd harm. (A)*	*5th harm. (A)*	*7th harm. (A)*	*9th harm. (A)*	$\varepsilon_{V_{PCC}}$ *(V)*	*Iconv (rms) (A)*
Converter off	*0.2133*	*273.1*	*47.9*	*26.01*	*18.77*	*2.92*	*2.50*	*0*
0	*0.4053*	*144.59*	*48.17*	*26.17*	*18.84*	*2.52*	*0*	*0*
20	*0.2734*	*136.01*	*33.28*	*14.21*	*7.40*	*2.54*	*95.70*	*20*
40	*0.1924*	*138.85*	*24.45*	*9.30*	*4.56*	*2.45*	*101.20*	*40*
60	*0.1351*	*152.97*	*19.10*	*6.86*	*3.29*	*2.38*	*113.73*	*60*
80	*0.0956*	*175.48*	*15.57*	*5.40*	*2.57*	*2.32*	*151.99*	*80*
100	*0.0691*	*203.52*	*13.10*	*4.45*	*2.10*	*2.29*	*175.13*	*100*
120	*0.0517*	*235.56*	*11.36*	*3.80*	*1.79*	*2.26*	*199.88*	*120*
140	*0.0396*	*270.38*	*9.99*	*3.31*	*1.55*	*2.24*	*225.46*	*140*
160	*0.0311*	*307.11*	*8.92*	*2.92*	*1.37*	*2.22*	*251.78*	*160*
180	*0.0249*	*344.45*	*8.04*	*2.62*	*1.23*	*2.20*	*278.71*	*180*
200	*0.0205*	*382.72*	*7.36*	*2.38*	*1.11*	*2.19*	*305.91*	*200*

TABLE 3.III

THD AND HARMONICS OF THE CURRENT THROUGH THE LINE DEPENDING ON K_1 (IN % NORMALISED TO THE FIRST HARMONIC)

k_1	*THD current*	*1st harm. (A)*	*3rd harm. (%)*	*5th harm. (%)*	*7th harm. (%)*	*9th harm. (%)*
Converter off	*0.2133*	*273.1*	*17.54*	*9.52*	*6.87*	*1.06*
0	*0.4053*	*144.59*	*33.31*	*18.09*	*13.02*	*5.49*
20	*0.2734*	*136.01*	*24.47*	*10.44*	*5.44*	*2.72*
40	*0.1924*	*138.85*	*17.60*	*6.69*	*3.28*	*1.73*
60	*0.1351*	*152.97*	*12.48*	*4.48*	*2.15*	*1.17*
80	*0.0956*	*175.48*	*8.87*	*3.07*	*1.46*	*0.80*
100	*0.0691*	*203.52*	*6.43*	*2.18*	*1.03*	*0.57*
120	*0.0517*	*235.56*	*4.82*	*1.61*	*0.75*	*0.42*
140	*0.0396*	*270.38*	*3.69*	*1.22*	*0.57*	*0.32*
160	*0.0311*	*307.11*	*2.90*	*0.95*	*0.44*	*0.25*
180	*0.0249*	*344.45*	*2.33*	*0.76*	*0.35*	*0.20*
200	*0.0205*	*382.72*	*1.92*	*0.62*	*0.29*	*0.16*

The graphical representation of TABLE 3.II is depicted in Fig. 3.9.

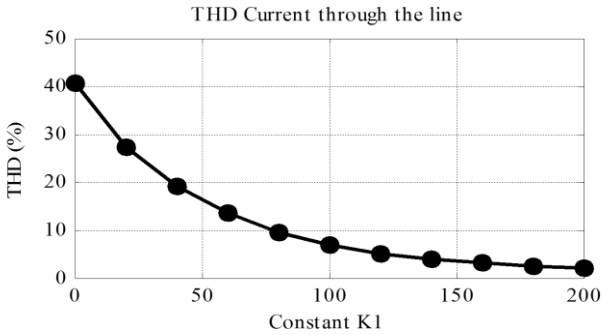

Fig. 3.9. Simulated THD of the current through the distribution line in function of constant k_1

The first conclusion about the reduction of the THD in Fig. 3.9 is simple. The more current the converter injects to correct the harmonic content, the less THD and thus, the less importance of the most harmful harmonics: 3rd and 5th. In Fig. 3.10 the evolution of the harmonics depending on the gain k_1 and hence, on the current injected by the converter is shown. It can be seen how the 1st harmonic increases while the odd harmonics are reduced. Fig. 3.11 depicts them normalised to the 1st one.

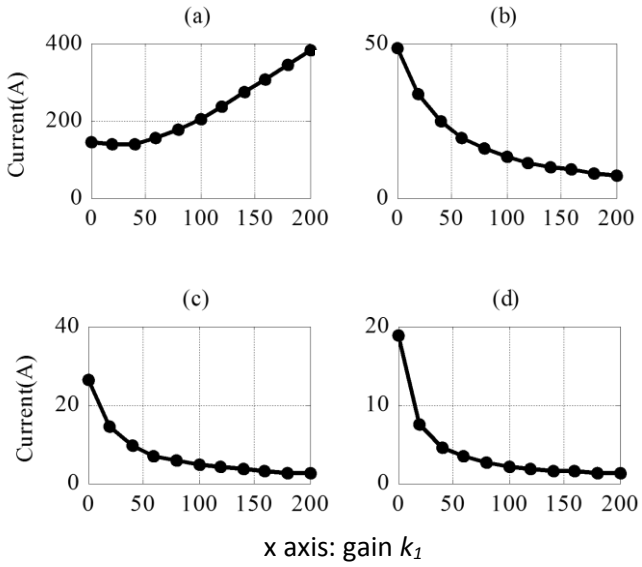

Fig. 3.10. Simulated harmonic content of the current through the distribution line for different values of k_1: (a) 1st harmonic. (b) 3rdharmonic. (c) 5th harmonic. (d) 7th harmonic

On the other hand, Fig. 3.12 shows the evolution of the *rms* current injected by the converter into the grid in order to correct the harmonic content, depending on the gain k_1. As mentioned before, the injected current rises continuously as gain increases. Consequently, the error would decrease down to zero for high currents. However, this situation would not represent a real case because the needed current would be need enormous.

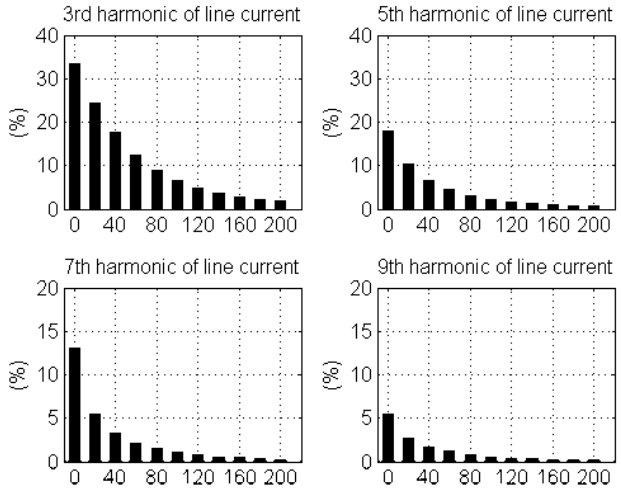

Fig. 3.11. Harmonic content of the current through the distribution line normalised to the first one

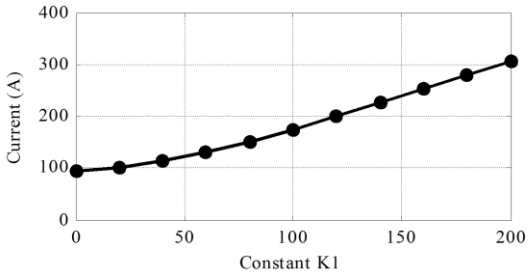

Fig. 3.12. Simulated rms current given by the converter

3.6 Selection of an optimal value for k_1 and analysis of the results

Thus, from the analysis carried out, an optimal value for the gain k_1 can be chosen. As mentioned before, according to the definition of a proportional controller, the best value for this gain would be infinite, or at least the highest feasible. However, a very large value of k_1 implies the injection of huge currents into the grid that would not represent a realistic situation, preventing the use of such an unclear condition.

By looking at TABLE 3.II and TABLE 3.III it can be appreciated that if a value of 40 is chosen for k_1, the harmonic content of the current is slightly below of the maximum values admitted by the IEC 61000-3-2:2005 regulation [36]. However, this margin is quite narrow, so it is better to choose a bigger value and thus, reduce even more the THD of the input current.

When the converter is off, the 3rd harmonic has a relative value of 17.54%. Hence, turning on the converter must mean an improvement in this value and also in the higher harmonics. A low THD of a 7% could be achieved with a k_1 equal to 100. Fig. 3.13 shows the difference between having the converter operating with this gain (right) and having no converter connected to the grid (left).

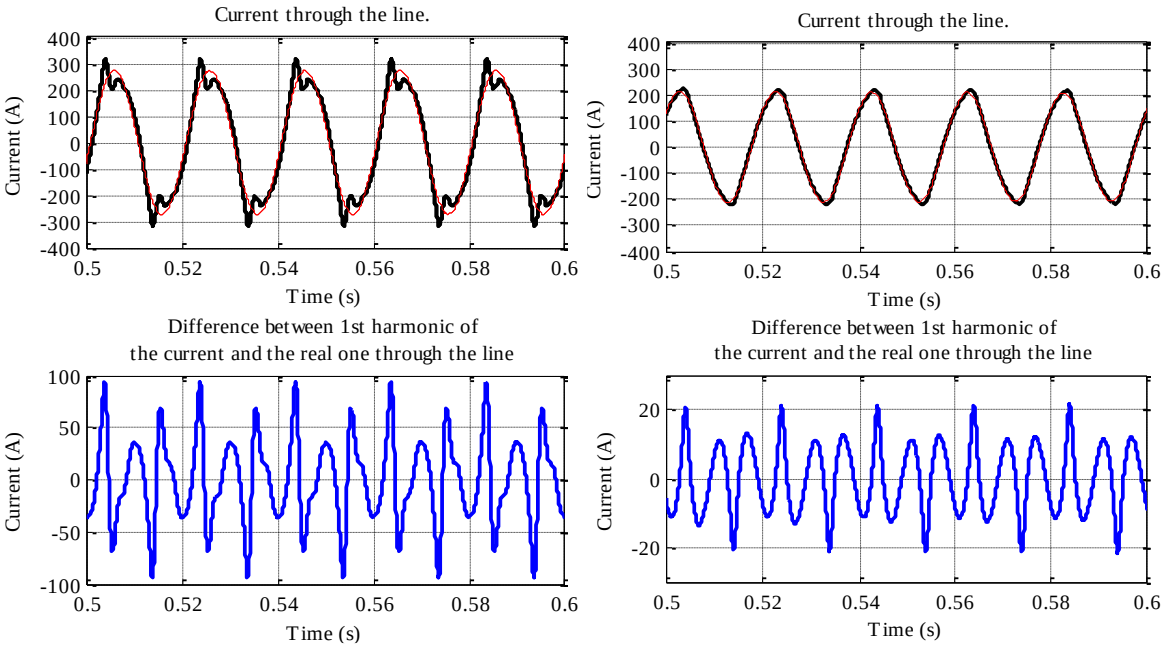

Fig. 3.13. Current through the distribution line (black), 1st harmonic of the current (red) and difference between both signals (blue). Left: converter off. Right: converter on when k_1=100

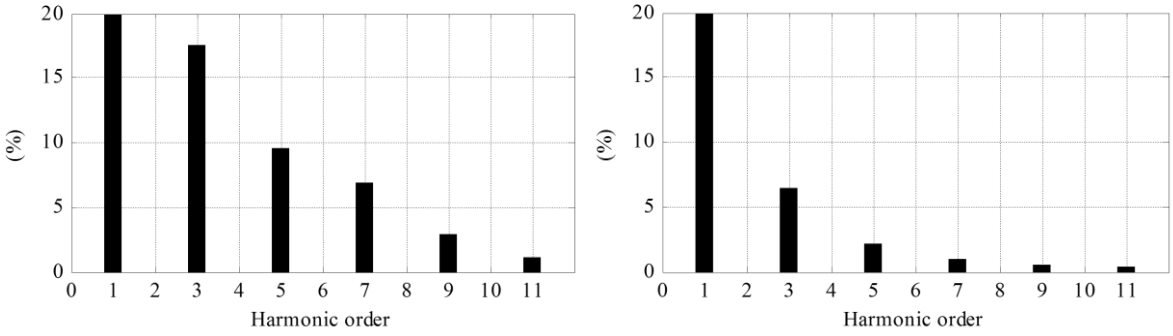

Fig. 3.14. Harmonic content of the current through the distribution line normalised to the 1st harmonic. Left: converter off. Right: converter on when k_1=100

Fig. 3.15 shows the current demanded by the loads as well as the current that the converter is injecting into the mains in order to correct the harmonic content generated by the loads. It is noticeable how the converter tries to compensate the peaks of the load current and do it the most sinusoidal it can.

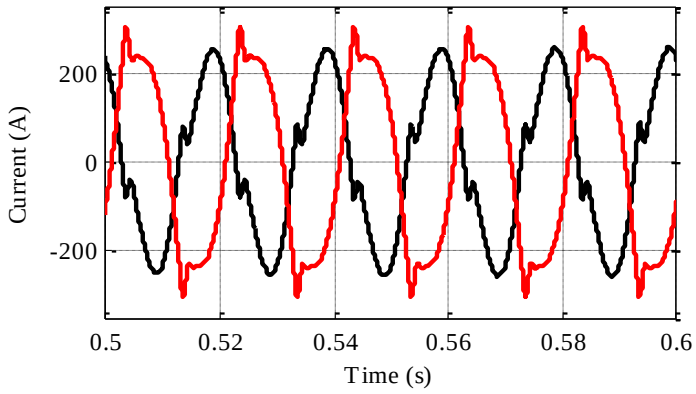

Fig. 3.15. Converter current (black) and demanded current by the loads (red)

3.7 Summary and conclusions

In this chapter a methodology to improve the THD of a given distribution line configuration with multiple linear and non-linear loads has been illustrated. The proposed method compensates the THD by measuring only the voltage at the PCC, thus avoiding the use of the line current measurement. The effect on the distortion of the distribution line current due the presence of such loads, represented by a set of HPS lamps + their associated LF ballasts, has been shown in detail. Particularly, the most harmful 3rd, 5th and 7th harmonics of the line current, as well as the total current THD, have been analysed and quantified. The proposed configuration has reduced significantly those harmonics and the final THD. In addition, the cost of implementing the proposed control system in an electronic ballast is low, provided that the needed electronics are already present in the system, including the voltage sensor.

As a future development of this topic, a deeper analysis can be carried out, in order to elucidate the real effect of the gain k_1 and an exhaustive analysis of the dynamics of the whole system. As it was

mentioned before, the larger the value of this gain, the better the THD of the line current, but physically is impossible to achieve an infinite value, so a compromise within the simulation values and the feasible ones is needed.

Chapter 4

Evaluation of control strategies to compensate the harmonic content generated by non-linear loads in microgrids and minigrids

This chapter proposes a study of two different control strategies based in active filters in order to reduce the harmonic content of a particular microgrid. The scheme of the grid is the one under study in the previous chapter, consisting in several non-linear loads, such as the LF electromagnetic ballasts and the HPS lamps considered. The main aim is to compare the behaviour of these alternative techniques in comparison with the simple, low cost solution shown in the previous chapter.

Harmonic correction in single-phase microgrids require different mathematical approaches when compared with three-phase system due to the fact that the transformations from stationary to synchronous reference frames and vice versa are the same. In this chapter, both synchronous and stationary reference frames shall be studied comparing their performances about selective harmonic compensation and also the computational cost they require.

4.1 Introduction

Microgrids are emerging as an appealing way for boosting the future smart distribution grids, due to its capability to operate in both island and grid-connected modes, their good efficiency and reliability and also their robustness to failures if they are well controlled. The integration of distributed generation (DG) units into the grid has been a trend since photovoltaic (PV) panels and wind turbines (WT) appeared in the market [60], [61]. The power converters that interface these DGs with the mains facility are generally controlled in current mode, in order to enhance the global performance of the microgrid. In most cases, the DGs are intended to maximise the active power injection into the grid by means of maximum power point tracker (MPPT) algorithms [62], [63].

A microgrid can be operated either in island mode or grid connected with a similar configuration [64], [65]. The main difference remains in the power balance in islanded microgrids, where energy generation and power consumption must be in equilibrium, therefore implying a tightly coordinated operation. Fig. 4.1 depicts a typical distribution network with a microgrid connected through a single PCC. This microgrid consists of generic devices such as loads, DGs -being either renewable energy sources (RES) or conventional sources- as well as Energy Storage Systems (ESS). Since the sources are connected directly to the voltage line, the power converters used for the interfacing must operate as current mode-voltage source inverters (CM-VSI), in order to support the distribution network [66], [67].

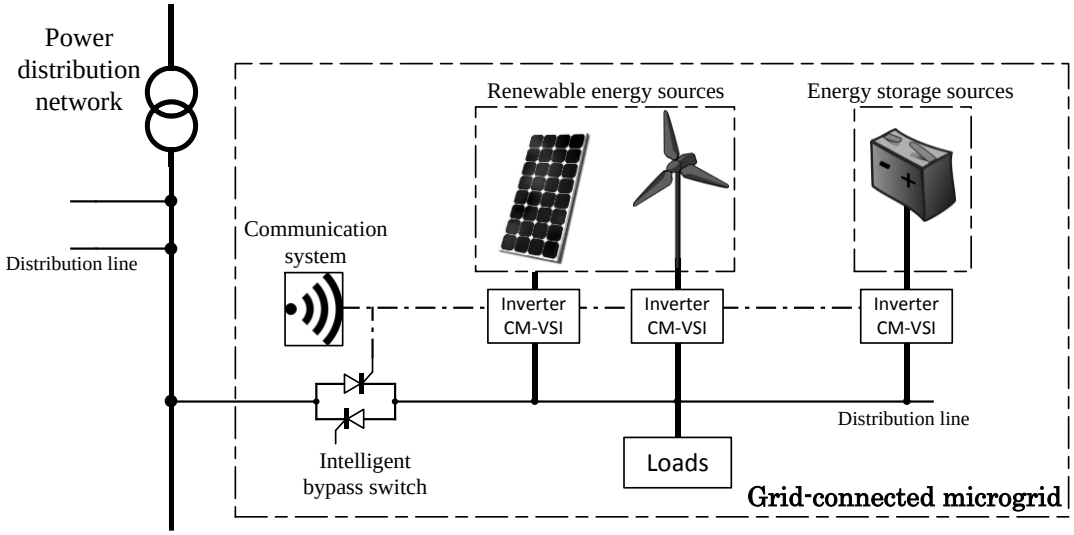

Fig. 4.1. Typical grid-connected microgrid with communications

On the other hand, when the microgrid is islanded (PCC disconnected), it requires a guarantee of reliability, security and power stability. Considering the stochastic intermittent nature of RES, this function must be done mainly by the ESS and its interfacing converters. A common operation strategy is to use the ESS as a backup compensator while RES inject the maximum power they can to the loads. If there is extra power in the islanded microgrid, the batteries of the ESS would charge, however, if they are completely charged, RES should reduce the power injection, moving away from the maximum power point (MPP) [65], [66], [67]. However, a practical islanded system may suffer from the lack of power generation or energy storage. These possible situations require to work in a flexible way combining MPPT algorithms for RES with the state of charge (SoC) of the ESS. A proper coordination between RES and ESS is key for avoiding unstable performance in the microgrid. However, islanded operations are not allowed yet in some countries due to security reasons [68].

Fig. 4.2 shows a typical islanded microgrid. The main difference with the one depicted in Fig. 4.1 is, besides the grid disconnection, the configuration of the power inverters. In this case, the inverter connected to the ESS operates as a grid forming voltage source inverter (VSI) while the RES units keep connected to the distribution line through CM-VSI.

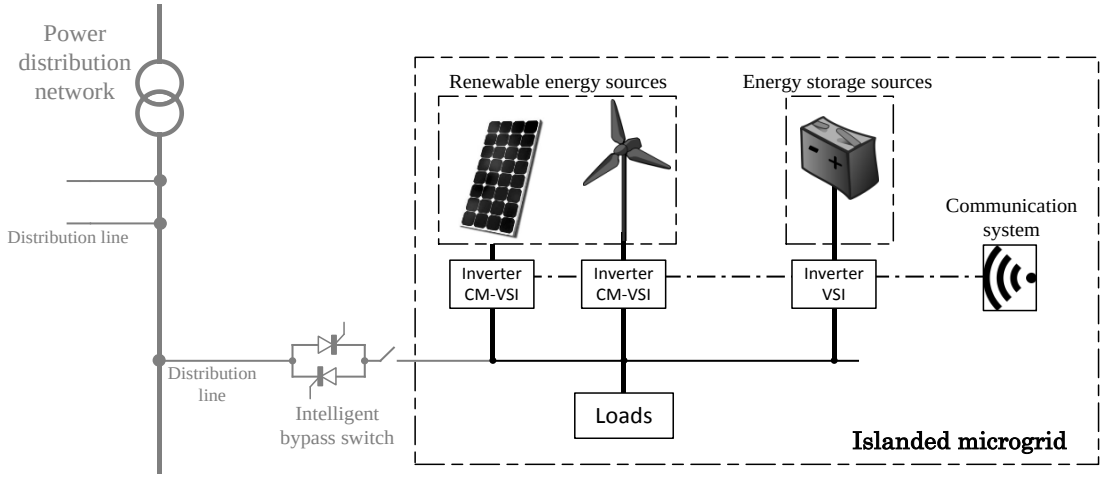

Fig. 4.2. Typical islanded microgrid with communications

In the case of islanded operation, the DGs are therefore connected to a microgrid that is usually much weaker than the traditional distribution grids. Consequently, the harmonic distortion tends to be more harmful [69]. There are many ongoing researches in the field of harmonic compensation for these systems. Active and passive power filters, or the combination of both -hybrid power filters-, are used for decreasing the harmonic distortion in the grid. Depending on the configuration, rather on series or shunt connection schemes, both the voltage ratings of the components and the characteristic impedances of the filtering units shall change [61]. Many control algorithms have been proposed for automatic and selective harmonic compensation [42], [60], [61]. In many cases, single-phase harmonics compensation techniques operate more effectively than three-phase methods due to unbalances in the phases [61].

4.2 Case of study

In this chapter, two different techniques for selective harmonic compensation in microgrids will be tested: a synchronous and a stationary reference frame control strategies. For these analyses, line current measurements will be needed, and therefore additional current sensors are required. This issue must be considered when presenting the conclusions to the comparison carried out, as it yields to a cost increase with respect to the previous solution proposed in chapter 3. Both control strategies will be compared in terms of harmonics reduction, THD and computational cost.

Fig. 4.3 shows the case under study. A total of 20 LF electromagnetic ballasts and their respective HPS lamps (for a rated power of 150 W) form the set of non-linear loads in a grid-connected microgrid. The harmonic compensation will be carried out by a front inverter interfacing the distribution line through a LCL filter with a dedicated ESS, in this case, a battery. Connected to the microgrid could appear other DGs and loads but, in order to simplify the case of study, just one converter and the lamps are attached.

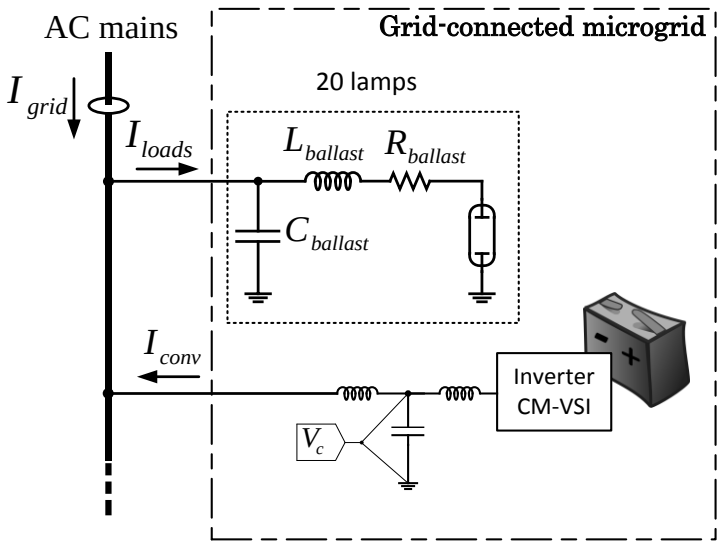

Fig. 4.3. Case of study

4.3 *dq* and αβ reference frames in single-phase converters

Most of the employed converters for interfacing power loads to grid, such as Active power filters, power factor correctors or uninterrupted power supplies (UPS), commonly make use of current control algorithms. However, provided that the electric variables are not constant but time variant in AC systems, the controllers cannot be tuned as simply as in the case of DC-DC. In the case of using the same techniques for tuning the DC controllers on AC ones, significant steady-state errors will occur [70], [71], [72], [73].

In three-phase systems, AC voltages and currents can be treated as DC magnitudes by means of mathematical functions, such as the transformation from *abc* stationary reference frame to *dq* synchronous reference frame. Nevertheless, performing this transformation in a single-phase system is not so straightforward. A second variable in quadrature with the variable to be transformed is needed. There are many ways to create this variable: by using the capacitor current feedback [71], by delaying the real one by ¼ of the line period, by means of notch filters tuned at twice the line frequency, etc. [70], [72], [73].

Fig. 4.4 shows the stationary αβ and synchronous *dq* reference frames. The *dq* axes rotate at ω*t*, being ω the line frequency and θ the angle between the α axis and the *d* axis. The transformation from αβ to *dq* can be found in (4.1) while the inverse transformation is written in (4.2):

$$\begin{bmatrix} d \\ q \end{bmatrix} = \begin{bmatrix} \cos(\theta) & \sin(\theta) \\ -\sin(\theta) & \cos(\theta) \end{bmatrix} \cdot \begin{bmatrix} \alpha \\ \beta \end{bmatrix} \quad (4.1)$$

$$\begin{bmatrix} \alpha \\ \beta \end{bmatrix} = \begin{bmatrix} \cos(\theta) & -\sin(\theta) \\ \sin(\theta) & \cos(\theta) \end{bmatrix} \cdot \begin{bmatrix} d \\ q \end{bmatrix} \quad (4.2)$$

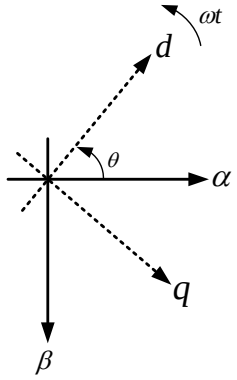

Fig. 4.4. Reference frames

Thus, a general *dq* current control block diagram can be found in Fig. 4.5. First, the variables (and the references) are transformed to a *dq* reference frame and hence, the PI controllers tuned for DC variables guarantee zero steady-state error. The gain ω*L* provides the decoupling terms for improving the transient response, but is not strictly necessary.

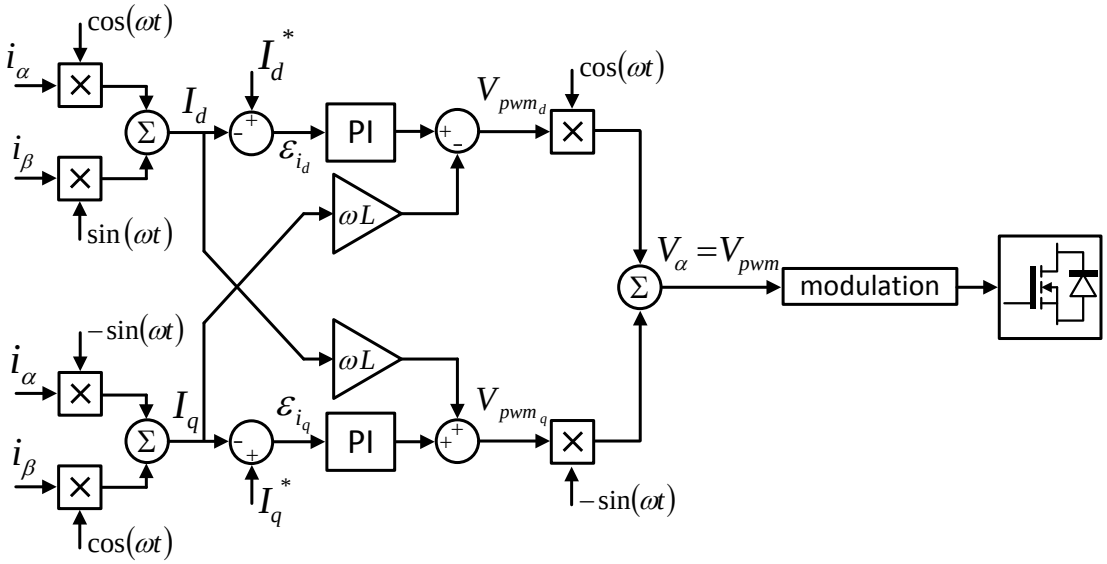

Fig. 4.5. Single-phase typical dq current control block diagram

However, if the purpose of the control is to be selective for the current harmonics (for instance, in order to remove these components), and given that thee harmonics take place at frequencies that are multiple of ω, then, this diagram needs to be modified.

4.4 Reduction of harmonic content using a *dq* reference frame

The control strategy thought to correct the harmonic content of a microgrid with non-linear loads is depicted in Fig. 4.6. It can be observed that there are many band-pass filters (BPF) whose mission is to extract the desired frequencies from the grid current. Considering that the most harmful components are the first odd harmonics ([74], [75], [76]), then these filters need to be tuned at 150

Hz, 250 Hz, 350 Hz and 450 Hz, corresponding to the 3rd, 5th, 7th and 9th harmonics. After the filters, the quadrature signals are created and finally the transformation from αβ to *dq* is carried out.

Since the aim of this control strategy is to reduce the harmonic content, the reference of these harmonics must be zero. Thus, PI controllers are used for cancelling the error for the high frequency current components.

Next, the inverse transformation from *dq* to αβ is done, and finally all the signals are added up and modulated in order to be sent to the inverter. Notice that this figure details the structure of the filter only for the 3rd harmonic, however the same structure is found in the rest of the harmonics. Only the harmonic order in the sine and cosine operations must be change by the correspondent harmonic order: 5, 7 or 9.

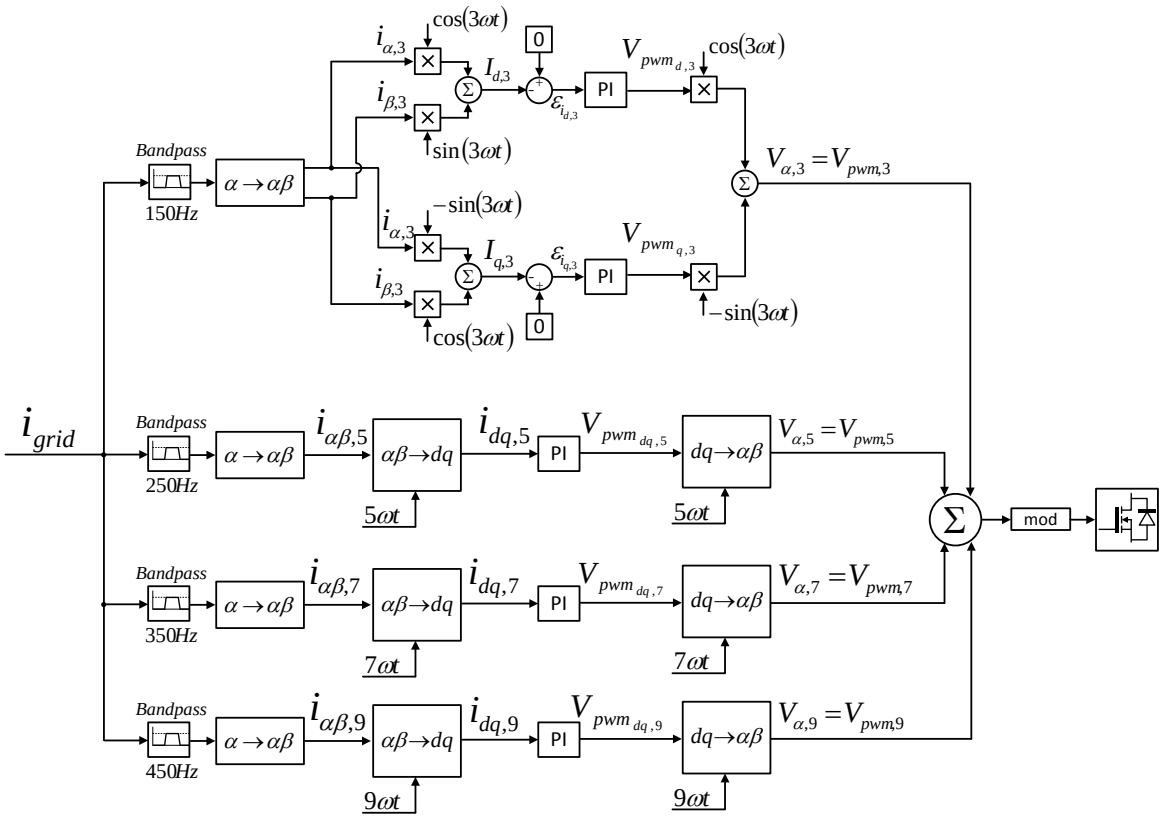

Fig. 4.6. dq control strategy carried out to reduce the effect of the harmonics

4.4.1 Alternative techniques to extract the harmonic content

Given that the design and performance of the input BPF can be a rather complex task, a comparative study between two options is carried out. The fast Fourier transformation (FFT) method has been compared with the Goertzel Algorithm. The computational cost of four FFT operating in parallel is a drawback in terms of execution time [77], [78]. The Goertzel algorithm is an effective convolutional form of the discrete Fourier transform for direct computation of the Fourier value at selected frequency position, i.e. evaluates the only selected bin of the Fourier spectrum [79]. In Fig. 4.7 the difference between using the BPF of Fig. 4.6 and the programmed FFT is shown. As it can be appreciated, the FFT filters in a better way the input current and improves the harmonic selection. Thus, the transformations to *dq* are better if using the FFT and therefore, this is the method that will

be used in the simulations. The calculations of these FFT are done with a dSPACE, hence there are no limitations in terms of computational power.

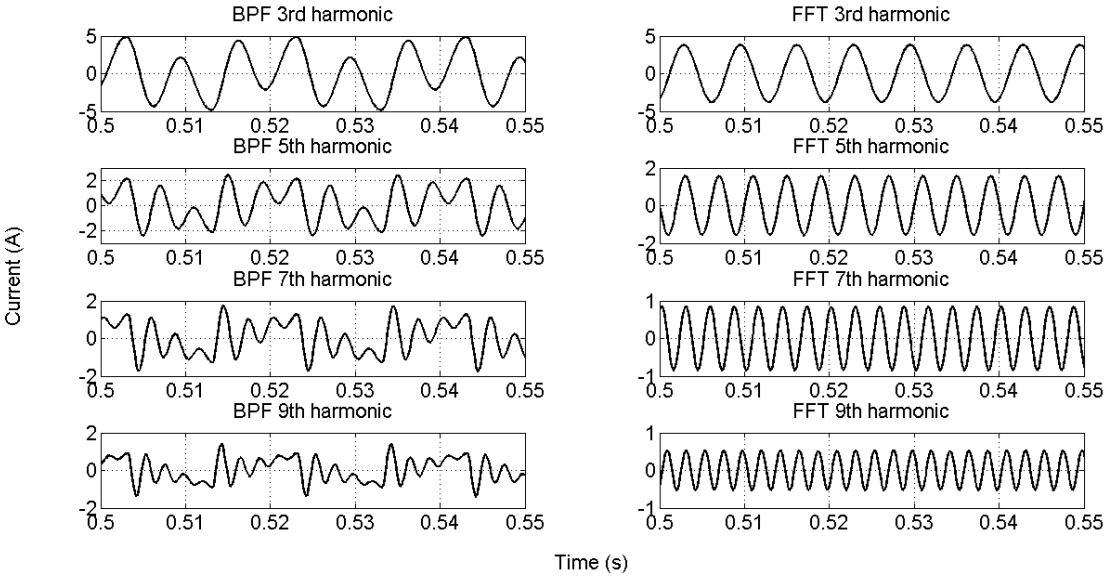

Fig. 4.7. Comparison between BPF and FFT when filtering harmonics

4.4.2 Selective harmonics correction in dq reference frame simulation results

The simulation results using a *dq* control strategy of Fig. 4.6 are shown ahead. The whole system was modelled in Simulink and then exported to a dSPACE platform. Thus, the presented results were obtained from the dSPACE software. In Fig. 4.8 the difference performance between a microgrid with and without the AF can be seen.

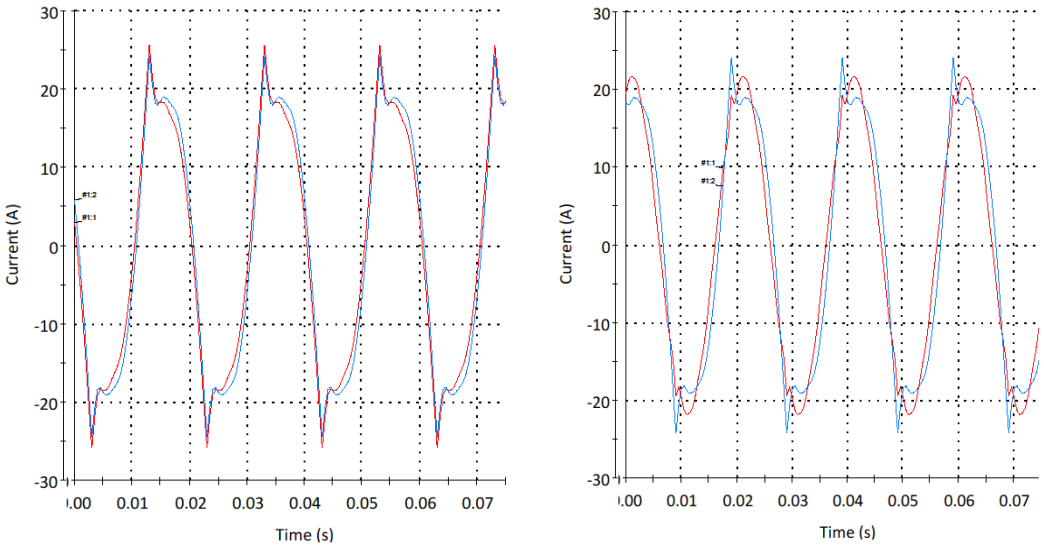

Fig. 4.8. Load current (blue) and grid current (red) when the converter is switched off (left) and when it is on (right) in a dq reference frame

The non-linear load demands a current waveform with a significant harmonic content. Fig. 4.9 depicts the THD of the line current in both cases. If the AF is not operating (before *t=0.65 s*), the THD is quite important. On the other hand, when the AF is switched on after *t=0.65* s, the converter compensates these harmonics by working as a grid supporting CM-VSI. The THD is reduced from 20% to less than 4%. In addition, Fig. 4.10 depicts the harmonic content of this current, normalised to the first harmonic whose information was obtained with the dSPACE.

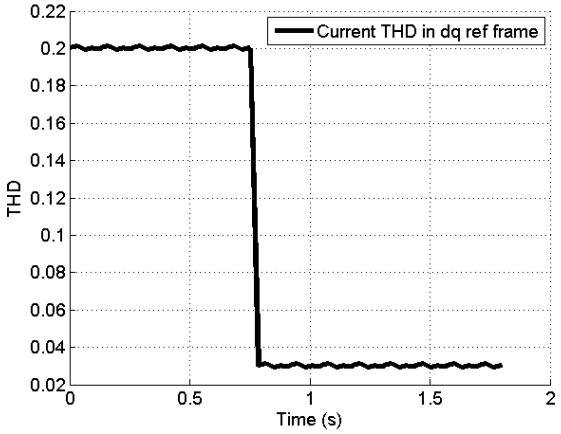

Fig. 4.9. THD of the grid current when the converter is off (left): 20% and THD when it is on (right): 3% in a dq reference frame

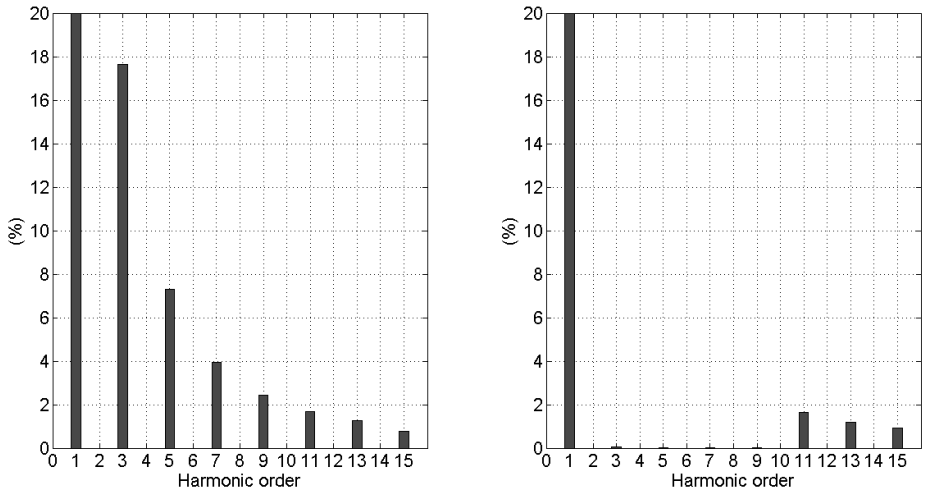

Fig. 4.10. Harmonic content when the converter is off (left) and on (right) in a dq reference frame

4.5 Reduction of harmonic content using a αβ reference frame

Due the aforementioned computational cost issues, the previous FFT based structure with several transformations from αβ to dq and vice versa is hardly found in real applications. For single-phase applications, most practical solutions make use of Proportional-Resonant (PR) regulators designed for controlling AC signals in αβ stationary reference frames [43], [44], [68].

In three-phase systems, the transformation from *abc* to αβ0 is a commonly used tool, which is mathematically performed by means of (4.3):

$$\begin{bmatrix} u_\alpha \\ u_\beta \\ u_0 \end{bmatrix} = \begin{bmatrix} \frac{2}{3} & -\frac{1}{3} & -\frac{1}{3} \\ 0 & \frac{1}{\sqrt{3}} & \frac{-1}{\sqrt{3}} \\ \frac{1}{3} & \frac{1}{3} & \frac{1}{3} \end{bmatrix} \cdot \begin{bmatrix} u_\mathrm{a} \\ u_\mathrm{b} \\ u_\mathrm{c} \end{bmatrix} \qquad (4.3)$$

Assuming that u_a, u_b, u_c quantities represent three sinusoidal balanced currents:

$$\begin{bmatrix} i_\mathrm{a} \\ i_\mathrm{b} \\ i_\mathrm{c} \end{bmatrix} = I \begin{bmatrix} \sin(\omega t) \\ \sin\left(\omega t - \frac{2\pi}{3}\right) \\ \sin\left(\omega t + \frac{2\pi}{3}\right) \end{bmatrix} \qquad (4.4)$$

These currents are flowing respectively into windings A, B, C of a three-phase winding, as Fig. 4.11 shows [80].

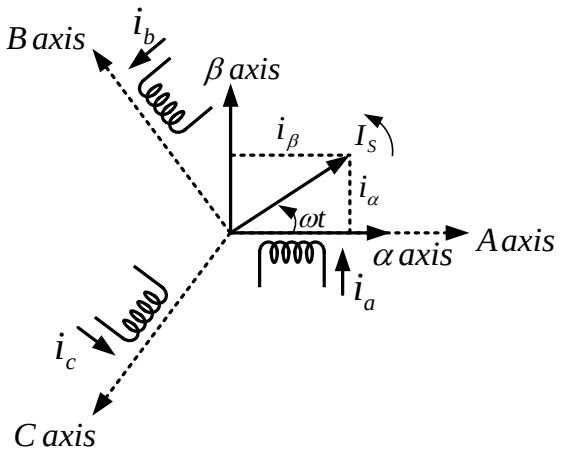

Fig. 4.11. abc and αβ *axis in a three-phase system*

In this case, the i_α and i_β components represent the coordinates of the rotating space vector I_s in a fixed reference frame whose α axis is aligned with phase A axis. I_s amplitude is proportional to the rotating magnetomotive force produced by the three currents. It is computed as follows:

$$I_S = i_\alpha + j \cdot i_\beta = \frac{2}{3}\left(i_a + i_b \cdot e^{j\frac{2\pi}{3}} + i_c \cdot e^{-j\frac{2\pi}{3}}\right) \qquad (4.5)$$

However, in single-phase systems, there is no need of such transformations. In a single-phase system, the component β of the stationary reference frame is useless because it is a virtual component used only for making synchronisation possible.

As mentioned before, in order to control AC signals, PR controllers are needed. Fig. 4.12 shows the bode diagram of several resonant controllers attacking different frequencies that match with the

harmonics order together with the block diagram of a typical resonant controller. The different depicted outputs represented in Fig. 4.12 depend on the value of the resonant frequency the controller is tuned to, which is ω_{res}. Therefore, having several block diagrams in parallel like the one shown in the left side of Fig. 4.12 but tuned for different values of ω_{res} would configure the final control technique in a stationary reference frame.

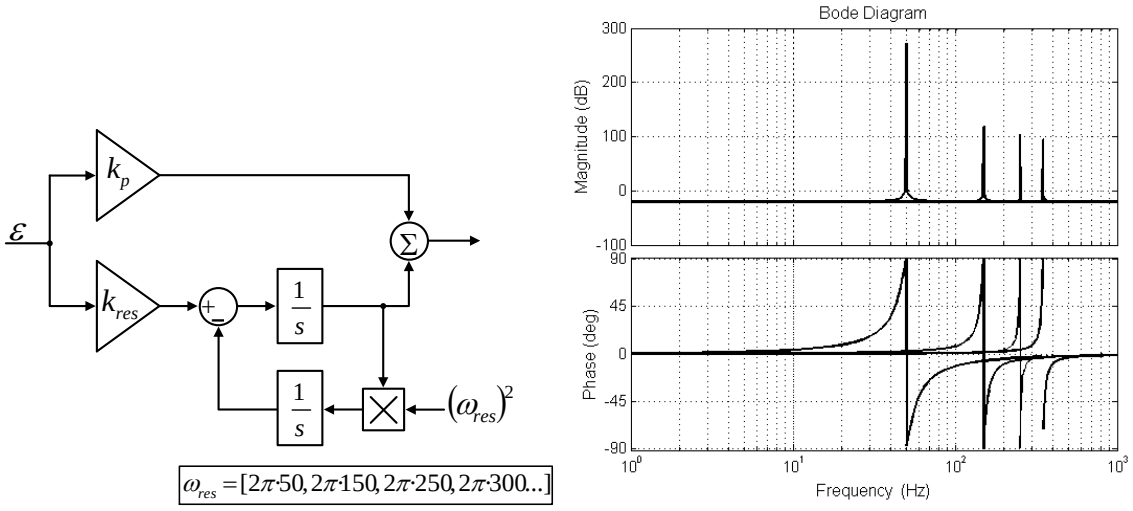

Fig. 4.12. Block diagram of a resonant controller and bode diagram attacking the 1st, 3rd, 5th and 7th harmonics if the natural frequency is 50 Hz

The control strategy changes considerably with respect to the previous synchronous control technique: first, a simple BPF is enough and no FFT is required to filter the first harmonic of the current. Then, instead of having a filter for each harmonic component, there would be a resonant controller and thus, the computational cost is reduced. As in the previous control strategy, there will be only one closed loop since the converter operates as a grid-tied CM-VSI. In Fig. 4.13 the control used in this section can be seen. The grid current is initially filtered and its first harmonic is extracted. Then, the whole harmonic content is compared with its first harmonic and the result is the error that the controllers will try to reduce.

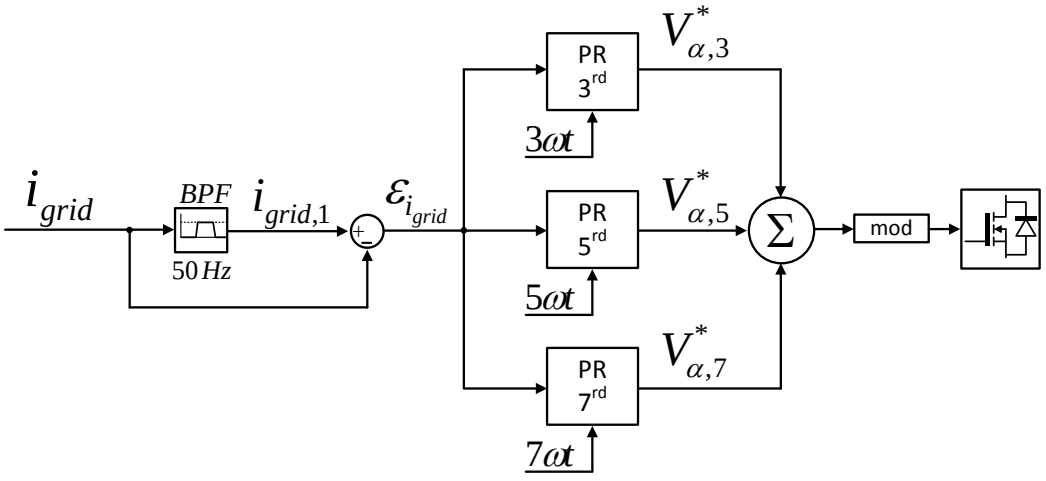

Fig. 4.13. αβ control strategy to reduce the effect of the harmonics

4.5.1 Selective harmonics correction in αβ reference frame simulation results

The simulation results using a αβ control strategy of Fig. 4.13 are shown ahead. Fig. 4.14 depicts the change in the grid current when the converter begins to support it correcting the harmonics. On the other hand, Fig. 4.15 shows the value of the THD before and after switching on the converter.

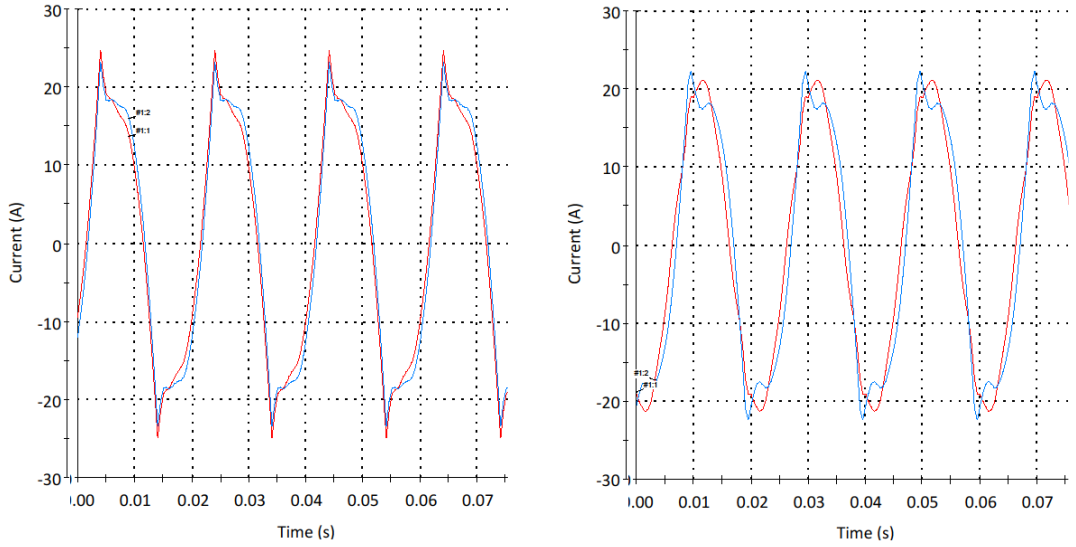

Fig. 4.14. Load current (blue) and grid current (red) when the converter is switched off (left) and when it is on (right) in a αβ reference frame

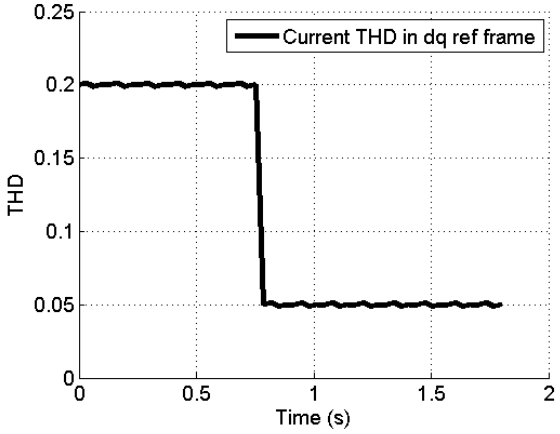

Fig. 4.15. THD of the grid current when the converter is off (left): 20% and THD when it is on (right): 5% in a αβ reference frame

With the previous simulation, the most remarkable issue that should be mentioned is the final THD value. Even though this parameter results slightly greater than in the *dq* case, the current method's computational cost is lower, and therefore depending on the application it could be a more interesting solution.

Finally, the harmonic content of this current normalised to the first harmonic is shown in Fig. 4.16. Notice that in this case, due to the whack-a-mole effect ([81]), we were only able to reduce the 3rd, 5th and 7th ones. It would need a more in deep study of the LCL filter and the tuning of the PR controllers in order to limit also the effect of the 9th harmonic.

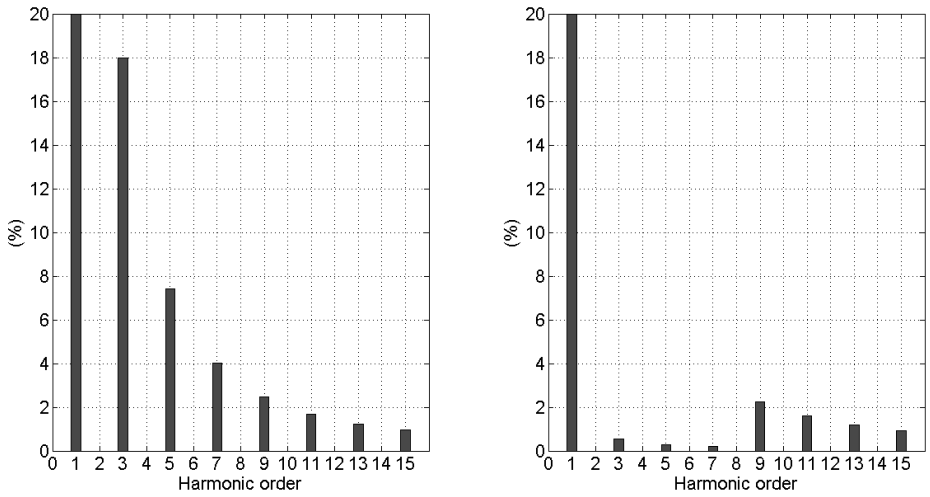

Fig. 4.16. Harmonic content when the converter is off (left) and on (right) in a αβ reference frame

Fig. 4.17 shows a comparative between both control techniques in terms of harmonics reduction.

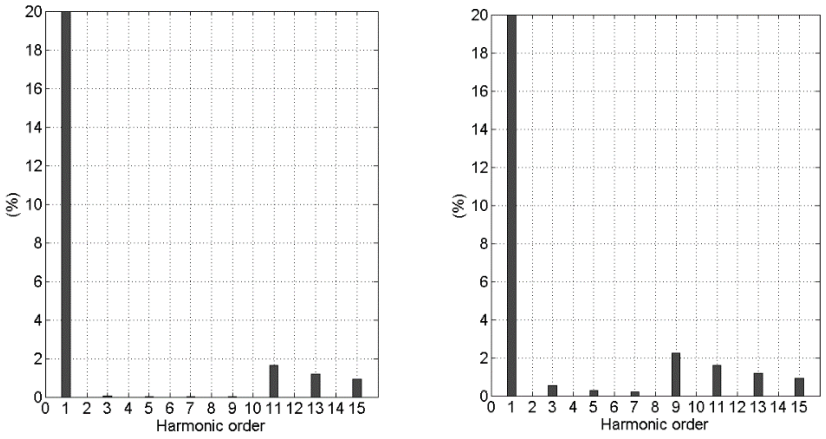

Fig. 4.17. Comparative between using synchronous (left) and stationary (right) reference frame harmonic reduction control techniques

In TABLE 4.I, the number of operations for both control strategies, synchronous and stationary, are summarised. In any case, it enables for a compromise solution between both the PR and the *dq* method.

TABLE 4.I

NUMBER OF OPERATIONS FOR BOTH PROPOSED CONTROL STRATEGIES

Type of calculation	*Computational cost*	*Number of operations in dq*	*Number of operations in αβ*
FFT	*High*	*4*	*None*
BPF	*Low*	*None*	*1*
PI controller	*Low*	*4*	*None*
PR controller	*Medium*	*None*	*4*
α→αβ	*Low*	*4*	*None*
αβ→dq	*Medium*	*4*	*None*
dq→αβ	*Medium*	*4*	*None*

The amount of calculations for the stationary control is lower and thus, it requires a less powerful microcontroller.

4.6 Summary and conclusions

In this chapter, two different control strategies to solve the harmonic content in microgrids have been studied. Both techniques have given good results when reducing the high frequency components of the grid current. These control strategies were proposed for single-phase microgrids, which is not a very common issue nowadays since most of them are actually three-phase systems. Both techniques were compared in terms of THD and harmonics reduction, control diagram complexity and computational cost.

The stationary reference frame control strategy has been proved to demand less computational cost since there is no need for FFT and other kind of mathematical transformations. On the other hand, the harmonic content is not reduced in the same amount as with the synchronous reference frame control strategy. In addition, it has been studied two kind of controllers: PI for DC signals and PR for AC signals. It was observed how the PR controllers are more sensitive to perturbations and difficult to tune, thus the system could go unstable more easily.

Therefore, in order to choose a technique for harmonics content reduction, there is no universal solution. A compromise choice has to be done, thinking in the computational power available and the desirable results.

Future developments of this research line include the study of how the EMI filters affect the resonant controllers and then allow the apparition of the whack-a-mole effect.

Chapter 5

A survey on the issues for integrating distributed renewable energy sources into the AC grid

In this chapter, a brief introduction to renewable energy sources compatible with a street lamppost shall be discussed. The interconnection between these sources and the AC grid will be studied in terms of the most common electrical topologies and configurations. Finally, a survey about hybrid generation systems that combine distributed generation and street lighting will be presented.

This chapter is intended to deal with certain issues that shall be applied later in chapters 6 and 7.

5.1 Introduction

Burning fossil fuels to generate a consistent supply of energy is the most common solution nowadays all over the world. Every year, the electricity demand increases, which means more and more power plants need to be built, thus increasing the pollutants dispensed into the environment. The strong energy dependence on fossil fuels, the negative effects of global warming related to greenhouse gases, as well as the growing social concern about negative effects of pollutant emissions and so on, have led some governments to promote the integration and use of renewable energy sources [82], [83]. The need to develop clean energy-producing systems that can perform as reliably as fossil fuel plants must be implemented throughout the world in order to decrease the effects man has on the planet [84], [85].

The Kyoto Protocol was signed by EU government in 1997, following the United Nations Framework Convention on Climate Change (UNFCCC) Conference. The EU committed to reduce its emissions of greenhouse gases by 8% by 2008-2012 (compared to 1990 levels). In May 2002, the protocol was ratified by all EU members and then, the EU legislation such as 2001/77/EC: Renewables Directive (now 2009/28/EC) as well as 2002/91/EC: Energy Performance of Buildings (now 2010/31/UE) was established. At this time, some EU members also agreed to reduce CO_2 emissions by 20% by 2010 and by 30% by 2020. These targets, published on the European Commission Climate Action website, indicate the relevance of this study [5].

Increasing integration of DG units and distributed storage systems (both renewable and non-renewable energy systems) is a fact [27], [67], [86], [87], [88], [89], [90], [91]. The installation of small PV generators and small WTs at user's home has become a "green" new trend in many countries, although the integration of low power RES into the grid is a key point to cope by researches around the world.

PV and wind energy is gaining more and more visibility at small-scale applications [92], [93]. Standalone systems where grid access is not available have been making use of this kind of technology for many years, but, on the other hand, when RES are connected to the mains, some concerns must be taken into account: harmonic content of the injected current, galvanic isolation or islanding detection among other issues such as reliability, cost, and lifespan [94]. If a RES unit is connected to the grid, in this case, the grid behaves as an energy storing subsystem with an ideal unlimited storage capacity. Virtually, it has no limit and the generated capacity can always be stored [27], [67]. Multifunctional systems that combine a lamp for street lighting and a RES unit for energy injection in the grid are becoming very interesting issues since they can afford money to local governments and help to prevent greenhouse effect [27], [28], [87].

As mentioned in chapter 1, a considerable amount of power is consumed in lighting. The global emissions would be potentially reduced whether more sophisticated lighting systems were employed or if the renewable energy sources were used to contribute supplying the lamps. Therefore, the less energy the lighting systems demand from the conventional power plants, the better for the environment.

Electric lighting requires, by definition, an artificial source of electrical energy. Most of the public lampposts are supplied by dedicated lines of the AC mains facility. In order to decrease the amount of budget of such consumptions, nowadays public institutions are trying to include RES units [95], [96]. Among the many suitable solutions for the lighting system, this work is focused on a hybrid bidirectional power converter, where energy would be able to flow from the grid to the lamp, but also from the RES units to the lamp and/or the grid, depending on the instant amount of available power.

There are different types of renewable energy technologies to consider, the main ones being:

- Wind energy
- Solar photovoltaic
- Hydroelectric
- Geothermal

For our case of study, only two of these sources can be installed in practice in a lamppost: a wind turbine or a PV panel.

5.2 Wind energy and small wind turbines

The conversion of air into electricity is the most chosen option of renewable energy in Europe [97], [98]. In 2014 the annual installations crossed the 50 GW mark for the first time. In 2013, the global installations were over 35.6 GW while a year later, more than 51 GW of new wind power capacity was installed. The previous record was set in 2012 with 45 GW of new capacity globally set up. In Fig. 5.1 the global annual installed wind capacity over the past 17 years can be seen.

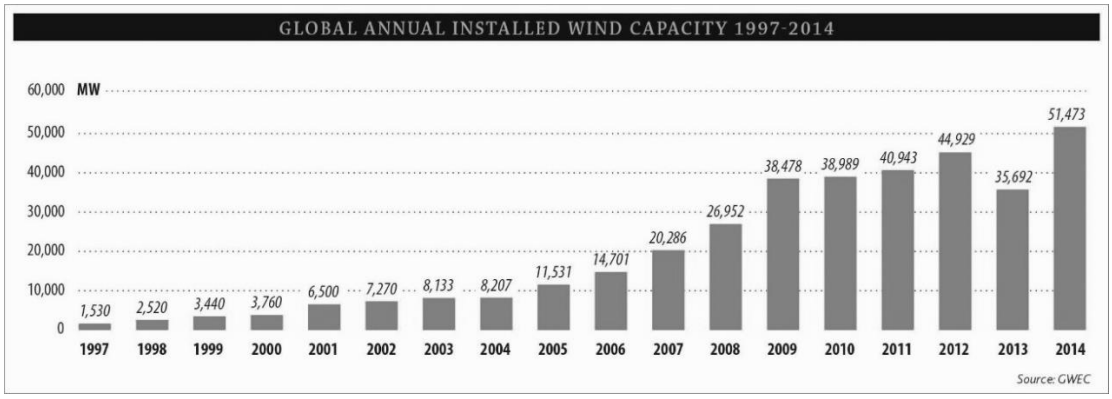

Fig. 5.1. Annual installed global capacity 1997-2014 [98]

Wind farms generate great amounts of "green" power that help to reduce the consumption of fossil fuels but with some drawbacks, like start-up cost or the visual and environmental impacts they cause in the area. Nevertheless, giant windmills, no matter if offshore or onshore, are not relevant at all in our case of study of street lighting systems and wind turbines.

The IEC Standard for small wind turbine safety, IEC 61400-2, defines a small wind turbine as having a rotor swept area of less than 200 m^2, which corresponds to a rated power of about 50 kW. In this thesis, the rated power is much lower: below 300 W [99], [100]. Small wind turbines have lower energy output than large commercial wind turbines, such as those found in wind farms [101]. Nevertheless, nowadays new small wind turbines start to be developed by wind companies and universities for its installation on streetlights or on roofs, for example [89].

There are many types of small wind turbines, but the most common are the Horizontal Axis Wind Turbine (HAWT) towered and Vertical Axis Wind Turbine (VAWT).

In VAWT, the axis of rotation is perpendicular to the wind stream and the ground. The modern concept of vertical axis wind turbines derived from the initial configurations Savonious (1922) and Darrieus rotor (1931) [102]. Darrieus rotors have good efficiency, but produce large torque ripple and cyclic stress on the tower, which contributes to poor reliability [103]. A Savonius is a drag type tur-

bine that is commonly used in cases of high reliability in many things such as ventilation and anemometers. Savonius are excellent in areas of turbulent wind and self-starting. The Savonius turbine of Fig. 5.2 can have three blades rather than two. This type of VAWT would be an optimal option for an installation on top of a lamppost.

The HAWT has an axis of rotation paralleling to the wind stream and the ground. Nowadays, it is the main installation type in the scaled commercial wind farms. In built environment, the HAWT are the most common type of turbine, which is now available on the market due to the good performance and more competitive installation cost [102]. However, the disadvantage of the horizontal axis turbine is that a yaw mechanism must keep the turbine rotor facing the varying direction of wind in order to make full use of the wind energy, which leads to a great restriction in application [102].

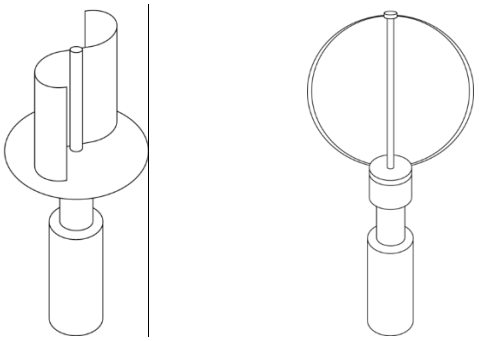

Fig. 5.2. Types of small VAWT: Savonius (left) and Darrieus (right). By Steffen Kuntoff. Creative Commons Attribution-Share Alike 2.0 Germany license

The global market for wind turbines has continued to grow in the past decade, but mainly considering the field of large utility scale wind turbines [104], [105]. Low energy harvesting and reduced cost/benefit ratio are two of the major reasons responsible for the continued low penetration of small WT and thus, this technology has not matured like its large-scale counterpart [106], [107], [108].

These analyses of costs, benefits and so on can be disappointing for small-scale standalone systems. For a streetlight, reducing the consumption during all nights may pay off the cost of the whole lamppost [104], [106], [109].

5.2.1 Small wind turbines connected to the grid

A micro-wind turbine below 300 W is usually designed for a charger system [110]. However, a grid-tied system omitting the battery would reduce cost and maintenance and increase the practicability of the small wind turbine system [111]. Classic topologies are not suitable for wind turbine generators (WTG) with a rated power below 300 W. Not only for that the cost is too high, but for that the generator voltage is usually too low that the front stage cannot step up the voltage to be a level high enough to supply the rear inverter stage [111].

To cope with those drawbacks, several solutions came up. In [111], a Flyback-based inverter is proposed. A rectifier and a Boost stage step-up the generator voltage as some of the classic topologies. Then, a Flyback inverter operating in Boundary Conduction Mode (BCM) for reducing the switch current and minimising the transformer size provides isolation. Finally, an H-bridge stage injects the wind turbine power into the grid (see Fig. 5.3).

There are also other options available for grid-tie wind turbines, such as [112] or [113] but in this case, the power of the wind turbine is quite greater than in [111], thus the topology does not need to be that complicated.

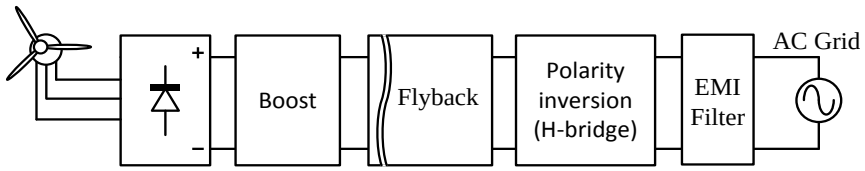

Fig. 5.3. Configuration of the grid-tie inverter for WTG proposed in [111]

5.3 Photovoltaic energy and PV panels

The primary and most abundant renewable energy source is the electromagnetic radiation coming from the sun. By geographical and climatic reasons, some areas in the world are more suitable than others to collect this energy. 2013 was a historic year for solar PV technology since at least 38.4 GW of solar PV capacity were installed worldwide. This figure boosted the value of cumulative installed capacity up to 138.9 GW. Besides, the new ruler in the newly-installed solar PV facilities has become Asia over Europe, representing 56% of the overall count [114].

Fig. 5.4 shows the cumulative installed capacity during the past 13 years. In 2013, Europe was still leading with a 59% of the total.

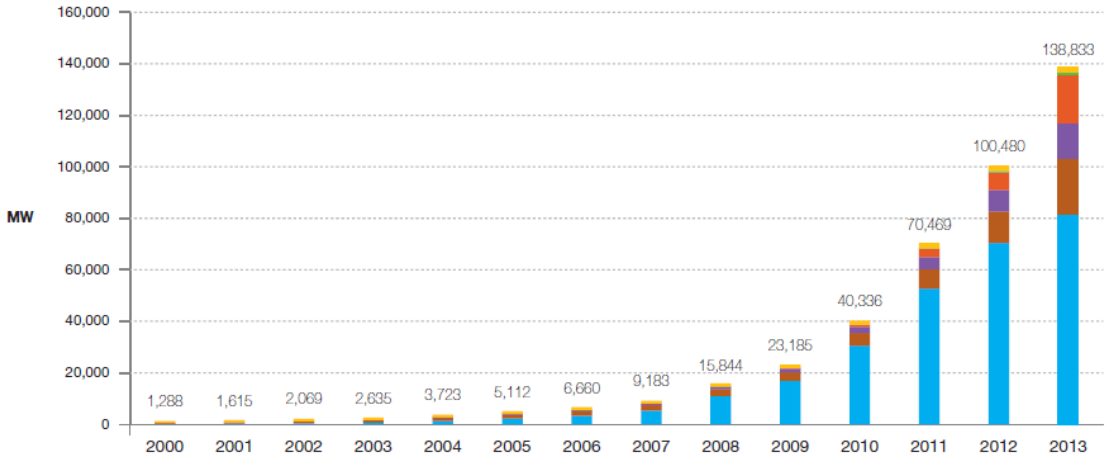

	2000	2001	2002	2003	2004	2005	2006	2007	2008	2009	2010	2011	2012	2013
RoW	751	807	887	964	993	1,003	1,108	1,150	1,226	1,306	1,590	2,098	2,098	2,098
MEA	n/a	n/a	n/a	n/a	1	1	1	2	3	25	80	205	570	953
China	19	24	42	52	62	70	80	100	140	300	800	3,300	6,800	18,600
Americas	21	24	54	102	163	246	355	522	828	1,328	2,410	4,590	8,365	13,727
APAC	368	496	686	916	1,198	1,502	1,827	2,098	2,628	3,373	4,951	7,513	12,159	21,992
Europe	129	265	399	601	1,306	2,291	3,289	5,312	11,020	16,854	30,505	52,764	70,489	81,464
Total	1,288	1,615	2,069	2,635	3,723	5,112	6,660	9,183	15,844	23,185	40,336	70,469	100,480	138,833

Fig. 5.4. Evolution of global PV cumulative installed capacity 2000-2013 [115]

Solar panels were meant to transform the sun radiation into electrical. The production of the electricity is done through cells connected in series and/or in parallel. These cells capture the photons to create free electrons that flow across to produce current [116]. The semiconductor material which

forms the PV panel determines the efficiency of the panel and hence, the manufacturing process. Solar panels came originally in three types: amorphous, monocrystalline, and polycrystalline but nowadays there are more than 20 [117]. A panel of 150 W has an area of around 1 m^2, but this information depends on the technology employed as well as in the manufacturing process.

5.3.1 Grid connected PV systems

If a PV system (or a wind turbine one) is connected to the grid, then the generated power has to comply with specific standards, which are regulated by the utility in each country. The main regulations that grid connected inverters have to comply with are [94], [118]:

- Total Harmonic Distortion (THD) and individual harmonic current levels.
- Power factor.
- Level of injected DC current.
- Voltage and frequency range for normal operation.
- Detection of islanding operation (islanding or non-islanding functions).
- Automatic reconnection and synchronizing.
- Grounding of the system.

PV generation systems are becoming more popular as their efficiency increases and the cost is reduced [119], [120]. These systems try to complement the electrical system they are connected to, helping to reduce CO_2 emissions to the atmosphere. In order to maximize the results of a PV panel, there are power converters or solar trackers that seek for its Maximum Power Point (MPP) [121], [122]. Depending on the sun conditions, the voltage and the current provided by the PV panel oscillate and this would be inefficient unless the Maximum Power Point Tracker (MPPT), that controls the interfacing power converter, would be constantly adjusting the maximum power output. The oscillating conditions are determined by environmental factors, chemical composition of the panel, and the angular position of the sun. There are many topologies and techniques, as it can be observed in the bibliography: [27], [59], [88], [94], [123], [124].

As it happened with the WT, the PV energy can be used either to charge batteries, to supply a load or to be injected into the grid. If there were not any kind of ESS, then all the energy generated would be injected into the electric distribution network. However, PV panels generate only DC currents and voltages, thus to move the energy from the panel to the grid an inverter is needed. There are many configurations available in order to attain the purpose. In the bibliography, several cases are mentioned: [125], [126], [127], [128], [129]. Each one of these solutions can be divided into one of the following groups:

- Non-isolated single stage topology
- Isolated single-stage topology
- Isolated multi-stage topology
- Non-isolated multi-stage topology

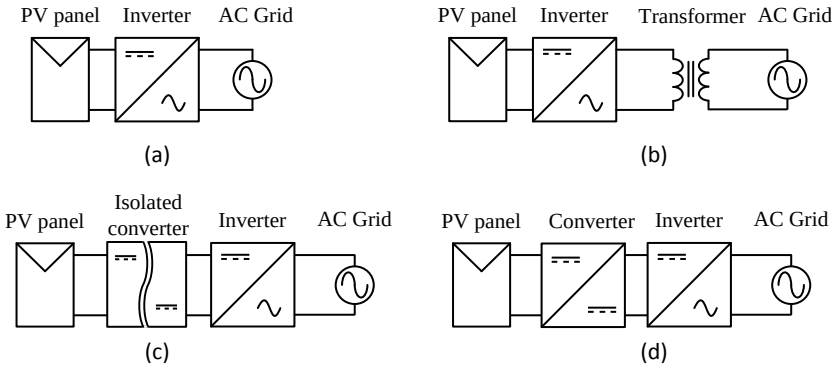

Fig. 5.5. Different grid connected PV panels: (a) non-isolated single stage; (b) isolated single-stage; (c) isolated multi-stage; (d) non-isolated multi-stage

The chosen option for this work has been a modification of Fig. 5.5c as it will be explained later. The reason is that the isolated converter and the inverter have been merged into one single isolated power converter.

5.4 Illumination and renewable energy sources in hybrid systems

Autonomous lighting systems with integrated RES and ESS have been working in applications for remote areas for many years (see Fig. 5.6). However, it is more interesting to consider that these systems could also operate connected to the grid and hence, the same scheme might be used but avoiding the use of battery banks. Therefore, the overall cost of the hybrid system is cut down and the rated power of the interface converter between the grid and the DC bus can be reduced.

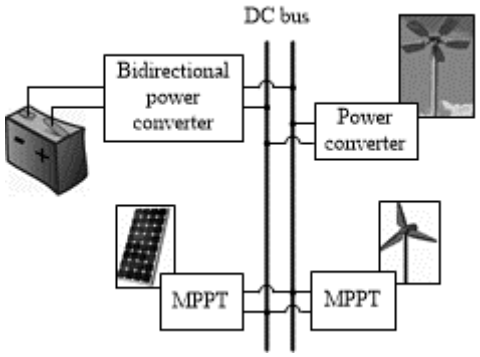

Fig. 5.6. Autonomous lighting system with RES units (images under Creative Commons license)

However, the type of RES integrated in a lamppost affects the behaviour of the whole system. The main difference is the amount of operating hours. A PV panel could be injecting energy in the grid during daytime, but nothing at night. Thus, depending on the sun hours, the net power balance between supplying the lamp at night and injecting power from the PV into the grid during the day could be positive, negative or zero. On the other hand, a wind turbine can operate whenever there is enough wind. Therefore, it could happen that there is not power exchange during the day, but at night there is enough available power as to avoid the lamp connection to the grid. Obviously, as it

happens with all renewable energies, and as it was mentioned before, the net power balance is unpredictable at this level. Both cases will be studied in this thesis and experimental results will be obtained.

Additionally, another important issue is the configuration of this hybrid system. There are many options: the traditional one, where the power flows of lamp and RES are fully decoupled and the one that will be proposed in this work with a bidirectional power converter that shall couple both power flows. The main difference between them, apart from the distribution of the subsystems, is the fact that the traditional configuration needs an extra power converter in order to inject the RES power into the grid while the proposed system, with just one bidirectional power converter, is able to move the energy in both ways.

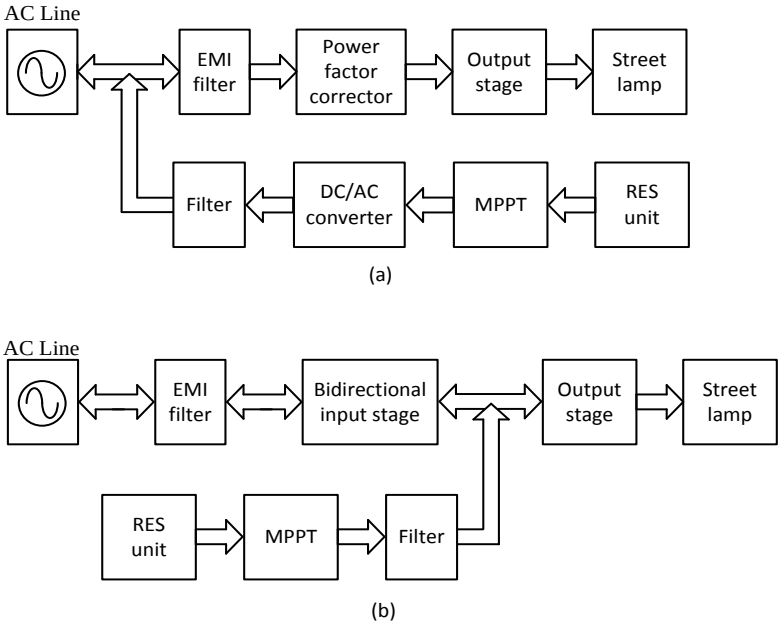

Fig. 5.7. (a) Traditional hybrid configuration; (b) Proposed configuration

All these details will be discussed in forthcoming chapters, including the control of the bidirectional input stage that shall operate also as a power factor corrector.

5.5 Summary and conclusions

In this chapter, a brief introduction to RES has been presented. The most suitable sources to be installed in street lampposts have been introduced: wind turbines and PV panels. Then, some common configurations of grid connection for both of them have been briefly studied.

Finally, a short introduction to hybrid systems that combine RES and illumination have been anticipated. These configurations are discussed more in detail in forthcoming chapters.

Chapter 6

State of the art of power factor correctors

This chapter deals with the conversion stage to interface the AC mains with a given power load. Thus, a primary concept in AC power supplies is introduced: the power factor correction (PFC).

Later, the main existing techniques for PFC will be summarised, making a classification between passive and active techniques, focusing in the discontinuous conduction mode (DCM) operation mode.

Afterwards, the different architectures of active solutions that can be found in the literature will be listed: one-stage, two-stage, three-stage or single-stage integrated converters.

Finally, a brief discussion about PFC front converters without diode bridge shall be studied in order to introduce the forthcoming chapter.

6.1 Introduction

With the ever-increasing use of electric energy consuming systems, power quality has become a significant requirement. Many electronic loads, like power supplies, lighting ballasts, low-cost AC/DC converters, etc. use power factor corrector (PFC) pre-regulators stages to guarantee the fulfilment of the input current operating standards mentioned in chapter 2 [130], [131], [132], [133], [134].

6.2 Power factor correction techniques

A variety of circuit topologies and control methods have been developed for the PFC application. It can be performed by several techniques achieving sinusoidal input current or just limiting the input current harmonic content [1], [120].

6.2.1 Passive techniques

Passive PFC techniques make use of uncontrolled devise and resistive and/or reactive elements. There are basically two types of circuits: passive filters and valley-fill circuits.

Passive filters

PFC based on passive elements are known as passive PFC and they consist of using passive elements such as inductors, resistors and capacitors combined with non-controlled rectifiers, as it is depicted in Fig. 6.1. It provides a high impedance for the considered input current harmonics, reducing their amplitude and smoothing the input current waveform [135].

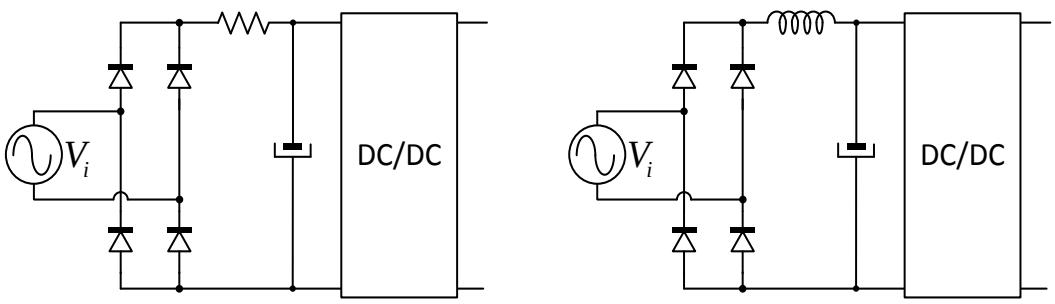

Fig. 6.1. Passive filters for improving PF: RC filter (left) and LC filter (right)

This solution offers a good trade-off between efficiency and cost and does not generate electromagnetic interferences (EMI). Nevertheless, high size of the inductor/resistor makes this solution only suitable for low power levels. Furthermore, the harmonic content is usually very close to the regulation limits [136].

Valley-fill circuits

The valley-fill topology (and its derivatives) improves the disadvantages of passive filters. It does not require a control circuitry and a 95% of PF can be reached. However, the Total Harmonic Distortion of the input current (THD_I) can match even a 40% [137], [138]. The simplest valley-fill topology can be seen in Fig. 6.2.

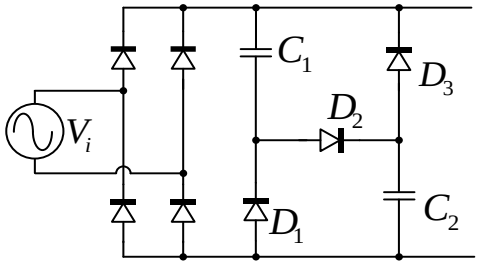

Fig. 6.2. Example of a valley-fill configuration

This solution has extensively been used for fluorescent lamp ballasts [137], [138], [139] and HID lamps [8], although it has also been applied for LED drivers, as a passive PFC in passive drivers [140], or as a decoupling stage in active LED drivers in order to avoid an electrolytic capacitor of the DC-link.

6.2.2 Active techniques: operation modes

Before deeper analyses of the different available techniques, it is important to mention that there are three different operation modes that determine the behaviour of the PFC converter.

Continuous conduction mode (CCM)

In this operation mode, the inductor current is never null within a switching period, and therefore it usually has a low high-frequency ripple. Thus, the EMI filter size can be made relatively small. In addition, due to the comparatively lower *rms* current through the switches, their losses are kept at a low level. However, the converter inductance tends to be high. Furthermore, since the current never reaches zero, there is hard switching, thus losses in the device can be increased and so it does the radiated EMI [1].

Discontinuous conduction mode (DCM)

In this operation mode, the inductor current always reaches zero level, thus the inductor is completely discharged at least once per switching period. When operating in DCM, several converters operate as a voltage follower under constant duty ratio, achieving almost unity PF with a single control loop. The main advantages of such operation mode in comparison with CCM can be related to cost: the inductor is smaller in DCM and the control circuitry can also be.

However, DCM operation means high conduction losses and current stresses on the switches. It also increases the size and weight of the EMI filter [130].

Boundary conduction mode (BCM)

In BCM, the inductor operates in the boundary between DCM and CCM. Compared to DCM operation, transistor conduction losses are reduced since the current *rms* values are lower owing to the variable frequency operation.

The main drawbacks of BCM are the higher complexity of the control loops and the design of the EMI filter [1], [141], [142].

6.2.3 Active techniques

There are other ways to reach high efficiency and high power factor. Active techniques use power converters which are placed between the load and rectifier bridge and they are called Power Factor Correctors (PFC). Fig. 6.3 shows the average waveforms of a sinusoidal-input current PFC. Input current and voltage are practically in phase and the power in the DC bus is pulsating with twice the line frequency. Despite of the higher complexity, cost and EMI emissions of these converters against the passive ones, they are considered the best solution for high power levels [140], [143], [144], [145], [146].

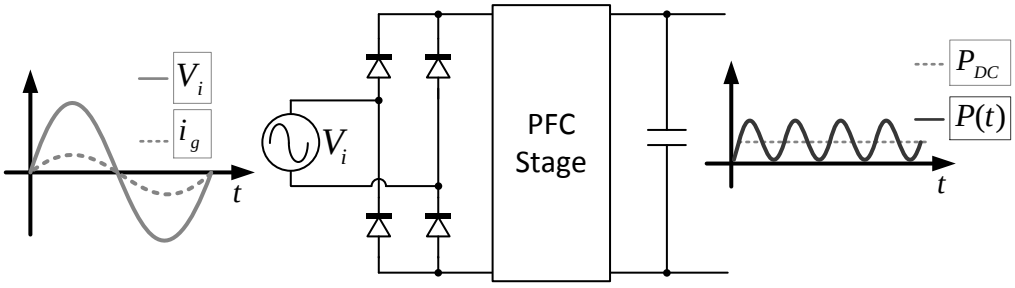

Fig. 6.3. Average waveforms of a sinusoidal-input current PFC

According to the input current, PFC can have a sinusoidal input current or a non-sinusoidal one:

Sinusoidal input current: ideal PFC stages

From the point of view of the AC grid, these converters absorb an instantaneous current value that is proportional to the instantaneous grid voltage. Therefore, they behave like a resistor, being the current and the voltage in phase. As the grid voltage is sinusoidal, the input current will also be. These converters comply with harmonics and THD standards since they are able to reach almost unity factor and very low THD_I. There are several solutions for implementing a sinusoidal PFC:

- **Resistor emulator**: these converters synchronise their input current with the line voltage. They absolutely need to measure the line voltage and make use of two control loops. One example is the Boost converter operating in Continuous Conduction Mode (CCM) [147].
- **Voltage follower**: some converters, due to operate in Discontinuous Conduction Mode (DCM), are able to behave as a voltage follower, maintaining a sinusoidal input current in phase with the grid voltage with just one control loop (or even without it). Some examples are the Buck-Boost, Flyback, SEPIC, etc. [136], [147].

Non-sinusoidal input current: Quasi-PFC Stages

There are two kinds of Quasi-PFC converters: either they feature a non-sinusoidal input current with limited harmonic content, or a highly distorted sinusoidal input current that comply with the regulations. The more significant converters are listed below:

- DC-DC converters: some DC-DC converters inherently behave as a Quasi-PFC. An example can be the Boost converter in DCM that shows an important third harmonic [148].
- Input current shapers: these topologies consist of the transformation of the original converter into another one with an additional output, generally from the converter transformer, between the input line and the DC bus capacitor. Some energy is recycled but efficiency is penalised [149].

6.2.4 Active PFC architectures with diode bridge

The most commonly employed topologies for performing PFC with a diode bridge at the input are listed as follows. LED drivers use typical DC-DC converter topologies adapted to the supply of LED lamps.

Single-stage converters

They consist of a unique stage that achieves high PF and supplies the load. Single-stage PFC are also called front-end converters. The most common are the Boost converter, the Buck-Boost and its derived topology, the Flyback converter. This Flyback based topologies are usually used in cost-effective, low power solutions since they can operate as a voltage follower working in DCM with a simple control, featuring galvanic isolation and an extra degree of freedom with the turns ratio [130], [145]. A single-stage PFC basic architecture is depicted in Fig. 6.4.

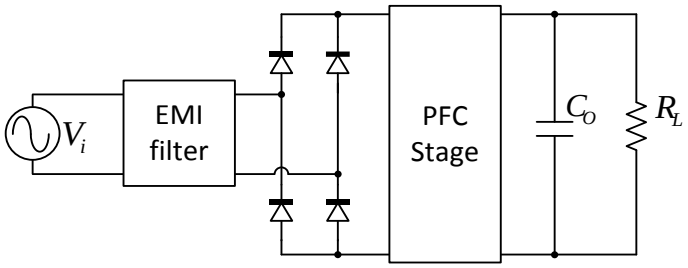

Fig. 6.4. Typical single-stage PFC converter

The main drawbacks of these PFC are the high peak current stresses and EMI problem caused by the DCM operation. Furthermore, in the DC bus there is an energy storage at double the line frequency and thus, big capacitors are needed [150].

Two-stage converters

This combination consists of a front-end PFC which absorbs energy from the AC mains and stores it in an intermediate DC bus, followed by DC-DC converter with a much higher bandwidth that will take the energy from the DC bus and drive the lamp. The DC bus is, therefore, used as a decoupling node in the circuit. This architecture easily allows dimming features and fast dynamics. In addition, smaller capacitors can be placed in the DC bus. Nevertheless, some drawbacks must be assumed: it is more complicated, more expensive and larger than the single-stage one due to the fact that the energy is processed twice and more components are needed [151]. Fig. 6.5 shows a basic configuration of a two-stage converter.

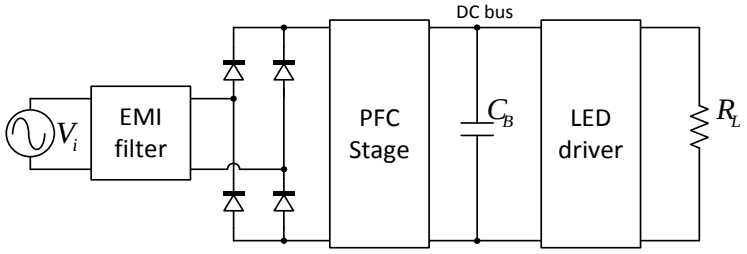

Fig. 6.5. Two-stage typical architecture

Three-stage converters

Although is not a very common architecture in the market due to its size and cost, in some cases, where high efficiency is pursued, three-stage converters are applied. The middle-stage use to provide galvanic isolation by means of a zero voltage switching – zero current switching transformer optimised for high frequency. Fig. 6.6 shows an example of this architecture.

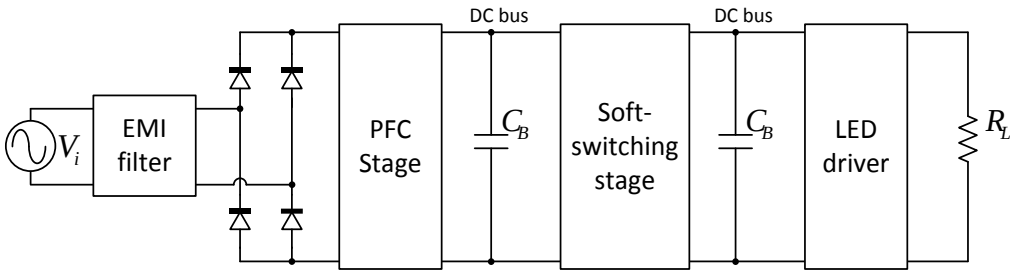

Fig. 6.6. A three-stage converter with a PFC.

Integrated power converters

Integrated power converters are a fine solution based on the integration of two different stages into a single one, which means the combination of the PFC and the DC-DC converter of a two-stage converter. Many integrated converters can be found in the literature: Buck converter integrated with a Flyback is one of the most famous [152].

They achieve a reduced size and thus, a reduced cost, complexity and weight. As a drawback, efficiency is usually lower than a two-stage converter because of the integration process [153], [154].

6.2.5 PFC front converters without diode bridge

One of the main drawbacks of the diode bridge in a PFC front converter is that it avoids the bidirectional power flow. In addition, efficiency can be improved if the input diodes are removed [87], [131]. Therefore, this kind of PFC converters avoid the use of a diode bridge and thus, they are connected directly to the AC grid. Hence, typical DC-DC topologies are not suitable anymore and they must be modified in order to deal with the sinusoidal nature of the grid voltage and current.

There are different approaches for this PFC front converter. For low power applications, one of the most appealing converters due to its galvanic insulation, short-circuit protection and simplicity is the Flyback converter. In addition, output voltage can be greater or smaller than the input voltage due to the turns ratio [131], [132], [133]. On the other hand, as it is well known, there are some remarkable drawbacks like semiconductor stresses due to Flyback transformer leakage inductance and drain to source switches capacitance interaction.

This work intends to deal with the use of a Flyback-based topology, which aims to remove the input diode bridge by using the integration of two power topologies, each one for a different polarity of the input voltage (see Fig. 6.7). The proposed topology (that will be analyse in detail later) has an extra feature as it can send energy from the DC bus back to the power line since the input diode bridge is removed. It can be used as an alternative to H-bridge-based topologies.

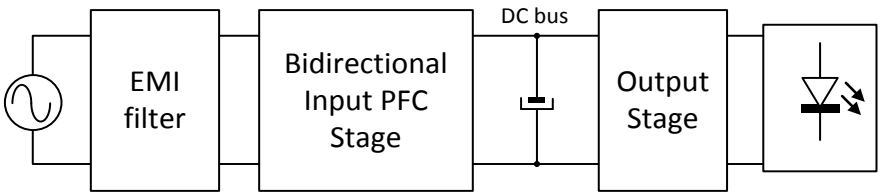

Fig. 6.7. Proposed PFC front converter block diagram

6.3 Summary and conclusions

The need for power factor correction has been studied in this chapter. The most common techniques and topologies dedicated to PFC applications has also been introduced although the main purpose of this work is to develop a bidirectional power converter able to move the energy from the AC utility grid to the DC bus and vice versa, operating either as a PFC front-end converter as well as a grid-tie inverter.

Chapter 7

Fast dynamics current control of DCM Flyback as PFC front converter for smart-lighting applications

In this chapter is proposed a simple wide bandwidth control technique for a PFC Flyback converter acting as front converter of a LED lighting system, that also reduces the harmonic content of the AC line current. The control scheme is discussed and implemented, and experimental results are presented.

7.1 Introduction

As mentioned in the previous chapter, a good solution for a LED driver consist of a single-stage front-end power factor preregulator (PFP) that supplies directly the lamp. However, for power levels beyond 25 W, this solution does not ensure the fulfilment of the Class C requirements [1]. Despite of the power being processed twice -and thus the overall efficiency will be affected- two-stage architectures are more suitable for medium power levels in lighting applications [143], [152], [155], [156], [157]. Two-stage approach provides much tighter design capability, as each stage can be optimised for independent issues, and therefore the overall controllability, versatility and performance is much better.

7.2 Rectifier mode background

The idea of this chapter is to design a PFC front converter for lighting applications with fast dynamics. This idea came up due to the study of PFC converters and their standard control methods limitation in terms of fast response to changes in the load or in the grid voltage. In this chapter, a control technique is proposed, which presents a faster response to changes in the load and/or in the AC mains with respect to previous methods, reducing THD and harmonic content.

For low-power level applications, the Flyback converter operating in DCM is widely used. As stated before, galvanic isolation, low cost and high efficiency make this converter a very appealing solution [27], [87], [131]. It also allows to achieve almost a unity PF by simply using a constant on-time control or fixing its duty ratio [130] and to have a smaller inductor. In addition, the required inductance values for such operation mode are usually small, which implies a compact design as well. However, DCM operation means high conduction losses and peak current stresses on the switches. It also increases the size and weight of the EMI filter [133]. Since the beginning of this work, DCM was employed.

The idea of having a Flyback connected directly to the AC grid without a diode bridge and operating as a PFC came up in [158], [159], [160], [161], [162], [163] but it was firstly applied to lighting systems in [87] and later in [131]. The first approach was to integrate two different Flyback stages, one for each polarity of the line voltage, into a single two-polarity stage. This way, bidirectional power flow in the input stage is enabled. In Fig. 7.1 this input stage is depicted. As it can be observed, there are five switches that allow energy to flow in both directions: from the grid to the DC bus will be called “rectifier mode” whereas from the DC bus to the grid shall be called “inverter mode”. At this point, the rectifier mode is being studied as the PFC performance will be evaluated. The load is represented by a resistor.

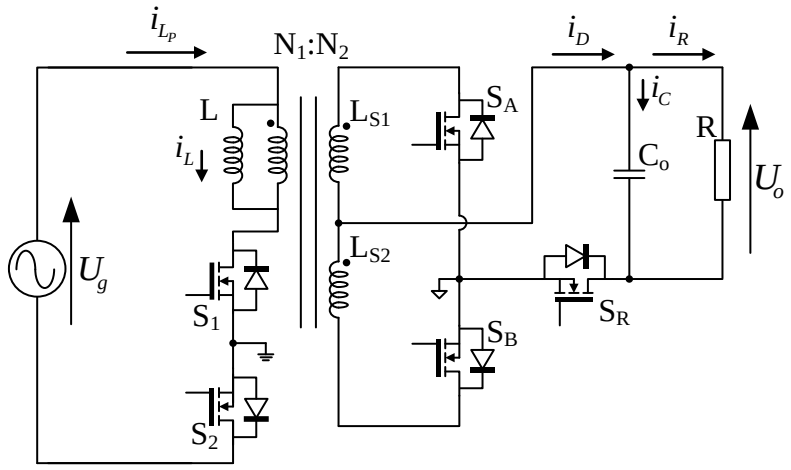

Fig. 7.1. Proposed input stage based in the integration of two Flyback stages with opposite polarities [87], [131]

7.2.1 Operational principles of the PFC input rectifier stage

In this operation mode, switches S_A and S_B do not need to be triggered unless synchronous rectification is desired. Hence, they both can be switched off and the current will be driven naturally through the antiparallel diodes.

There are three different intervals for each half-cycle of the grid. In the following discussion, the behaviour of the system for positive input voltage, U_g in Fig. 7.1, will be considered. The case of negative input voltage provides the same waveforms due the symmetry of the topology, however some references must then be reversed.

On the other hand, the DCM Flyback inductor currents and main voltages are depicted in Fig. 7.2 for positive input voltage. Since it operates in DCM, three intervals can be observed: charge of the magnetising inductor ($d_1 \cdot T$), discharge ($d_2 \cdot T$) and a dead time ($d_3 \cdot T$).

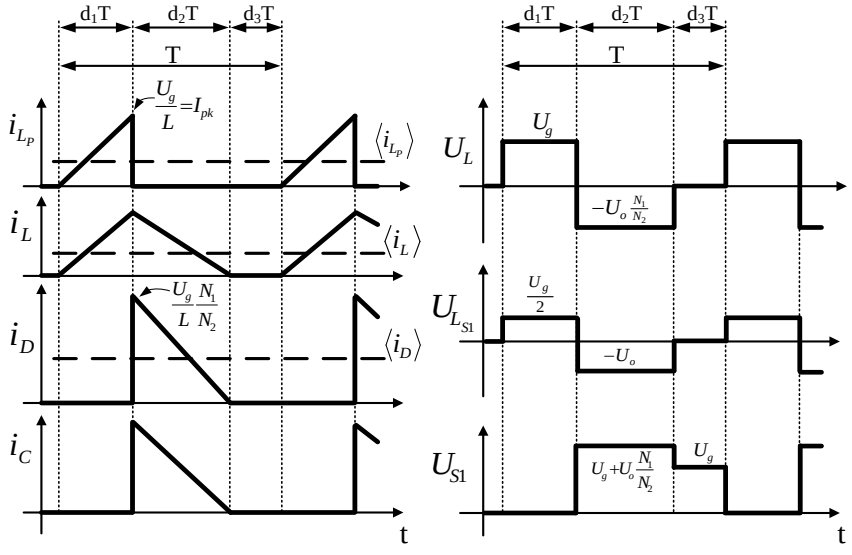

Fig. 7.2. Main Flyback waveforms

First interval

During this interval, the magnetising inductor at the primary side of the transformer, *L*, is charged, from the initial zero value, through switch S_1 and the diode of S_2. The grid voltage is directly applied to the inductor *L*. Since S_R is switched off and S_A and S_B diodes are reverse-biased, the current will not flow in the secondary side. Capacitor C_O is then responsible of keeping the load voltage ripple between reasonable margins. Fig. 7.3 shows this first interval. Those devices that are conducting current are coloured in black, whereas the devices with no current flowing are depicted in grey.

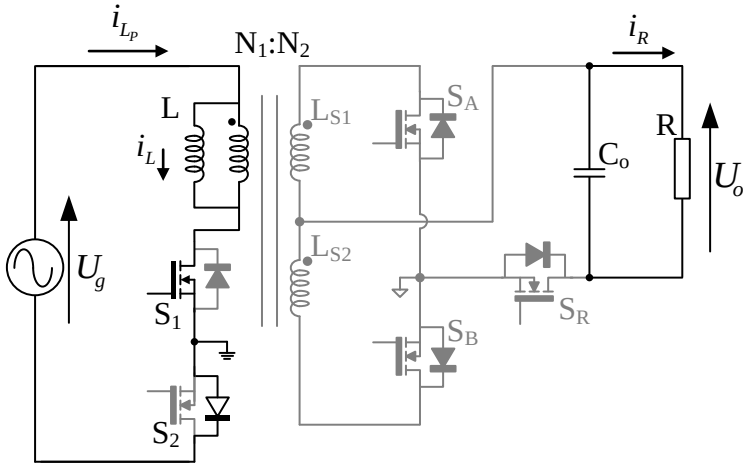

Fig. 7.3. First interval of the converter when the grid voltage is positive

Second interval

The second interval, depicted in Fig. 7.4, begins when S_1 is switched off. The energy stored in the inductor *L* is discharged in the secondary side through L_{S1}, the switch S_R and the body diode of S_A. S_R must start to operate when S_1 is off. The DC bus is therefore charged during this interval.

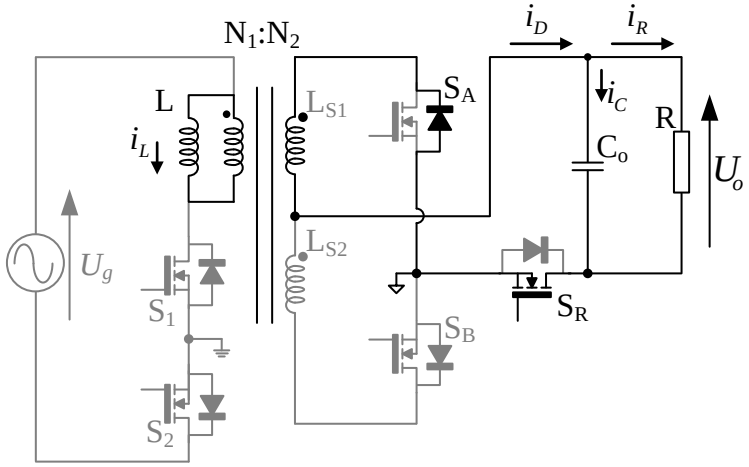

Fig. 7.4. Second interval of the converter when the grid voltage is positive

Third interval

Since the Flyback is operated in DCM, the third stage corresponds to the moment when the magnetising inductor current goes naturally to zero and thus, there is no energy stored in the transformer. As in the first stage, the capacitor C_O must supply the load (see Fig. 7.5).

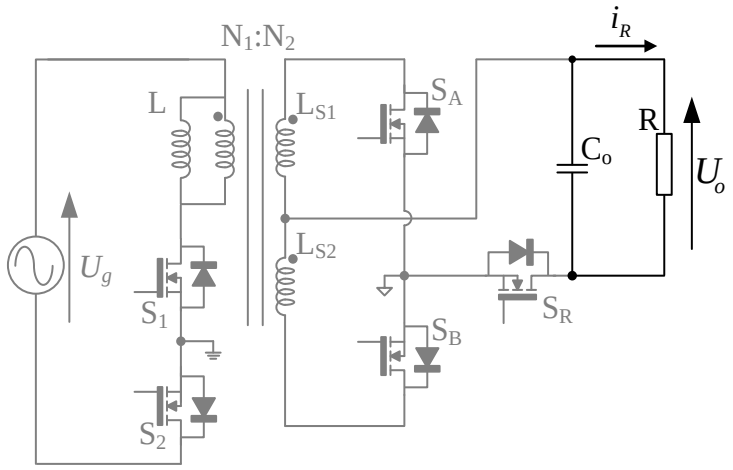

Fig. 7.5. Third interval of the converter when the grid voltage is positive

In order to consider the operation intervals during the negative cycle of the grid voltage, the main changes are that now S_2, L_{S2} and the diode of S_B are used instead of S_1, L_{S1} and the body diode of S_A. The main switching waveforms, however, present similar expressions in this case.

7.2.2 First version of the DCM Flyback as PFC front converter

The first approach of this PFC was carried out in [87] and [131]. In both works, the secondary side of the converter had two diodes instead of the switches S_A and S_B (see Fig. 7.6). The Flyback transformer was designed just for the rectifier mode which means that the bidirectional power flow was not studied in detail.

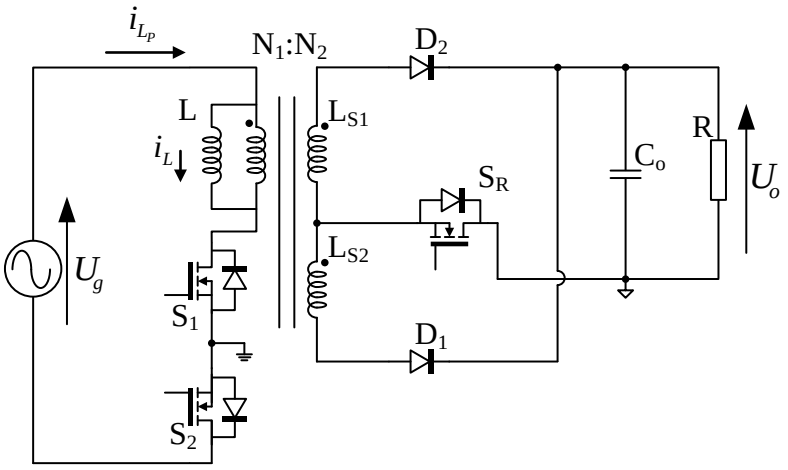

Fig. 7.6. First version of the DCM Flyback as PFC front converter done in [72] and [116]

In these works, a slow control loop that sensed the DC link voltage and kept constant duty ratio in every line period was implemented, so the maximum bandwidth of that regulator was limited by the 50 or 60 Hz, depending on the grid frequency. However, the conclusions showed that the proposed topology provides a higher efficiency than the standard diode bridge and Flyback PFC stage circuit. On the other hand, more components are needed: two more switches, an extra secondary winding in the transformer and an additional diode.

7.2.3 Second version of the DCM Flyback as PFC front converter

The next update was done in [27]. In this work, both rectifier and inverter modes were studied. Hence, it was the first step towards the combination of a lighting system and a RES. In this case of study there were only one stage that would supply the lamp and operate as an inverter when it was necessary. The RES unit would be a PV panel, thus both lighting and renewable energy systems would never work at the same time. A relay would make sure of this operation mode. In Fig. 7.7 can be seen the idea behind this explanation.

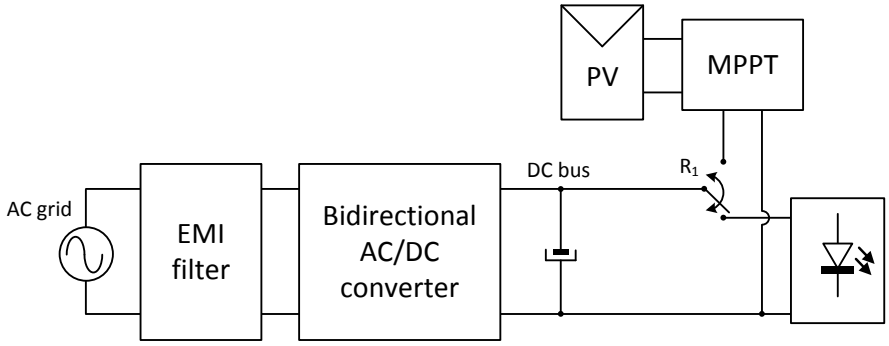

Fig. 7.7. Block diagram of the proposed topology in [27]

The firing of the switches and the topology employed was already explained in Section 7.2.1. However, the important issue of this work was the mathematical methodology developed in order to obtain the parameters of the bidirectional Flyback converter, in DCM, valid for both rectifier and inverter modes. In addition, a complete discussion about the operational principles and experimental

results were obtained. This section will be focused in the rectifier mode since the operation of the Flyback as a PFC is being studied. However, in following chapters, the inverter mode, as well as the continuous, swift transition between both modes, shall be explained.

If the reported work ([87] and [131]) had a slow control loop, the later study in [27] lacked of a closed loop control strategy. In rectifier mode, that is supplying the lamp from the grid, the duty ratio was not controlled by any kind of regulator but by an open loop scheme. In this strategy, the duty ratio was given by an equation that would depend on two fundamental parameters: the peak value of the grid voltage and the DC bus instantaneous voltage. This equation comes from considering the average voltage in the inductor but it does not consider any distortion in the grid voltage (that would be transferred to the lamp) and it neither consider changes in the load.

Fig. 7.8 shows the scheme of the power converter used in this work. Notice that in this case, a simple LC low-pass EMI filter was used, and the DC bus was kept steady with a bulk electrolytic capacitor.

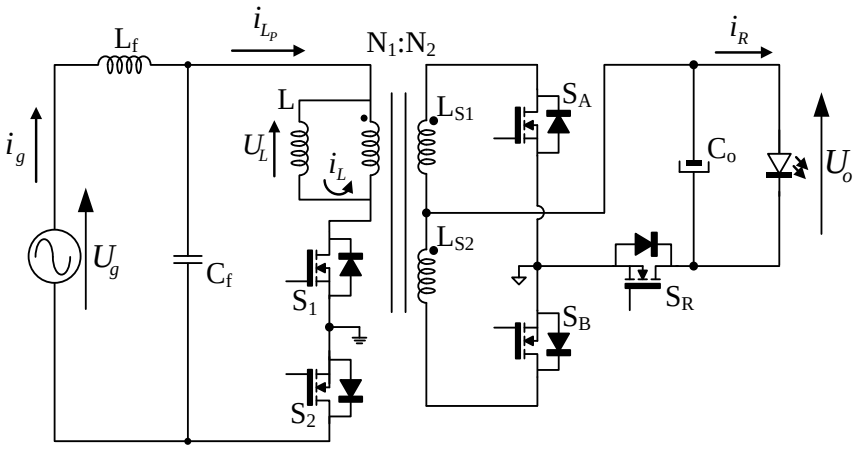

Fig. 7.8. Proposed bidirectional Flyback in [27]

The voltage in the primary side magnetising inductor for every switching cycle (when positive input voltage) can be seen in Fig. 7.2. To ensure steady state operation of the converter, the average value of the inductor voltage in a switching period is made equal to zero. Based on the DCM waveforms in Fig. 7.2, the average voltage of the inductor can be defined as:

$$U_g \cdot d_1 \cdot T = U_o \cdot \frac{N_1}{N_2} \cdot d_2 \cdot T \qquad (7.1)$$

In addition, in order to attain the maximum value of the duty ratio (BCM, where d_3=0), then $d_2=1-d_1$ and $U_g \rightarrow U_{g\_pk}$. Therefore (7.1) can be expanded as:

$$d_{1max} = \frac{U_o \cdot N_1}{U_{g_{pk}} \cdot N_2 + U_o \cdot N_1} \qquad (7.2)$$

The obtained expression in (7.2) gives the maximum duty, $d_{1\,max}$, that can be used in rectifier mode for avoiding CCM, depending on the peak value of the grid voltage and on the DC bus voltage. Thus, sensing both voltages and using some digital controller (in this case a C2000 Texas Instruments TMDS320F28335), the adequate duty ratio can be calculated and implemented. However, this is not entirely a closed-loop operation mode. Basically, the converter was working as a traditional PFC with

a big capacitor in order to stabilize output voltage. Another further update needs to be done in order to have a full control of the converter in rectifier mode.

7.3 Proposed control strategy for the PFC Flyback bidirectional converter operating in rectifier mode

This section deals with the study of an optimized control method for the rectifying mode of the bidirectional converter. It will be proved that a simple PI regulator is able to control the DCM bidirectional input PFC stage shown in Fig. 6.7 and keep a steady bus voltage fulfilling the desired reference with a higher bandwidth than classic controllers and rejecting disturbances. Furthermore, the power topology can be designed in order to reduce the bus capacitor size for rectifier mode. Although the target application is for smart lighting ballasts of low to medium power ratings, it must be noticed that this methodology control could be applied to any kind of power converter.

The bidirectional two-stage power topology shown in Fig. 7.9 is considered. The first stage, a PFC, is the already explained modified Flyback connected to the AC grid. The second stage is just a DC-DC Buck converter that would drive a LED lamp. In order to test the proposed control strategy for the PFC, this second stage of the driver would be modelled as a variable resistance.

It must be commented that, for simplicity, the power generation stage that would be connected to the DC link, is not represented at this point. This issue must be taken into account in order to understand the apparently paradox of presenting an input stage with bidirectional power capability connected to a unidirectional power flow LED driving.

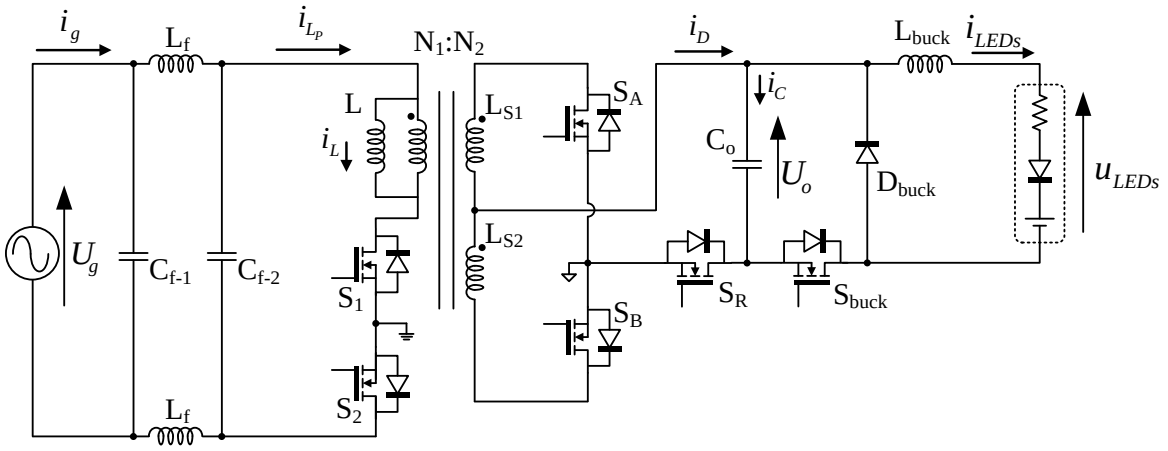

Fig. 7.9. Proposed electronic driver for a LED lamp

Hence, the power topology we are dealing with in this chapter is the one shown in Fig. 7.10.

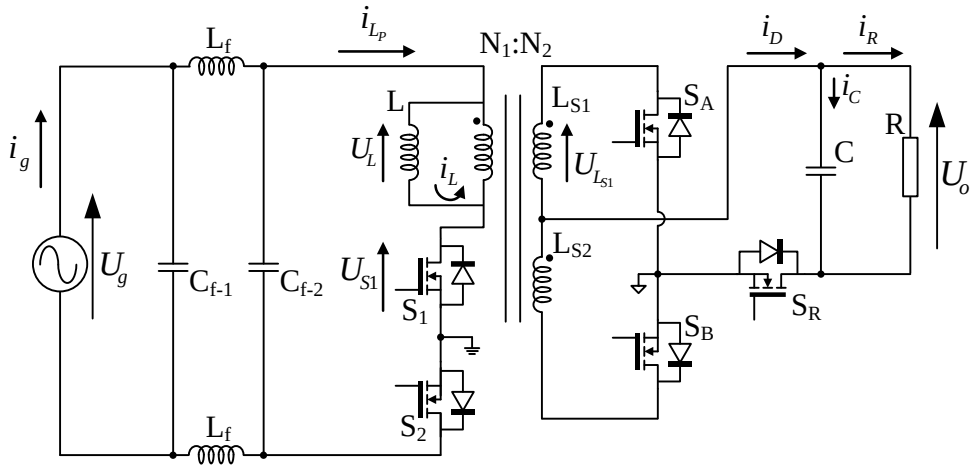

Fig. 7.10. Proposed bidirectional PFC stage

In the technical literature, different control techniques are tested for the DCM Flyback [27], [130], [131], [132], [164]. However, all of them have a common point and it is the lack of a fast response in the DC bus. If the load was a single lamp, it is not a big deal to have a low but reliable control loop. Nevertheless, if the case of study for a full lighting system and its effect in the quality of the power line, then it could be an issue the fact of not responding quickly enough to disturbances.

In some cases, like [27], the control is based on an equation that does not guarantee total reliability and in other cases, as [130], [131], [140], the control is relatively slow. In this work, a control technique is proposed, which presents a faster response to changes in the load and/or in the AC mains with respect to previous methods, reducing THD and harmonic content.

Prior to the control design, the converter will be analysed in detail in order to model it. In [165], [166] is explained why PFC Flyback converters working in DCM behave like first-order systems. However, a complete small-signal model of the converter is needed in order to ensure the ability to carry out the proposed control design.

The DCM Flyback inductor currents and main voltages are depicted in Fig. 7.2 for positive input voltage (similar equations apply to negative input voltage). Since it operates in DCM, three stages can be observed: charge of the magnetising inductor ($d_1 \cdot T$), discharge ($d_2 \cdot T$) and a dead time ($d_3 \cdot T$).

So, the average value of the input current for every switching period can be easily written as:

$$\langle i_{L_P} \rangle = \frac{1}{T}\int_0^{d_1 T} \frac{U_g}{L}\, t\, dt = \frac{1}{T}\frac{U_g}{L}\left.\frac{t^2}{2}\right|_0^{d_1 T} = \frac{U_g {d_1}^2 T}{2\,L} \qquad (7.3)$$

where T is the switching period, L is the magnetizing inductor of the transformer seen from the primary side, U_g is the input voltage and d_1 the duty cycle.
Considering U_g as a pure sinusoidal voltage source ($U_g = U_{g_{pk}} \sin(\omega t)$) without any extra harmonic content, i_{LP} would result in:

$$i_{L_P} = \frac{U_{g_{pk}} \sin(\omega t)\, {d_1}^2 T}{2\,L} = I_{L_{P_{pk}}} \sin(\omega t) \qquad (7.4)$$

Thus, the peak value of the input current can be defined as:

$$I_{L_{P_{pk}}} = \frac{U_{g_{pk}} {d_1}^2 T}{2\,L} \tag{7.5}$$

This means that the peak values are related and hence, for pure sine waves, we can use a DC circuit to analyse the relationships between peak values in the AC-DC converter, therefore being able to use large and small-signal methods.

7.3.1 Large-signal AC model (averaged dynamic model)

So as to properly design the fast dynamics feedback loop, a dynamic model of the whole system is needed. The behaviour of the system can be simplified by studying only the low frequency evolution of the signals (avoiding the effects of switching [167], [168]). In Fig. 7.2 the main waveforms are depicted in order to proceed to this large-signal analysis. Equations (7.6), (7.7) and (7.8) show the different values for the inductor current, inductor voltage and capacitor current during the three possible stages, respectively.

$$i_L(t) = \begin{cases} \dfrac{U_g(t)}{L} t & 0 < t \le d_1 T \\ I_{pk} - \dfrac{U_o(t)}{L}(t - d_1 T)\dfrac{N_1}{N_2} & d_1 T < t \le (d_1 + d_2) T \\ 0 & (d_1 + d_2) T < t \le T \end{cases} \tag{7.6}$$

$$U_L(t) = \begin{cases} U_g(t) & 0 < t \le d_1 T \\ -U_o(t)\,\dfrac{N_1}{N_2} & d_1 T < t \le (d_1 + d_2) T \\ 0 & (d_1 + d_2) T < t \le T \end{cases} \tag{7.7}$$

$$i_C(t) = \begin{cases} \dfrac{-U_o(t)}{R} & 0 < t \le d_1 T \\ i_D - \dfrac{U_o(t)}{R} & d_1 T < t \le (d_1 + d_2) T \\ \dfrac{-U_o(t)}{R} & (d_1 + d_2) T < t \le T \end{cases} \tag{7.8}$$

Considering steady state, the average inductor voltage is zero. From (7.1) it can be stated that:

$$d_2 = d_1 \frac{U_g}{U_o} \frac{N_2}{N_1} \tag{7.9}$$

It is turn to average the equation systems previously shown. Averaging (7.7):

$$\langle U_L \rangle = L \frac{d\langle i_L \rangle}{dt} = d_1 \langle U_g \rangle - d_2 \langle U_o \rangle \frac{N_1}{N_2} + 0 \tag{7.10}$$

And given that U_g and U_o remain constant in a switching period, substituting (7.9) in (7.10):

$$\langle U_L \rangle = d_1 \langle U_g \rangle - d_1 \frac{\langle U_g \rangle}{\langle U_o \rangle} \frac{N_2}{N_1} \langle U_o \rangle \frac{N_1}{N_2} = 0 \quad (7.11)$$

Which indeed proves that the average voltage in the inductor is zero in DCM.

The same procedure shall be done with the output capacitor current, (7.8).

$$\langle i_C \rangle = C \frac{d\langle U_o \rangle}{dt} = -d_1 \frac{\langle U_o \rangle}{R} + \left(d_2 \langle i_D \rangle - d_2 \frac{\langle U_o \rangle}{R} \right) - d_3 \frac{\langle U_o \rangle}{R} \quad (7.12)$$

On the other hand, from Fig. 7.2, the maximum value of input current i_{LP} can be defined as I_{pk}:

$$I_{pk} = \frac{U_g \, d_1 \, T}{L} \quad (7.13)$$

In addition, the average value of the current in the secondary side, $\langle i_D \rangle$, can be calculated as follows, taking into account (7.13):

$$\langle i_D \rangle = \frac{1}{T} \int_0^{d_2 T} \left(I_{pk} \frac{N_1}{N_2} - \frac{\langle U_o \rangle}{L} \left(\frac{N_1}{N_2} \right)^2 t \right) dt =$$

$$= \frac{1}{T} \int_0^{d_2 T} \left(\frac{\langle U_g \rangle \, d_1 \, T}{L} \frac{N_1}{N_2} - \frac{\langle U_o \rangle}{L} \left(\frac{N_1}{N_2} \right)^2 t \right) dt = \frac{1}{T} \left[\frac{\langle U_g \rangle \, d_1 \, T}{L} \frac{N_1}{N_2} \, d_2 T \right. \quad (7.14)$$

$$\left. - \frac{\langle U_o \rangle}{L} \left(\frac{N_1}{N_2} \right)^2 \frac{{d_2}^2 T^2}{2} \right] = \frac{1}{T} d_2 T \left[\frac{\langle U_g \rangle \, d_1 \, T}{L} \frac{N_1}{N_2} - \frac{\langle U_o \rangle}{L} \left(\frac{N_1}{N_2} \right)^2 \frac{d_2 T}{2} \right]$$

In (7.9) was defined the relation between d_1 and d_2. Thus, including it in (7.14):

$$\langle i_D \rangle = \frac{1}{T} d_1 \frac{U_g}{U_o} \frac{N_2}{N_1} T \left[\frac{\langle U_g \rangle \, d_1 \, T}{L} \frac{N_1}{N_2} - \frac{\langle U_o \rangle}{L} \left(\frac{N_1}{N_2} \right)^2 \frac{d_1 \langle U_g \rangle \, N_2}{2 \langle U_o \rangle \, N_1} \right] = \frac{{d_1}^2 \langle U_g \rangle^2 \, T}{2 \, L \, \langle U_o \rangle} \quad (7.15)$$

So, if (7.12) and (7.15) are merged, finally the average value of the capacitor current is derived:

$$\langle i_C \rangle = C \frac{d\langle U_o \rangle}{dt} = -d_1 \frac{\langle U_o \rangle}{R} + \frac{{d_1}^2 T}{2 \, L} \frac{\langle U_g \rangle^2}{\langle U_o \rangle} - d_1 \frac{N_2}{N_1} \frac{\langle U_g \rangle}{\langle U_o \rangle} \frac{\langle U_o \rangle}{R} - d_1 \left(\frac{\langle U_o \rangle}{R} \right)^2$$

$$+ d_1 \frac{\langle U_o \rangle}{R} \frac{\langle U_g \rangle}{\langle U_o \rangle} \frac{N_1}{N_2} = -\frac{\langle U_o \rangle}{R} + \frac{{d_1}^2 \langle U_g \rangle^2 \, T}{2 \, L \, \langle U_o \rangle} \quad (7.16)$$

So far, the large-signal model has been obtained. However, in order to obtain the transfer functions of the dynamic model, extra transformations consisting in the linearise + perturb approach, need to be done.

7.3.2 Small-signal AC model

All variables will be perturbed from an equilibrium situation, in order to achieve a linear and time invariant (LTI) system. It must be noticed that the following calculations will be done for instant values of the grid line, not considering power balance in a line period. As it will be shown in forthcoming sections, this issue will ultimately allow to use the model for large bandwidth control schemes.

Based on the large signal model, the average value of any signal can be represented as steady-state value and small change in the signal as shown in the following equation:

$$\langle X \rangle = X + \hat{x} \tag{7.17}$$

where:

$\langle X \rangle$: the average value in a switching interval

X: the steady-state value

$\hat{x}$: the small-signal perturbation

Therefore, applying this concept to equations (7.11) and (7.16):

$$(U_L + \hat{u}_L) = L\frac{d(I_L + \hat{\imath}_L)}{dt} = 0 \tag{7.18}$$

After applying the steady-state condition, the small-signal mesh equation from (7.18), can be written as:

$$\hat{u}_L = L\frac{d\hat{\imath}_L}{dt} = 0 \tag{7.19}$$

Obviously, provided that the inductor is a LTI system, (7.19) states the same information that was already known in the large-signal equation. However, this is not generally true for every device in the system under study.

On the other hand, the same approach with the node equation, (7.16), can be done taking into account that the derivative of a quotient of functions on the same variable is defined as:

$$\left(\frac{f(x)}{g(x)}\right)' = \frac{f'(x)\,g(x) - f(x)\,g'(x)}{g(x)^2} \tag{7.20}$$

Thus,

$$(I_C + \hat{\imath}_C) = C\frac{d(U_o + \hat{u}_o)}{dt} = -\frac{(U_o + \hat{u}_o)}{R} + \frac{\left[\left(U_g + \hat{u}_g\right)^2 {D_1}^2\, T + {U_g}^2\left(D_1 + \hat{d}_1\right)T\right] 2\, L\, U_o - \left[{U_g}^2 {D_1}^2\, T\, 2\, L\right](U_o + \hat{u}_o)}{(2\, L)^2\, {U_o}^2} \quad (7.21)$$

After applying the steady-state conditions:

$$\hat{\imath}_C = -\frac{\hat{u}_o}{R} + \frac{2\, U_g\, \hat{u}_g\, {D_1}^2\, U_o\, T}{2\, L\, {U_o}^2} + \frac{2\, {U_g}^2 U_o\, D_1\, \hat{d}_1\, T}{2\, L\, {U_o}^2} - \frac{{U_g}^2 {D_1}^2\, \hat{u}_o T}{2\, L\, {U_o}^2} \quad (7.22)$$

And simplifying terms:

$$\hat{\imath}_C = \hat{u}_o\left[-\frac{1}{R} - \frac{{U_g}^2 {D_1}^2 T}{2\, L\, {U_o}^2}\right] + \hat{u}_g\frac{U_g\, {D_1}^2\, T}{L\, U_o} + \hat{d}_1\frac{{U_g}^2 D_1\, T}{L\, U_o} \quad (7.23)$$

Therefore, the small-signal model can be represented graphically as in Fig. 7.11. Take into account that the terms that are multiplying the variable $\hat{u}_o$ are draining current due to its sign. However, in the circuit they shall appear as their inverse in order to place impedances and not admittances.

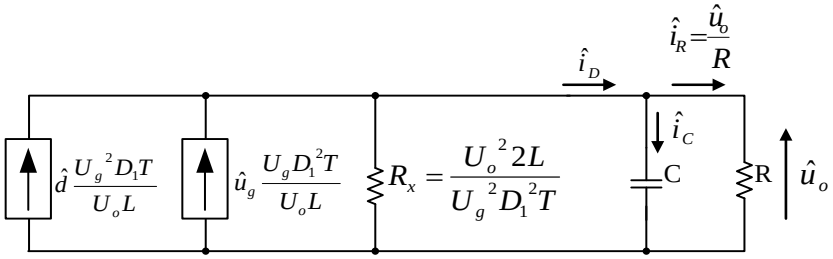

Fig. 7.11. Final model of the bidirectional DCM Flyback converter

We need to ensure that the $\hat{\imath}_D$ term accounts for effectively the same current in both Fig. 7.10 and Fig. 7.11. On one hand, in Fig. 7.10, i_D can be defined as:

$$i_D = \frac{U_o}{\frac{R}{1 + sCR}} \quad (7.24)$$

If the small-signal analysis is applied to (7.24), then:

$$(I_D + \hat{\imath}_D) = \frac{U_o + \hat{u}_o}{\frac{R}{1 + sCR}} \rightarrow \hat{\imath}_D = \frac{\hat{u}_o}{\frac{R}{1 + sCR}} \quad (7.25)$$

Therefore, as it was depicted in Fig. 7.11, they are indeed equivalent.

Special attention is given to the resistor R_x in Fig. 7.11. The value of this draining-current resistor can be proved that is the same as R. By definition, in DCM:

$$\frac{U_o}{U_g} = d_1\sqrt{\frac{R\,T}{2\,L}} \rightarrow \left(\frac{U_o}{U_g}\right)^2 = {d_1}^2\left(\frac{R\,T}{2\,L}\right) \qquad (7.26)$$

If (7.26) is substituted in R_x:

$$R_x = \frac{2\,L\,{U_o}^2}{{U_g}^2{d_1}^2 T} \rightarrow R_x = \frac{2\,L\,{d_1}^2 R\,T}{{d_1}^2 T\,2\,L} = R \qquad (7.27)$$

The model was tested using the software *PSIM*. Fig. 7.12 depicts the comparison between the simulated bidirectional Flyback operating as a PFC and the model developed in this section. Furthermore, a small perturbation in the duty cycle of the switches is applied to both cases in order to check that they effectively behave the same way.

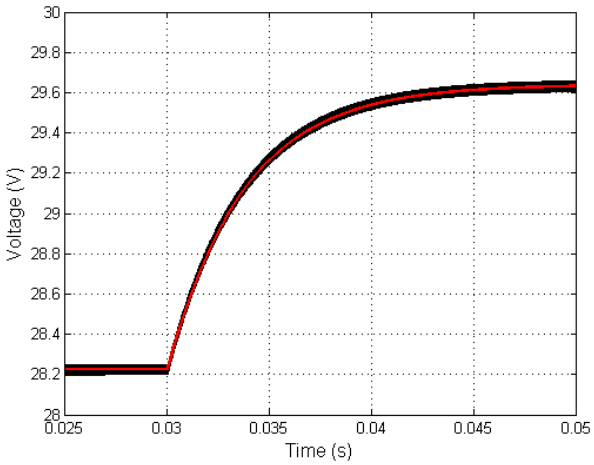

Fig. 7.12. Comparative between the simulated circuit (black) and the small-signal model (red) response

7.3.3 Analysis of control approaches

Once the converter is modelled, different control strategies can be carried out in order to regulate the DC bus voltage.

A. Classic control

The most simple control scheme of the DCM Flyback inverter for active PFC, consists on keeping the duty ratio constant during a line period [87]. In the case of ideal components, the input current would track down the input voltage waveform and thus, PFC is easily achieved. The duty ratio reference used to be calculated with a slow control loop with very small bandwidth controller that regulates the DC bus voltage. Nevertheless, there are some drawbacks in this operation mode: non-ideal effects like line voltage harmonics, high frequency switching delays, voltage snubbers needed due the leakage inductance of the transformer, and so on can spoil the sinusoidal shape of the line current.

Thus, the classic control is based on obtaining the transfer function between the variable to be controlled, U_o, and the control signal, d_1. Then, knowing the root locus of this transfer function, a controller would be designed, but keeping in mind that the bandwidth should be quite low.

Hence, from Fig. 7.11, the transfer function $G(s) = \frac{U_o}{d_1}$ can be defined as:

$$G(s) = \frac{U_o}{d_1} = \frac{{U_g}^2 d_1 T}{U_o L} \frac{R'}{1 + sCR'} \quad (7.28)$$

Where $R' = \frac{R_x R}{R_x + R}$

The bode diagram of this transfer function can be seen Fig. 7.13.

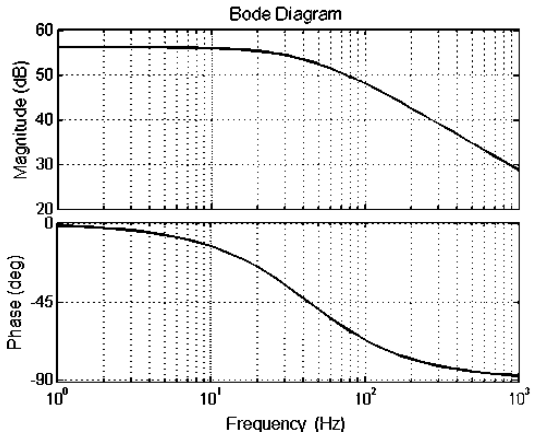

Fig. 7.13. Bode plot of the transfer function between the output voltage and the duty ratio

B. Proposed control: dynamic feature

The proposed control technique is based on designing the proper controller for the target transfer function compound by the output resistance (load) and the output capacitor: $G(s) = R/(1 + sCR)$ and it is also based on synchronise with the sinusoidal input voltage.

This target transfer function does not depend on any line frequency or input voltage but only in the RC system, which is constant and linear in every operation condition. Since a simple PI controller is desired in order to simplify the control algorithm, a zero-pole cancellation technique shall be applied, choosing the bandwidth of the controller at will. A first approach of the control diagram is depicted in Fig. 7.14. There is a voltage command that is compared to the actual voltage in the DC bus and then a PI controller corrects the error.

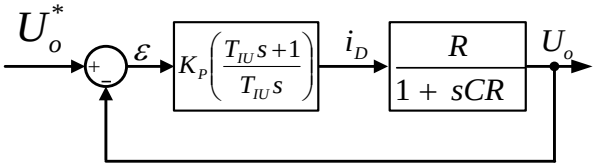

Fig. 7.14. Basic control diagram: first approach

Nevertheless, what is shown in Fig. 7.14 is not as simple as it seems. If the model is observed (Fig. 7.11), it can be seen that i_D and U_g are fully decoupled. However, the variable that is used to completely control a power converter is the duty ratio. It is needed to find the relationship within this duty and the current i_D like in Fig. 7.15. This dependence will be analysed taking into account the model of Fig. 7.11 and it shall be called "dynamic control". Later, even a simpler control will be performed and a different name shall be needed.

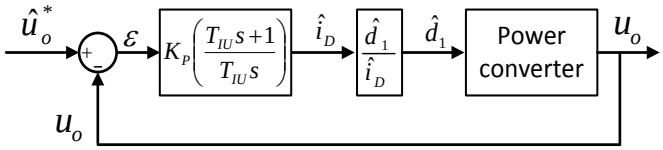

Fig. 7.15. Dynamic control diagram

Thus, this intermediate transfer function $G(s) = \hat{d}_1/\hat{\imath}_D$ is:

$$G(s)\rfloor_{\hat{d}_1,\hat{\imath}_D} = \frac{\hat{d}_1}{\hat{\imath}_D} = \frac{\hat{d}_1}{\hat{u}_o}\frac{\hat{u}_o}{\hat{\imath}_D} = \frac{2\,L\,U_o}{{U_g}^2\,d_1 T}\cdot\frac{\frac{s}{2}+\frac{1}{RC}}{s+\frac{1}{RC}} \qquad (7.29)$$

However, as mentioned before, the controller is tuned for the transfer function of the RC output net. The regulator is defined as:

$$R(s) = K_p\left(\frac{1+s\,T_{iu}}{s\,T_{iu}}\right) \qquad (7.30)$$

Considering zero-pole cancellation, the parameters K_p and T_{iu} can be calculated knowing the values of the output capacitor, the resistance and obviously, the desired bandwidth (B_w):

$$K_p = 2\,\pi\,Bw\,C \qquad (7.31)$$

$$T_{iu} = R\,C \qquad (7.32)$$

Fig. 7.16 shows the root locus of the system with a zero-pole cancellation controller tuned with a 100 Hz bandwidth as well as the step response upon a step in the reference, just to prove the time response of the system. Theoretically, this bandwidth has no limitation due to the resulting root locus.

On the other hand, Fig. 7.17 depicts different bode diagrams of the closed-loop system for several controller bandwidths. Therefore, the most bandwidth the controller has, the bigger the overall bandwidth of the close-loop system is.

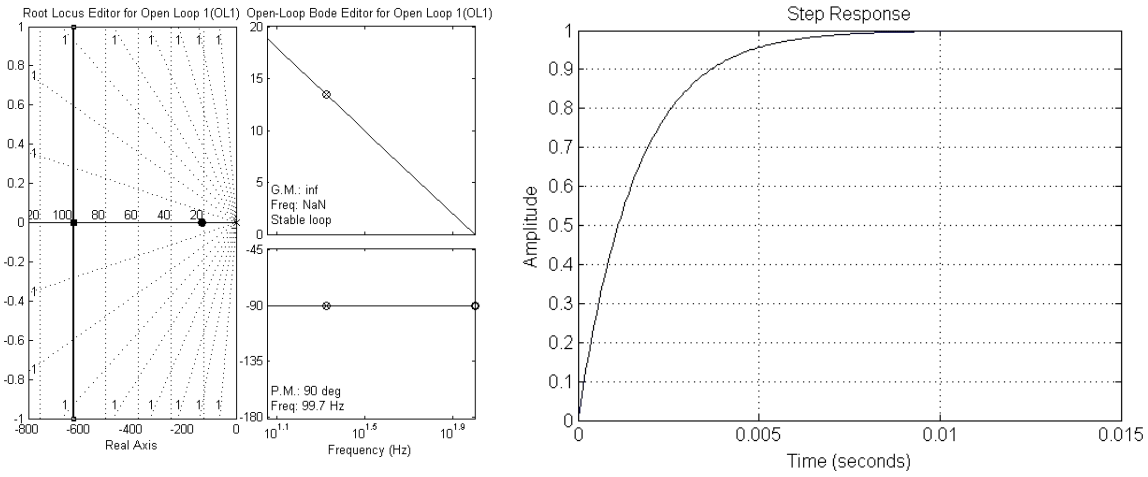

Fig. 7.16. Root locus with a 100 Hz bandwidth controller and step response

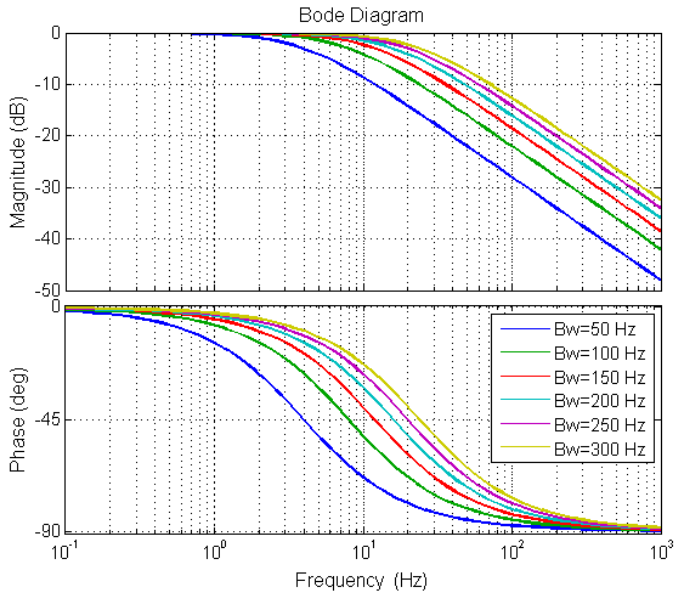

Fig. 7.17. Closed-loop bode diagram depending on the bandwidth of the controller

C. Proposed control: static feature

Instead of using the adjustment proved in (7.29), which introduces additional dynamics that might destabilise the closed-loop operation performance, there is the possibility of employing a simpler expression. This ratio can be based on a constant relationship, therefore avoiding the extra dynamics, but guaranteeing a proper closed-loop operation. Assuming that the input and the output powers are equivalent, which is assuming the efficiency is a 100% and neglecting the effect of the input filters, it can be stated (according to Fig. 7.2):

$$\langle P_i \rangle = \langle P_o \rangle \rightarrow U_g \langle i_{L_P} \rangle = U_o \langle i_D \rangle \qquad (7.33)$$

Including (7.3) and (7.15) in (7.33):

$$d_1 = \sqrt{\frac{2\,L\,U_o}{\left(U_{g\_pk}\right)^2\,T}\langle i_D\rangle} \qquad (7.34)$$

That is the relation between the output current and the duty ratio. Graphically, it can be represented as in Fig. 7.18:

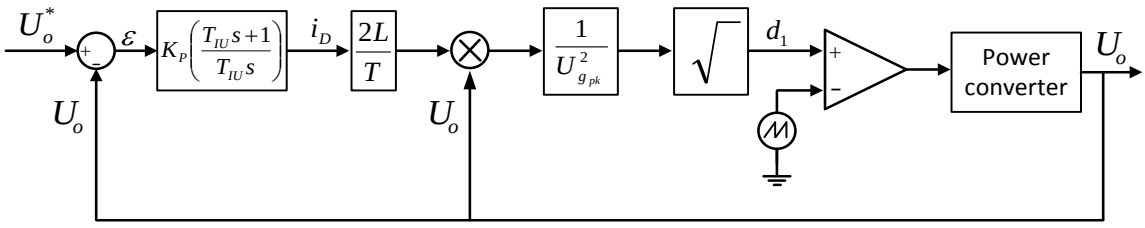

Fig. 7.18. Static control diagram

The design of the PI controller is exactly the same as the one proposed before, considering only the RC output network. The only change is the adaptation between i_D and d_1.

7.3.4 Experimental results

A built prototype of the PFC stage has been built and tested. TABLE 7.I gathers main converter parameters. In the annexes the methodology to obtain those values can be found.

Fig. 7.19 shows the full control scheme. The voltage sensors measure both the grid and DC bus voltages and then, after the adequate signal conditioning, the signals are translated to the digital signal processor (DSP) voltage levels, which is between 0 and 3.0 V. Then, the analog-to-digital converter (ADC) of the microcontroller processes the information and the control makes a decision. The PWM module generates the pulses for the switches and an intermediate driver transform these signals to the adequate gating signals.

TABLE 7.I

PROTOTYPE COMPONENTS

Parameter	***Symbol***	***Value***
Grid side winding	L	$500\,\mu H$
Load side windings	L_{s_1}, L_{s_2}	$125\,\mu H$
DC bus capacitor	C	$75\,\mu F$
Primary switches	S_1, S_2	*FQA8N100C*
Secondary switches	S_A, S_B, S_C	*MUR860*
Digital signal processor (DSP)		*F28335PGFA*
Average DC link voltage	U_o	*100 V*
Nominal output power	P_o	*100 W*
Average output current	i_D	*1 A*
Output power step	ΔP_o	*23%*
Input voltage step	ΔU_g	$30\ V_{rms}$

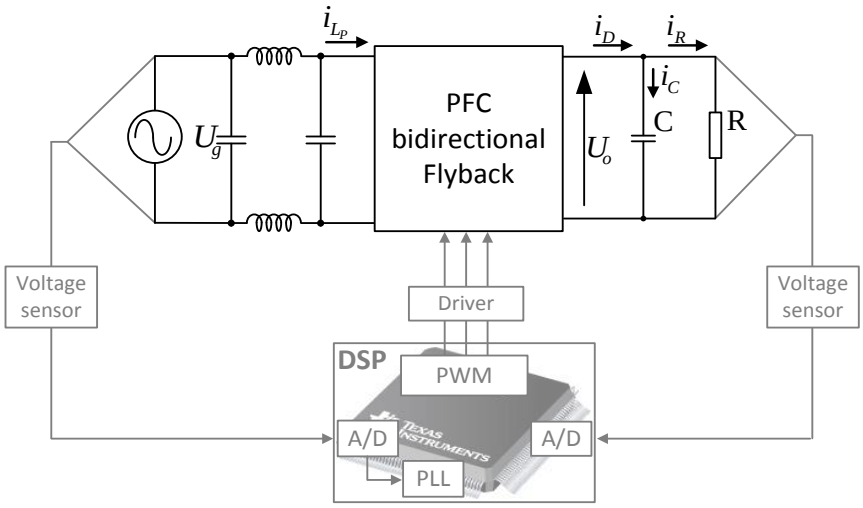

Fig. 7.19. Complete control scheme

The next paragraphs deal with a comparison between both control techniques outlined in the previous analysis, the classic control and the proposed one. Initially, both controllers have the same bandwidth in order to compare their behaviour to changes in the load or in the input voltage. Furthermore, the analysis of the harmonic content of the input current and the THD will be reflected. Both dynamic and static feature control techniques were tested experimentally. However, the static one showed a better performance at high bandwidths.

In Fig. 7.20 and Fig. 7.21 the experimental results upon input voltage and load disturbances with 50 Hz classic control are shown. As it can be seen, the system needs in the order of 20 ms to recover from any disturbance. The red rectangle marks when these changes happen.

On the other hand, Fig. 7.22 and Fig. 7.23 show the same experiments but using the proposed control, also with a 50 Hz bandwidth.

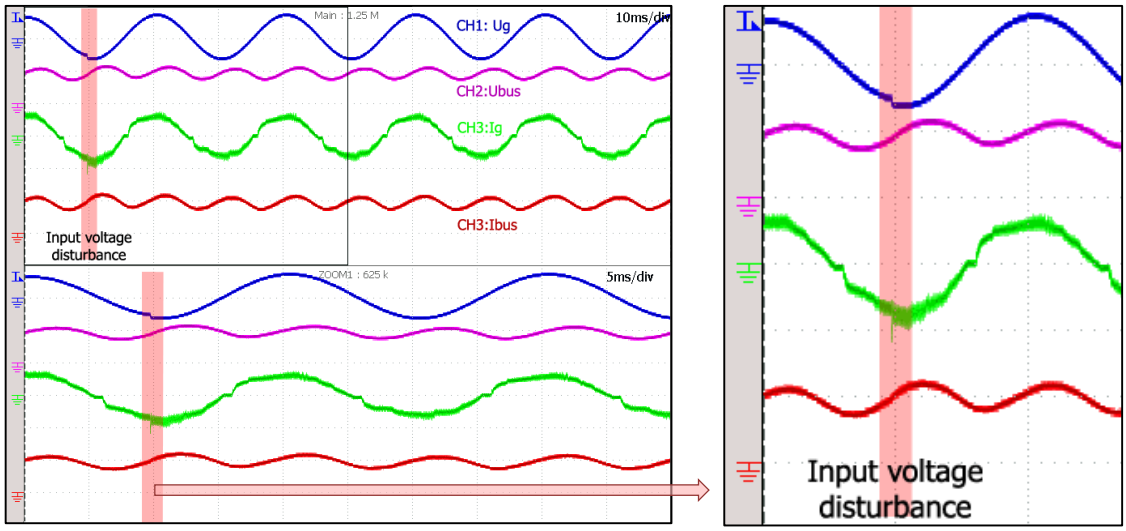

Fig. 7.20. Experimental waveforms with a 50 Hz bandwidth classic controller and a sudden change in the input voltage (210 to 240 V_{rms}). U_g: input voltage (500 V/div); U_{bus}: bus voltage (100 V/div); I_g: input line current (1 A/div); I_{bus}: bus current through the load (1 A/div)

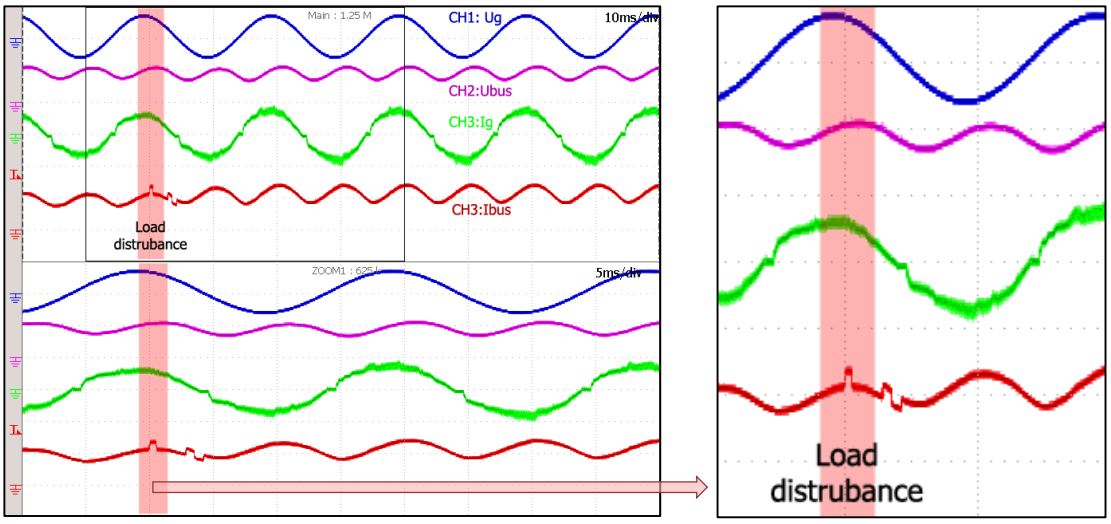

Fig. 7.21. Experimental waveforms with a 50 Hz bandwidth classic controller and a sudden change in the load (23%). U_g: input voltage (500 V/div); U_{bus}: bus voltage (100 V/div); I_g: input line current (1 A/div); I_{bus}: bus current through the load (1 A/div)

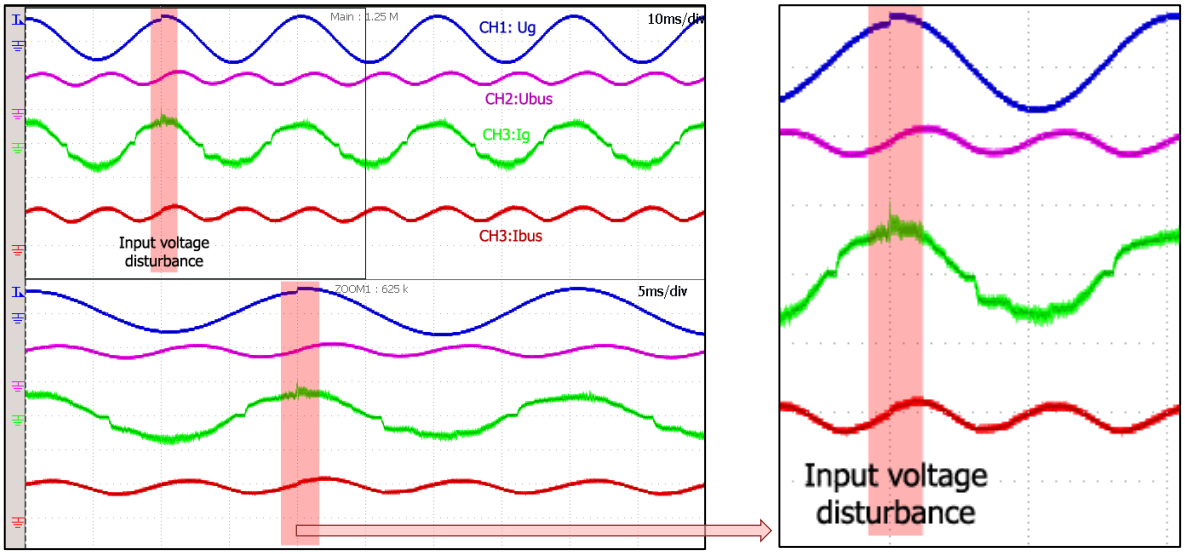

Fig. 7.22. Experimental waveforms with the 50 Hz bandwidth proposed controller and a sudden change in the input voltage (210 to 240 V_{rms}). U_g: input voltage (500 V/div); U_{bus}: bus voltage (100 V/div); I_g: input line current (1 A/div); I_{bus}: bus current through the load (1 A/div)

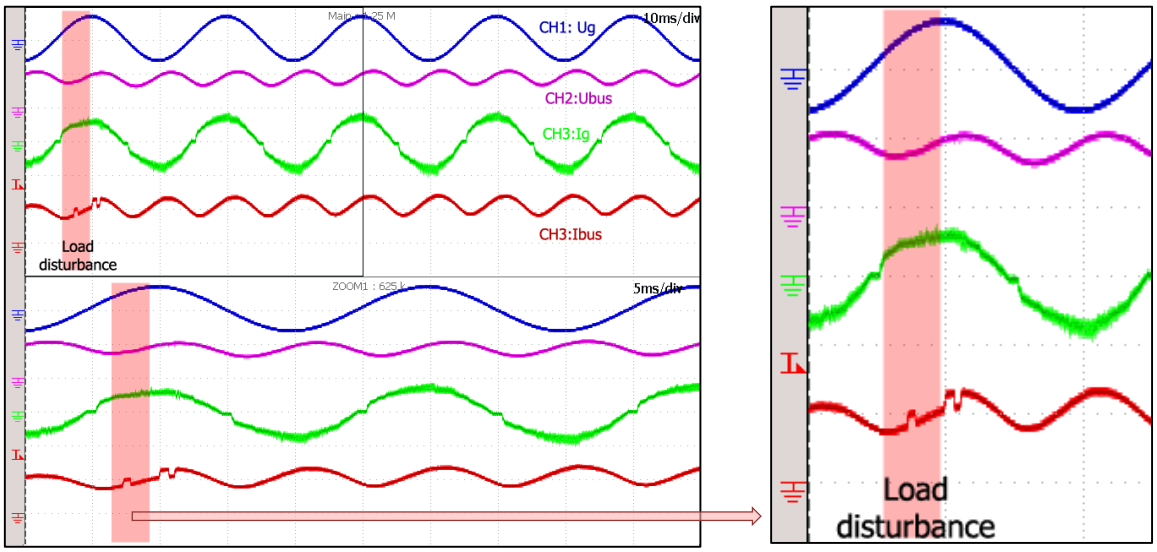

Fig. 7.23. Experimental waveforms with the 50 Hz bandwidth proposed controller and a sudden change in the load (23%). U_g: input voltage (500 V/div); U_{bus}: bus voltage (100 V/div); I_g: input line current (1 A/div); I_{bus}: bus current through the load (1 A/div)

At a first sight, it may seem that both controllers have the same behaviour (see Fig. 7.24). In terms of settling time they behave in a similar manner, but, the analysis of the harmonic content and the THD is revealing, as it can be seen in Fig. 7.25. With the same bandwidth, the proposed controller behaves better in terms of THD and harmonic content.

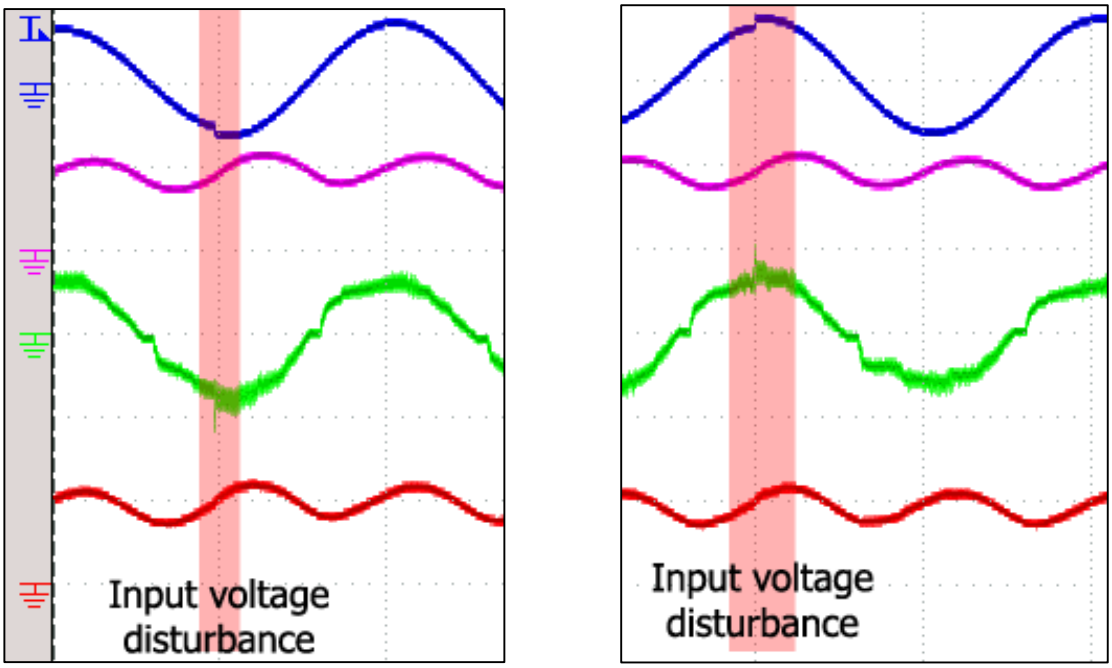

Fig. 7.24. Comparison between classic control (left) and the proposed one (right)

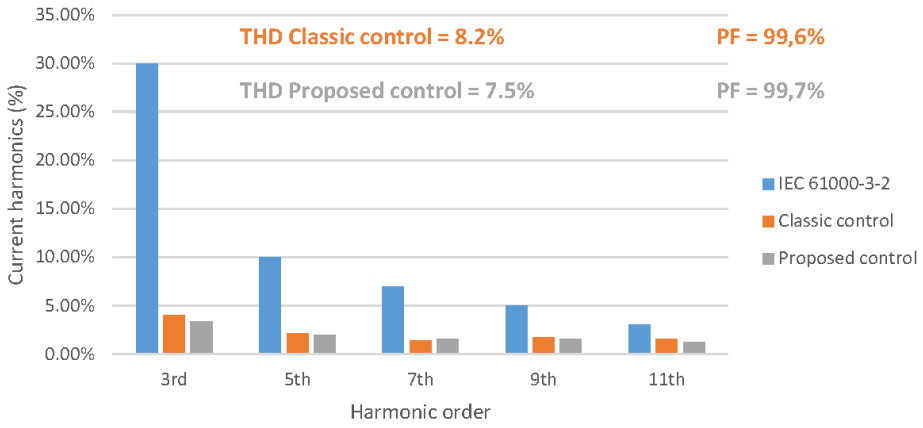

Fig. 7.25. Measured harmonics of the input current and imposed limits by the IEC 61000-3-2

High bandwidth control experiment

Finally, it was tested the power converter with a 250 Hz bandwidth controller. The classic control was not able to reach it but, on contrary, the proposed control did. Fig. 7.26 shows the experimental results with the proposed control operating with a high bandwidth of 250 Hz.

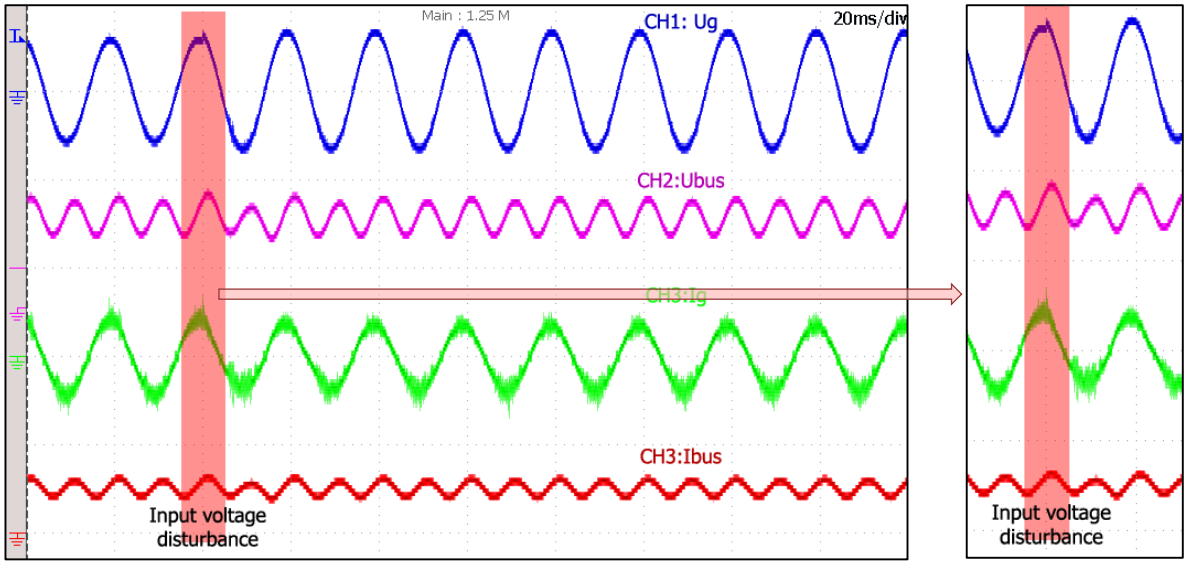

Fig. 7.26. Experimental waveforms with the 250 Hz bandwidth proposed controller and a sudden change in the input voltage (210 to 240 V_{rms}). U_g: input voltage (500 V/div); U_{bus}: bus voltage (100 V/div); I_g: input line current (2 A/div); I_{bus}: bus current through the load (2 A/div)

In Fig. 7.27 are depicted the experimental waveforms with the maximum bandwidth reached with the classic controller, 70 Hz.

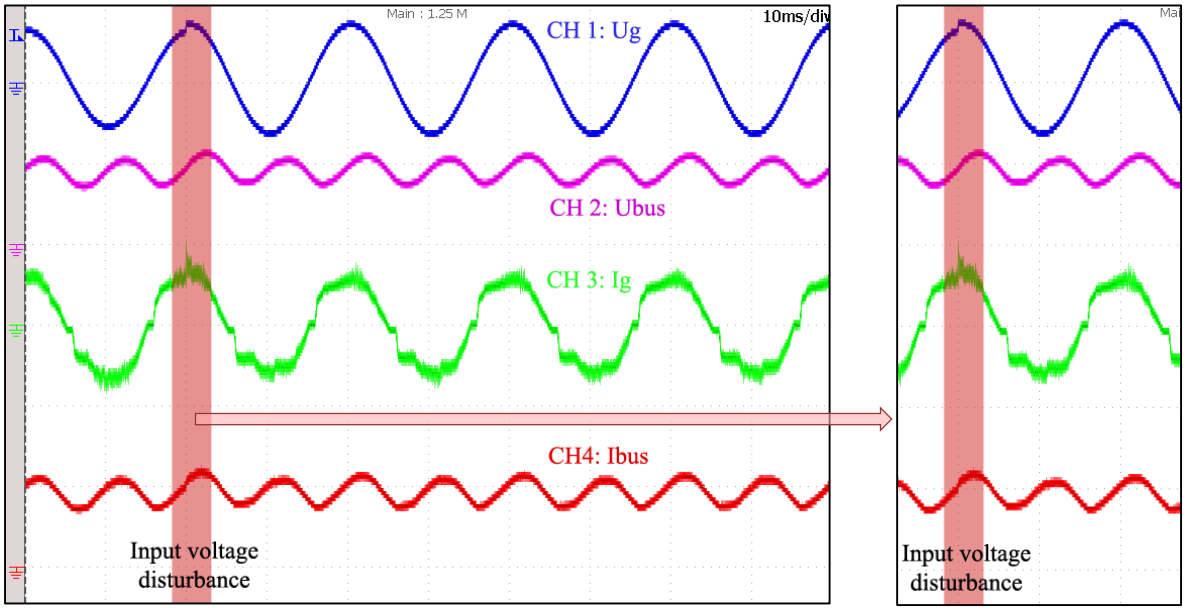

Fig. 7.27. Experimental waveforms with a 70 Hz bandwidth classic controller and a sudden change in the input voltage (210 to 240 V_{rms}). U_g: input voltage (500 V/div); U_{bus}: bus voltage (100 V/div); I_g: input line current (1 A/div); I_{bus}: bus current through the load (1 A/div)

Fig. 7.28 compares the harmonic content obtained with the proposed controller for different bandwidths. The results were stunning since the THD and the harmonic content was even improved when the bandwidth was increased.

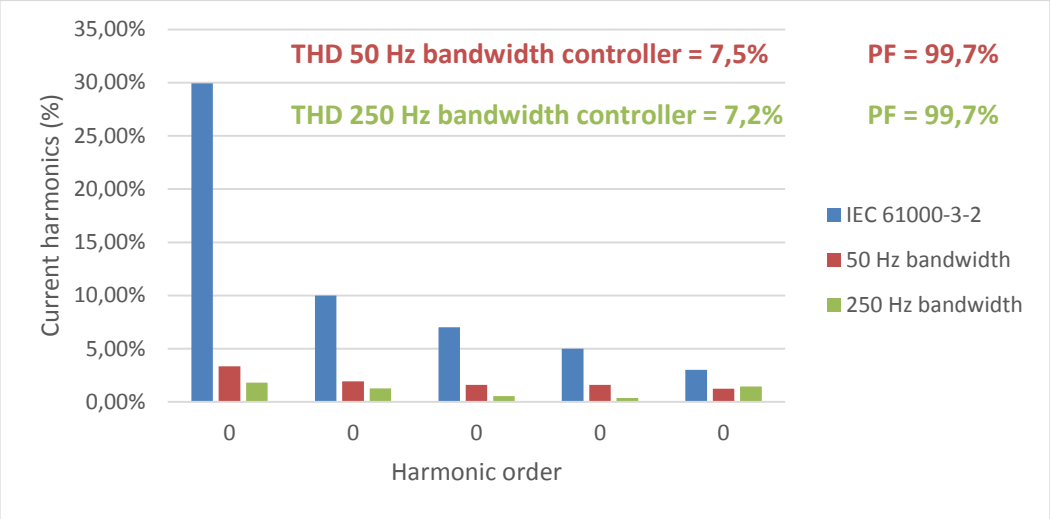

Fig. 7.28. Measured harmonics of the input current comparing two different bandwidths of the proposed controller

In terms of efficiencies, TABLE 7.II summarises the obtained information.

TABLE 7.II

EFFICIENCY OF THE CONVERTER DEPENDING ON THE CONTROL

Type of control	*Bandwidth*	*Efficiency*	*THD*
Classic control	50 *Hz*	*88.1 %*	*8.2%*
Proposed control	50 *Hz*	*87.8 %*	*7.5%*
Proposed control	250 *Hz*	*85.1 %*	*7.0%*

7.3.5 Effect of the leakage inductance

The effect of the leakage inductance can be seen in the voltage stress of the grid side switches. There is an overshoot when the switch is turned off and the current stops circulating through.

In this built prototype, the leakage inductance accounts for 1.5% of the magnetising inductor and the effect can be appreciated in Fig. 7.29.

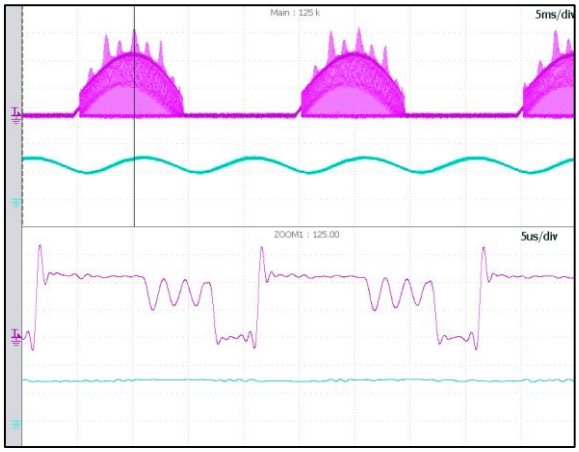

Fig. 7.29. Effect of the leakage inductance in one of the grid side switches. CH1: mosfet S_1 voltage (purple, 200 V/div). CH2: input current (green, 500 mA/div)

These voltage stresses can be reduced by placing a snubber circuit in the grid's side of the Flyback transformer. There are several kind of snubbers: active clamps, RCD dissipative networks, regenerative circuits with inductors and capacitors. These circuits are well known for classic DC-DC Flyback converters but they need to be modified for the bidirectional one due to the both directions current circulation. In the case, there is no snubber, thus the semiconductors have to be oversized in order to bear with the voltage stresses.

7.4 Summary and conclusions

This chapter has studied a novel kind of control scheme for DCM PFC Flyback converters. First of all, the mathematical model of the converter was developed using the small-signal analysis. It was proved that this analysis is valid also to AC inputs if peak values are taken into account. Then, a classic control strategy was studied and experimental results were obtained.

Afterwards, the proposed control technique was explained and tested with simulations and experimentally. Finally, they were compared in terms of bandwidth of the regulator, harmonic content of the input current and its THD, yielding to a better performance than the one obtained with the standard controller.

Thus, the proposed control with high bandwidth improved the THD and the harmonic content of the input current when compared to the classic control. Nevertheless, this novel kind of control scheme affects the efficiency of the converter. The dynamics involved in the whole system (control and power converter) avoid reaching higher bandwidths experimentally. Further studies in this issue can be done in order to detect the exact reason why the converter trips at bandwidths beyond 250 Hz.

Chapter 8

Unified switching strategy for the bidirectional DCM Flyback converter for grid interface

This chapter defines, explains and implements a unified switching pattern for the switches in a bidirectional DCM Flyback converter, used for connecting the individual elements (nodes) of a street lighting system to the mains facility. In every node, the DC bus links the different existing stages, such as lamp driver, energy storage stage, power generation stage and PFC grid interface. The proposed switching patterns enable for a smooth transition between the behaviour of the grid interface stage from inverter to rectifier mode, therefore enabling for a unified control method of the converter, valid for every operation condition.

The output of the proposed strategy provides the pulses for every switch in the converter in the adequate sequence, therefore simplifying the design and implementation of the power and control stages. The proposed switching pattern is validated through simulation and experimental results.

8.2

8.1 Introduction

As mentioned in previous chapters, small-scale applications for PV and wind energy exploitation are gaining more and more visibility. From the point of view of the interfacing stage to the harvesting system, the connection with the grid can be isolated or non-isolated by means of a transformer. It depends on the local country regulations [94]. In some cases, the galvanic isolation requirement is done either by a low-frequency (LF) step-up transformer on the grid side or by a high-frequency (HF) transformer on the DC side of the converter (see Fig. 8.1). In other cases, the galvanic isolation can be avoided whether another technological solution is used to prevent undesired common mode voltages or harmful current loops through groundings or neutral connections.

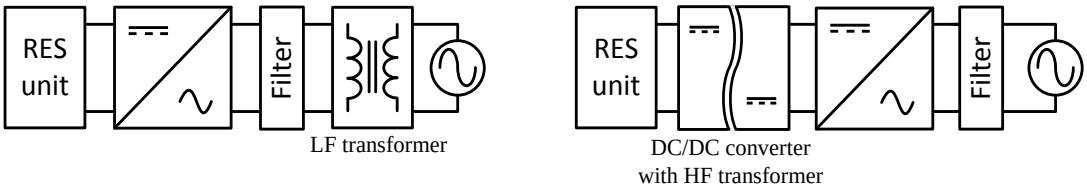

Fig. 8.1. Grid-connected RES system using an inverter with galvanic isolation: (left) grid-side LF transformer or (right) DC side HF transformer

A manifold of different power injection topologies have already been studied and are extensively reported in the technical literature [27], [88], [90], [91]. Most of the power inverter stages consist of an H-bridge converter due to its modularity, high reliability, good performance and low cost [88]. However, the DC bus voltage in such topology must have a value higher than the peak value of the mains voltage, in order to be able to inject current into the mains (Fig. 8.1, right). Alternatively, this condition might be fulfilled by including a step-up bulky LF transformer which would increase cost and size of the stage (Fig. 8.1, left).

However, the scheme can be modified as depicted in Fig. 8.2. By using a single DC-AC stage that includes a HF transformer, on the stages discussed above would be avoided. This option provides galvanic isolation and operates as an inverter. The bidirectional Flyback studied in the previous chapter would accomplish these conditions. In addition, this topology solves the high voltage mismatch between terminals [27], [169], [170], [171], [172] and it can be used as an input PFC converter, as well as a High Frequency (HF) inverter.

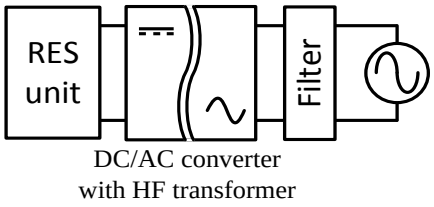

Fig. 8.2. Grid-connected RES system with galvanic isolation and one single power stage

8.2 Inverter mode background

At this point, the inverter mode operation of the Flyback based stage under study needs to be explained. Under inverter operation, the energy would flow from the DC bus to the utility grid. As it will be shown, every existing switch shall be used. The first detailed analysis of the inverter mode was done in [27] although in this case both lamp and renewable energy source and its correspondant maximum power point tracker (RES+MMPT) can be simultaneously connected to the DC bus and sharing energy. In [27] there was a relay which allows to choose between the lamp or the RES that makes the system valid only for a PV panel. For example, if the RES is a WT, then the relay would be useless because a WT does not distinguish day from night since it can be operating all day. In [27], the relay was placed in order to connect the PV panel during the day and the lamp during the night.

8.2.1 Operational principles of the inverter stage

Like in the rectifier mode, there are different operation intervals during the inverter mode operation. The most basic control was proposed originally in [27]. The circuit is based on the bidirectional Flyback inverter plus a LC filter with a cut-off frequency a decade below switching frequency in order to eliminate the HF ripple as depicted in Fig. 8.3. In the following subsection, the most basic switching strategy upon inverter mode is explained. However, this concept is presented just to enlighten the circulation of the current through the switches, as it was done in the previous chapter with the rectifier mode. In this current chapter, the following basic switching strategy developed in [27] is not applicable due to the fact that it is not compatible with the rectifier mode and therefore, a common solution for both modes shall be studied and tested.

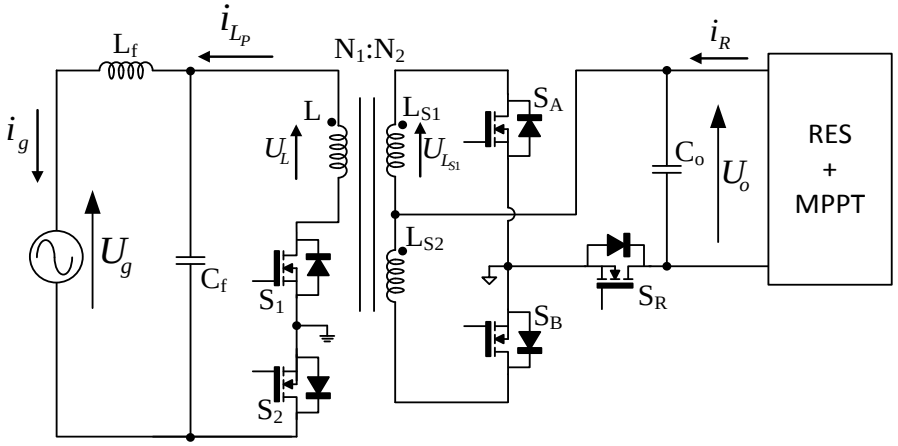

Fig. 8.3. Inverter mode during the positive semi cycle of the grid voltage

According to [27] and the arrows depicted in Fig. 8.3, the main waveforms of voltages and currents are shown in Fig. 8.4. Notice that the employed nomenclature corresponds to [27] and it will vary in the forthcoming sections of this chapter.

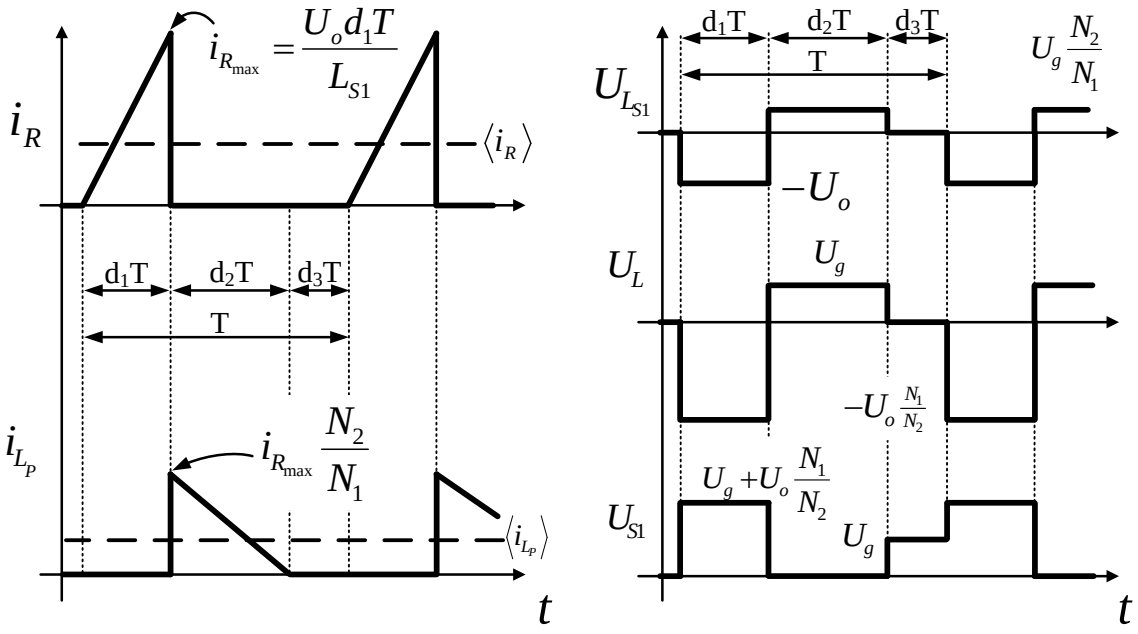

Fig. 8.4. Main Flyback waveforms according to [27]

Thus, for a switching period, *T*, the intervals of the power converter during the positive semi cycle of the grid voltage are explained ahead. It would be analogue for the negative one by changing the switches that are fired and the bus side inductors. The injection of a sinusoidal current into the AC mains is done by firing the switches S_1 and S_2 with a sinusoidal pulse width modulation (SPWM), as depicted in Fig. 8.5.

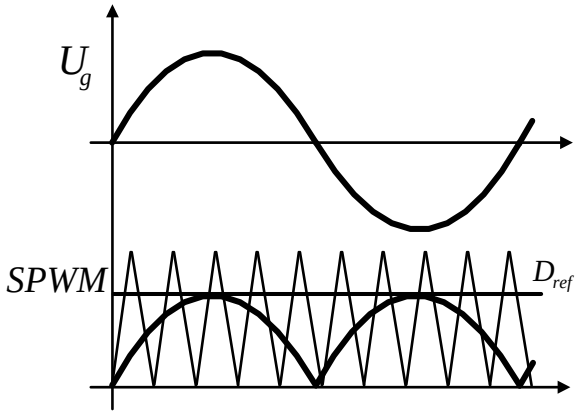

Fig. 8.5. SPWM modulation

First interval

During the first interval, the inductor L_{S1} is charged through the switch S_A and the diode of S_R (Fig. 8.6). Therefore, the magnetising inductor during inverter mode is in the bus side and it depends on the sign of the grid voltage.

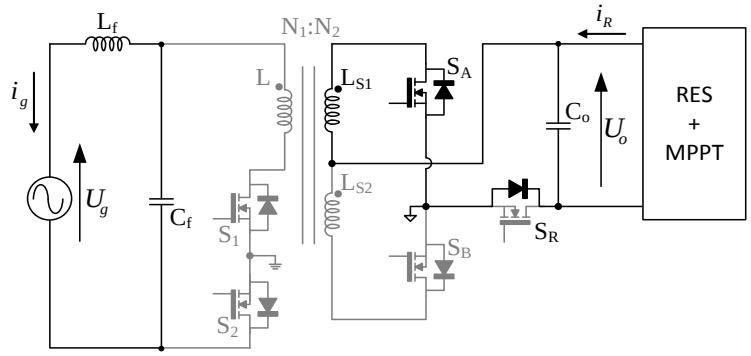

Fig. 8.6. First interval during inverter mode

Second interval

During the second interval, the energy stored in L_{S1} flows towards L in the grid side. In order to inject the current into the mains, switch S_1 must be turned off while S_2 is turned on (Fig. 8.7). During the negative semi cycle, the current would flow through S_1 and the diode of S_2.

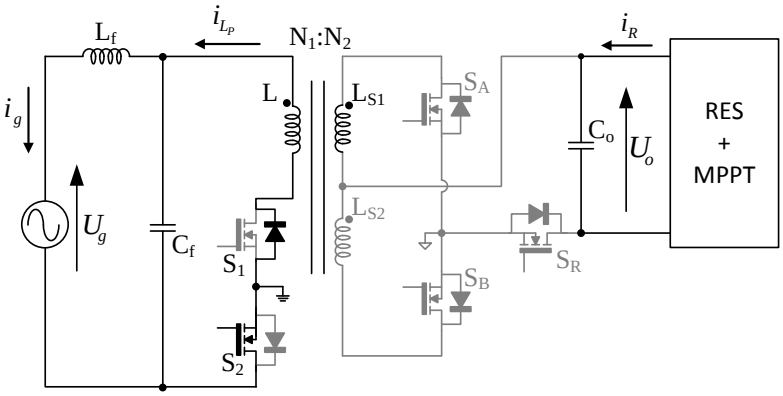

Fig. 8.7. Second interval during inverter mode

Third interval

The third interval starts when the inductor is fully discharged. During this interval, the filter capacitor, C_f, must be able to provide the injected current with a small voltage variation (Fig. 8.8).

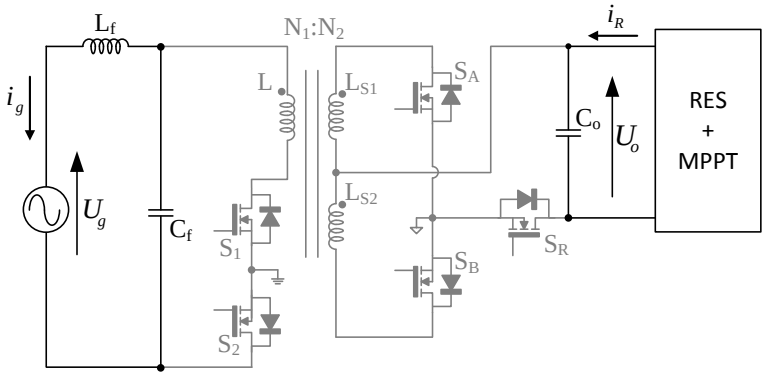

Fig. 8.8. Third interval during inverter mode

8.3 Proposed power stage

So far, the operation of the electronic stage, within a switching period, in both inverter and rectifier mode has been discussed. Therefore, from the input voltage point of view, the device can operate within the four quadrants. Indeed, for positive input voltage, the current can be positive or negative (rectifier or inverter mode), and thus the circuit can work in I and II quadrants). Considering the AC line input voltage, the same discussion can be carried out for negative input voltage, yielding to III and IV quadrants operation. Therefore, theoretically it is possible to operate the system for an arbitrary current waveform, what enables the system for line compensation. Fig. 8.9 depicts the basic diagram of a lighting system with PV and WT generators, the lamp and the AC mains. Each arrow represents a power conversion and its direction: unidirectional or bidirectional. As it can be seen, there are different power stages, which are all connected in one common point, the DC bus.

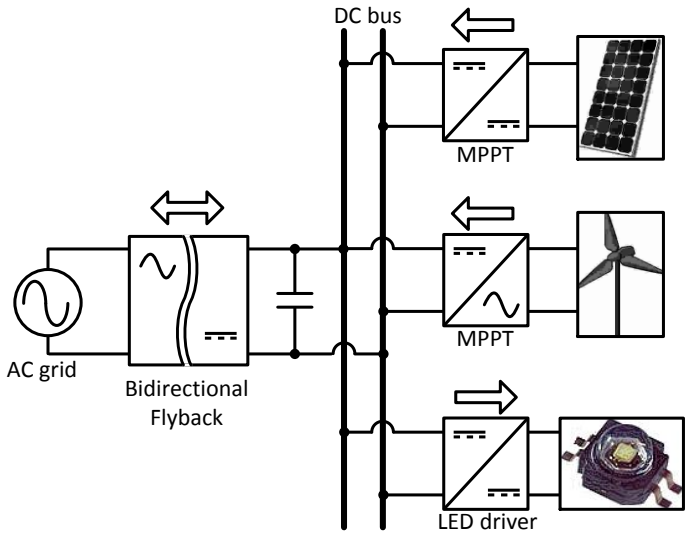

Fig. 8.9. Conceptual electrical diagram

In the case a WT is connected to the DC bus through a dedicated converter, and considering the energy flow towards the utility grid, the configuration shown in [27] (Fig. 7.8) using a relay switch is not valid, as mentioned before.

Unlike the control of a full bridge that does automatically move the power to or from the DC bus without changing the firing scheme of the switches, in [27], the bidirectional Flyback converter operates in both rectifier and inverter modes with different firing schemes. This issue is solved in this section where a PWM switching strategy of the bidirectional Flyback converter in DCM is proposed and experimentally validated, for both power flow directions.

From Fig. 8.9, considering the operation mode in which the lamp is turned on and the PV panel is disabled (e.g. night operation of the system). Upon no energy generation from the WT (i.e. no wind or almost no wind), the bidirectional Flyback is operating as a PFC, maintaining a certain level of voltage in the DC bus. However, if there is a sudden change in the conditions and wind starts to blow, the WT begins to generate power enough to increase the DC bus voltage. This, in turn, tends to decrease the power demanded from the mains and thus, the PFC begins to demand less current to keep the DC bus steady.

Nevertheless, at a given point, the power from the WT might be greater than the power required by the lamp. Hence, the extra power could be send back to the utility grid and thus the grid current must be negative if the DC bus voltage is kept constant. Therefore, the Flyback must work as a controlled inverter and not as a PFC anymore. In addition, this change must be fluent and neat, keeping the DCM condition unchanged.

The topology described above can be seen in Fig. 8.10, where the resistor accounts for the lamp stage and the WT with the MPPT can be simulated as a dedicated block.

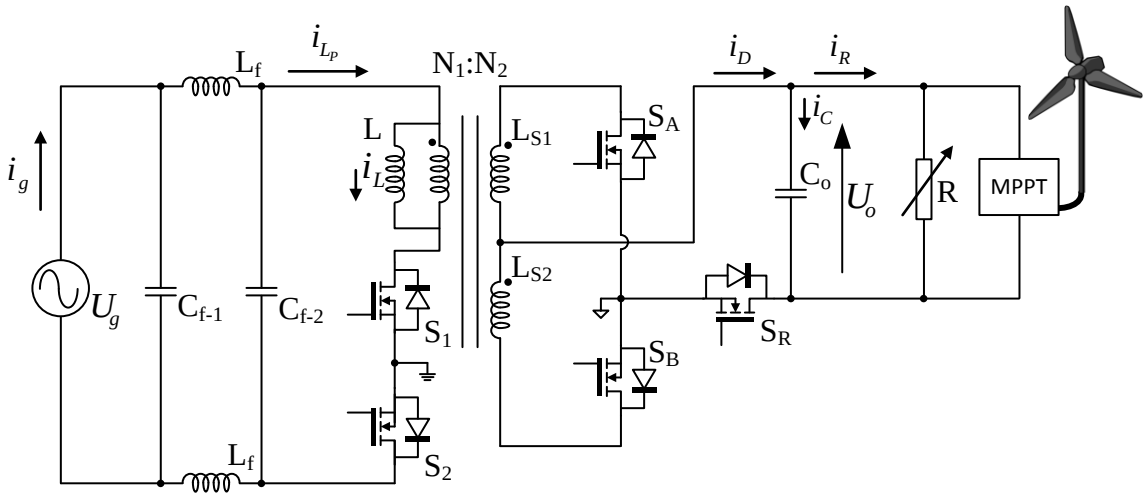

Fig. 8.10. Proposed topology changing the lamp stage by a variable resistor

8.3.1 Switching scheme of the bidirectional Flyback converter

In order to define the switching pattern compatible with both rectifier and inverter modes, and taking into account that the change of operation mode might take place stochastically, the following considerations need to be taken into account:

- DCM operation is kept during both operation modes thus the magnetising inductor has to be discharged in every switching period.
- There are three possibilities for the magnetising inductor depending on the operation mode and on the sign of the grid voltage.
- The converter is working in steady state, therefore every parameter instant value is repeated each switching time, *T*.

Duties calculation

When the converter operates as a PFC (rectifier mode), the line input voltage and the most characteristic currents can be depicted as in Fig. 8.11:

- i_g: grid current
- U_g: grid voltage
- i_D: bus current
- i_{LP}: grid side inductor current

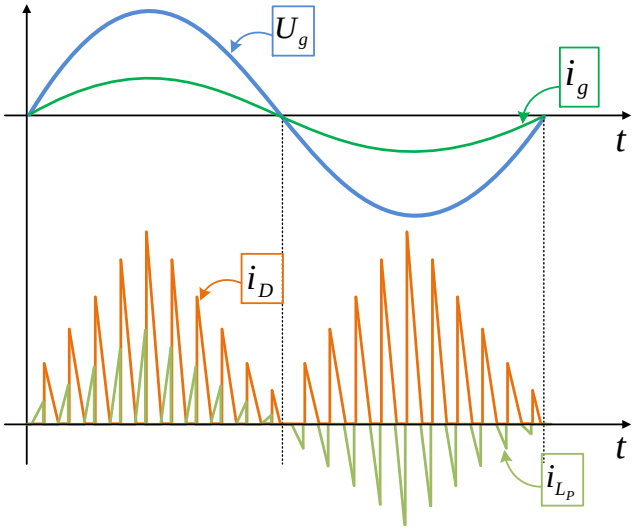

Fig. 8.11. Input voltage and currents through L_f, L and i_D during rectifier mode

These currents are detailed for a switching period, *T*, in Fig. 8.12.

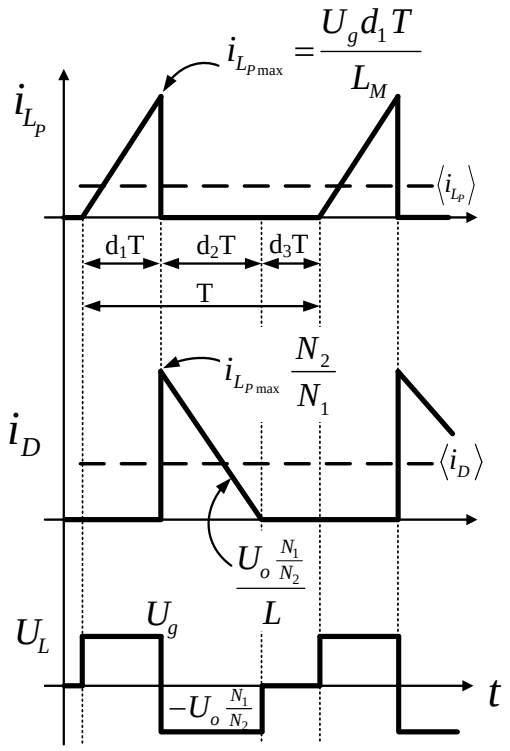

Fig. 8.12. Flyback inductor currents and inductor voltage (rectifier mode) seen from grid side

Assuming that d_1 is the duty ratio of the grid side switches, S_1 and S_2 while d_2 shall be the one of the bus side switches, S_A and S_B and then, according to Fig. 8.12, the average input current for every switching period can be defined as:

$$\langle i_{L_P} \rangle = \frac{1}{T}\int_0^{d_1 T} \frac{U_{g_{pk}} \sin(\omega t)}{L}\,\tau\, d\tau = \frac{U_{g_{pk}} \sin(\omega t)}{L}\frac{{d_1}^2 T}{2} = I_{pk}\sin(\omega t) \qquad (8.1)$$

where d_1 is the duty ratio of the grid side switches, S_1 and S_2, d_2 is the duty ratio of the bus side switches, S_A and S_B, T is the switching period, L the magnetising inductance of the grid side inductor and $U_{g\,pk}$ the peak value of the grid voltage.

Thus, from (8.1), a new expression for d_1 can be written:

$$d_1 = \sqrt{\frac{I_{pk}\sin(\omega t)}{U_{g_{pk}}\sin(\omega t)}\frac{2L}{T}} = \sqrt{\frac{I_{pk}}{U_{g_{pk}}}\frac{2L}{T}} \qquad (8.2)$$

The expression of d_2 that guarantees DCM operation is obtained based on assuring the fully discharge of the inductor, that, seen from the grid side, yields to:

$$i_{L_P} = i_{L_{Pmax}} - \frac{U_o \frac{N_1}{N_2}}{L} d_2 T \qquad (8.3)$$

Thus, making $i_{LP} = 0$:

$$i_{L_{Pmax}} = \frac{U_o \frac{N_1}{N_2}}{L} d_2 T \rightarrow d_2 = \frac{i_{L_{Pmax}} L}{U_o \frac{N_1}{N_2} T} \qquad (8.4)$$

On the other hand, $i_{LP\,max}$ can be calculated for every switching period as follows:

$$i_{L_{Pmax}} = \frac{U_{g_{pk}} \sin(\omega t)}{L} d_1 T \qquad (8.5)$$

Thus, combining (8.4) and (8.5):

$$d_2 = \frac{\frac{U_{g_{pk}} \sin(\omega t)}{L} d_1 T\, L}{U_o \frac{N_1}{N_2} T} = \frac{U_{g_{pk}} \sin(\omega t) d_1}{U_o \frac{N_1}{N_2}} \qquad (8.6)$$

And since the duty cannot be negative:

$$d_2 = \frac{\left|U_{g_{pk}} \sin(\omega t)\right|\, d_1}{U_o \frac{N_1}{N_2}} \qquad (8.7)$$

After the discharge of the inductor, the system keeps $i_L = 0$ until the next switching period begins. This last interval is called dead time (d_3).

As shown in Fig. 8.10, the operative sequence is d_1T for charging, d_2T for discharging and d_3T as the dead time when the converter is operating as controlled rectifier.

However, it is critical to notice that the duty ratio intervals sequence will change upon inverter mode as it may be seen in Fig. 8.13 whether it is considered d_1 for the grid side switches duty ratio and d_2 for the bus side ones.

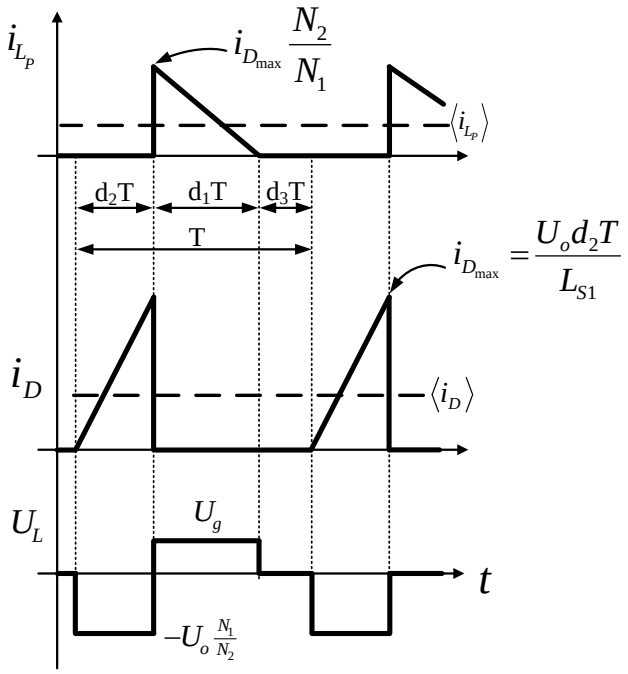

Fig. 8.13. Flyback inductor currents and inductor voltage (inverter mode)

This time, the magnetising inductor is the one on the bus side and it will be charged through the switches S_A and S_B (depending on the grid voltage sign) for a time interval equal to $d_2 T$. Afterwards, it comes the discharge of the Flyback transformer in the grid side by means of the switches S_1 and S_2, lasting d_1T seconds. Finally, so as to fulfil the DCM requirement, the dead time shows up, d_3T.

Even though rectifier mode and inverter mode have different sequences, the mathematical expressions to calculate the duties are the same in both cases. The switching pattern for both modes in terms of the magnetising inductors can be seen in Fig. 8.14. In rectifier mode, the transformer charges through L and during inverter mode, through L_s.

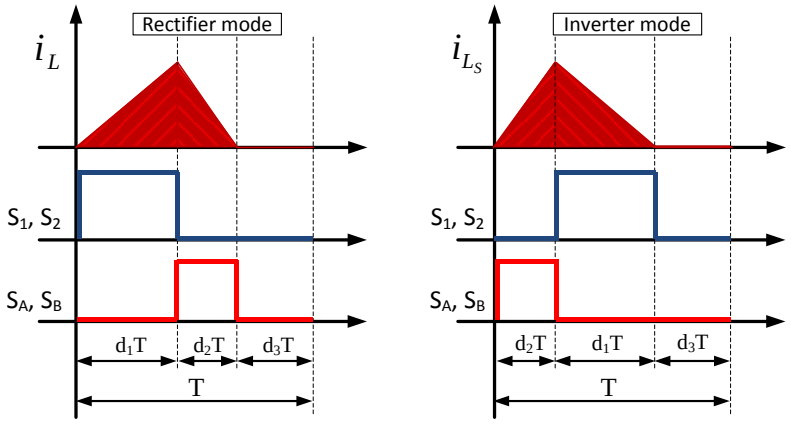

Fig. 8.14. Switching patterns in (left) rectifier mode and (right) inverter mode

References convention for duty ratios and current signs

Hence, Fig. 8.14 defines a problem. The control programed in the DSP must identify the operation mode that is currently needed and it has to adapt the switching of the transistors. Therefore, an agreement for the duty ratios is needed. By convention, it is assumed that if the current reference I_{pk} that is shown in (8.2) is bigger than zero, then the converter will operate in rectifier mode and the Flyback transformer would be charged through the inductor *L*. On the other hand, when I_{pk} would be lower than zero, then it would work in inverter mode. This convention allows to define d_1 and d_2.

Fig. 8.15 summarises all the possible cases. Notice how the axes are not conventionally depicted in terms of signs. In inverter mode (yellow area), the current reference of the converter is lower than zero $(I_{pk} < 0)$ and thus, d_1 will be considered positive while d_2 negative. On the contrary, in rectifier mode (the green area), it goes just the opposite way: d_1 shall be negative and d_2 positive. It must be appreciated how in inverter mode d_2 goes before d_1 and vice versa in rectifier mode. The represented curves for d_1 and d_2 of Fig. 8.15 came from (8.2) and (8.6).

However, this step only defines signs and values for the duties but another issue needs to be considered: the definition of the firing scheme of the transistors regardless of the operation mode of the converter.

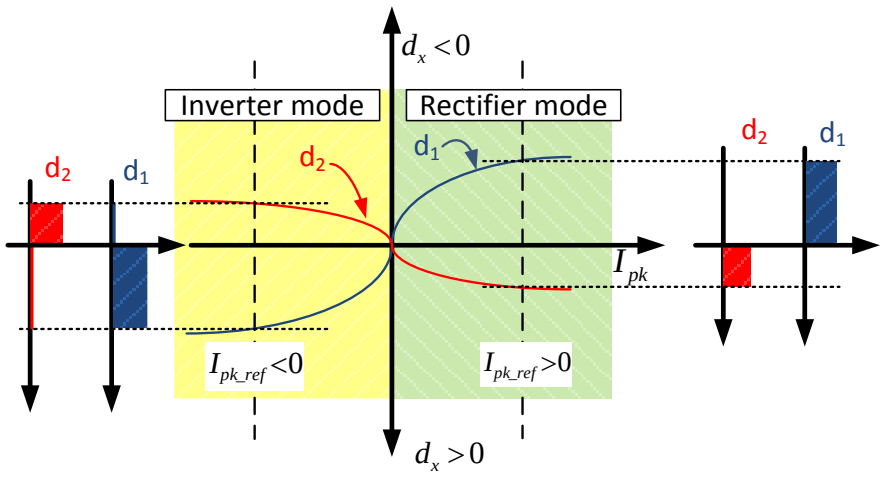

Fig. 8.15. Graphical representation of the switching pattern

Switching pattern

Unlike in [27], all the switches must operate in both operation modes in order to change automatically between them in a neat way. Hence, so to try to find a common pattern between rectifier and inverter modes, TABLE 8.I and TABLE 8.II summarise all the possibilities, being "1" an on state, "0" an off state and "x" meaning irrelevant.

TABLE 8.I shows the different states of all the switches during rectifier mode. In the grid side, when the input voltage is positive, $U_g > 0$, the transistor that must drive the current is S_1 while the diode of S_2 would be direct biased, being the state of S_2 irrelevant. A similar operation is achieved upon negative input voltage, but interchanging the switches, hence they can be turned on simultaneously.

On the other hand, in order to discharge the Flyback transformer, S_R must be turned on after S_1 is turned off. S_A and S_B do not affect this discharge due to the fact that their diodes would be actually direct biased and driving the current.

TABLE 8.I

RECTIFIER MODE SWITCHING MAP

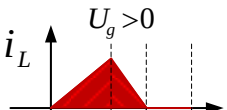

S_1	1	0	0
S_2	x	x	x
S_A	0	x	0
S_B	0	0	0
S_R	0	1	1

S_1	x	x	x
S_2	1	0	0
S_A	0	0	0
S_B	0	x	0
S_R	0	1	1

The inverter mode switching map is shown in TABLE 8.II. It can be seen that in this case, the transformer charges through the proper inductor in the bus side and thus, only S_A or S_B could be turned on but never at the same time, depending on the grid voltage sign. The diode of S_R direct biased, hence the state of the switch is irrelevant in this mode.

However, it is showed that whether S_1 is turned on, the state of S_2 is irrelevant and vice versa in this operation mode, thus they can be triggered at the same time.

TABLE 8.II

INVERTER MODE SWITCHING MAP

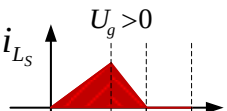

S_1	x	x	0
S_2	0	1	x
S_A	1	0	0
S_B	0	0	0
S_R	x	x	x

S_1	0	1	x
S_2	x	x	0
S_A	0	0	0
S_B	1	0	0
S_R	x	x	x

Hence, summarising both tables:

- S_1 and S_2 can be turned on always simultaneously.
- S_R must operate with a “not” gate regarding S_1 (or S_2).
- S_A and S_B will be turned on depending on the current reference sign.

Perform these conditions with logic gates can be a tough task, as Fig. 8.16 depicts.

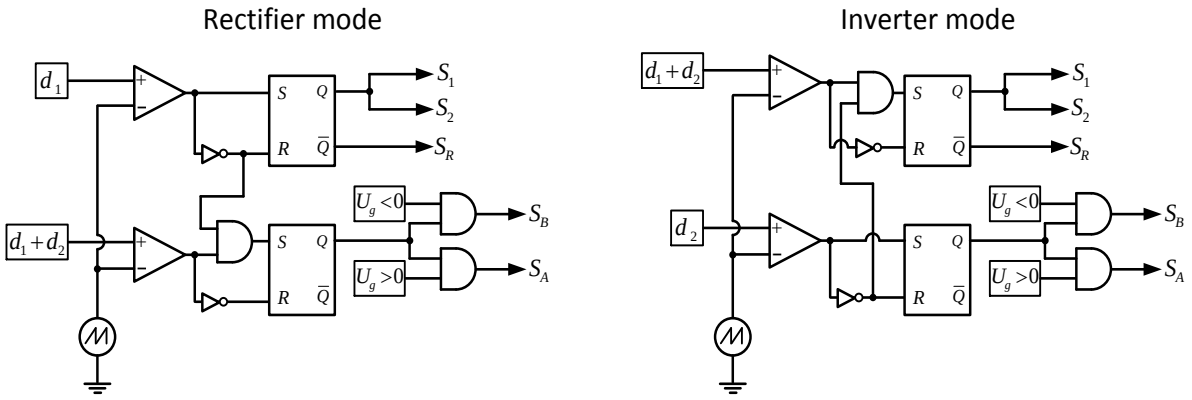

Fig. 8.16. Switching pattern using logic gates

Translation to DSP digital logic

Even though the previous section may look complicated to understand, when a DSP is involved, the problem can be efficiently solved just by code programming. Both duty ratios, d_1 and d_2 will be compared to a triangular sawtooth waveform and then, the pulses for the switches can be obtained.

In the DSP F28335, the register that accounts for the maximum value of the sawtooth counter is called TBPRD. It sets the PWM frequency. There are two different counter-compare registers for each triangular signal (CMPx) that are continuously compared to the time-base counter, TBCTR. When the values are equal, an event is sent to the action-qualifier where a decision is made depending on the configuration of the AQCTLx register: it can ignore the event, clear, set or toggle the PWM.

The proper and individual programing for all the sawtooth comparators needs to be done in order to achieve a proper triggering of the switches. Thus, a graphic example of how this triggering is accomplished is given in Fig. 8.17. In this case, two different values for d_1 and d_2 have been chosen in order to see the pulses, as it is depicted, representing two results given by (8.2) and (8.7).

If the converter would be operating in rectifier mode, the DSP would have a positive current reference and thus, it would proceed as follows: since d_1 is the duty for the grid side switches, it would remain invariant. Nevertheless, d_2 would be redefined as $D_2= d_1+ d_2$. This is just a mathematical instrument needed for the programing of the sawtooth comparators.

On the other hand, if the DSP detects a negative current reference, then inverter mode shall begin and the counter-compare registers change, as it may be appreciated in Fig. 8.17. This time, d_2 remains equal to the calculated one and d_1 is redefined as $D_1= d_1+ d_2$. This way, the switches related to d_1 (S_1, S_2) are triggered after S_A and S_B.

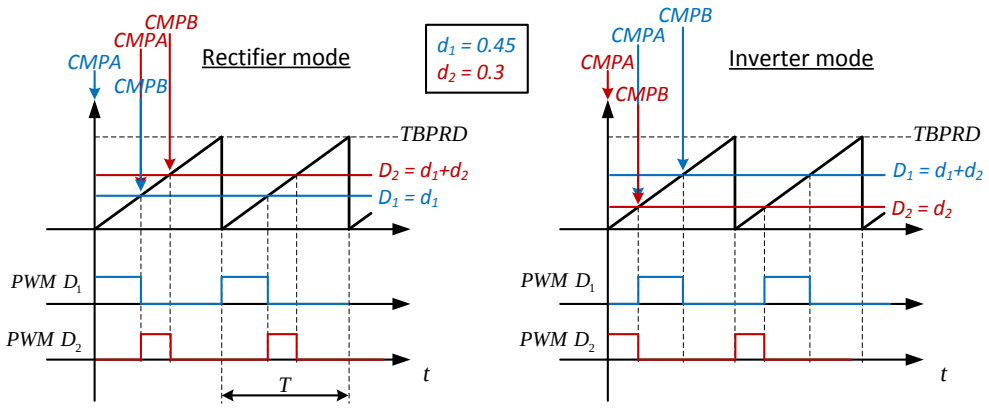

Fig. 8.17. DSP logic to trigger the switches

8.3.2 Simulation results

The parameters of the converter are the ones depicted in TABLE 7.I about the power converter is also valid for this chapter. Several simulations were performed in order to test the proposed technique.

Fig. 8.18 shows the topology employed in the simulation. The WT has been modelled as a voltage source in series with a resistor in order to work as a real voltage source. This model can represent the behaviour of any power generator. Particularly, the desired current control can be easily implemented in such model of the generator block. This way, the exact behaviour of the existing interfacing converter for the WT can be used.

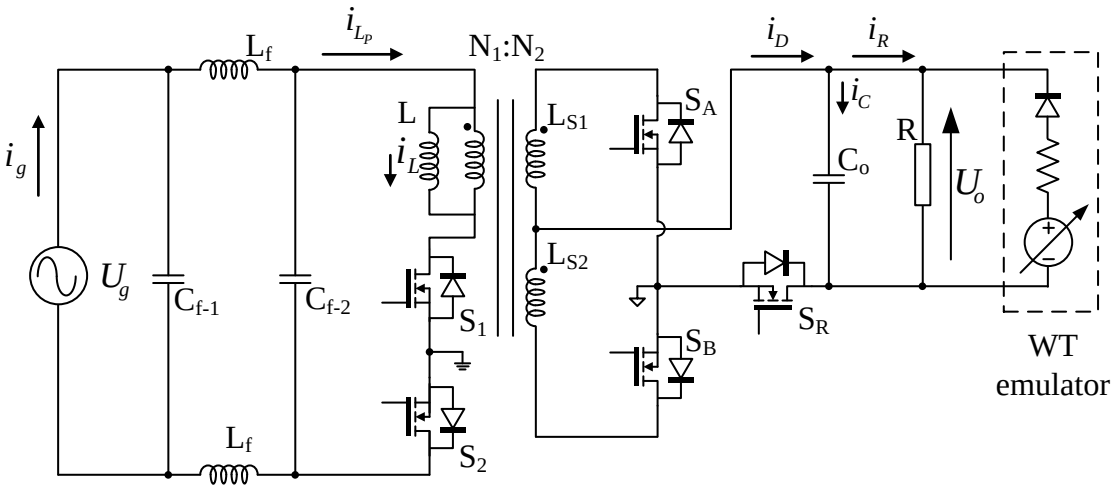

Fig. 8.18. Electrical circuit of the simulation

Thus, the first simulation was done in order to ensure the DCM operation of the system in steady state, considering the switching pattern developed for both rectifier and inverter modes in a switching period.

Rectifier mode test

The main waveforms for a switching period during rectifier mode with the proposed switching pattern are shown ahead. They match with the expected curves of a DCM Flyback converter. The magnetising inductor charges by the grid side and discharges by the DC bus side, staying always in DCM.

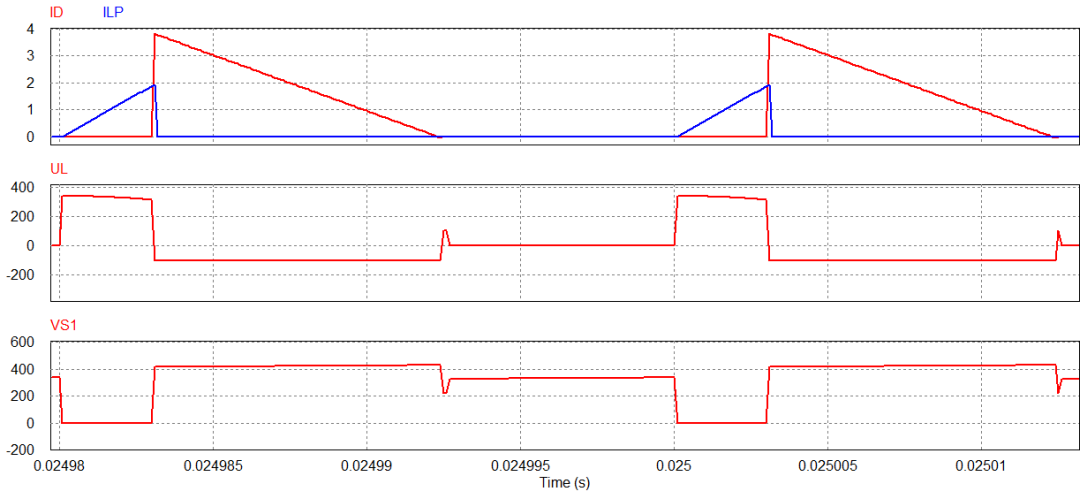

Fig. 8.19. Rectifier mode simulation waveforms with the proposed switching pattern

Inverter mode test

The same test was performed for the inverter mode. In this case, the magnetising inductor charges through the DC bus side, as it can be seen in Fig. 8.20, and therefore, the waveforms for a switching period must change with respect the ones shown in Fig. 8.19. In addition, they are consistent with Fig. 8.4.

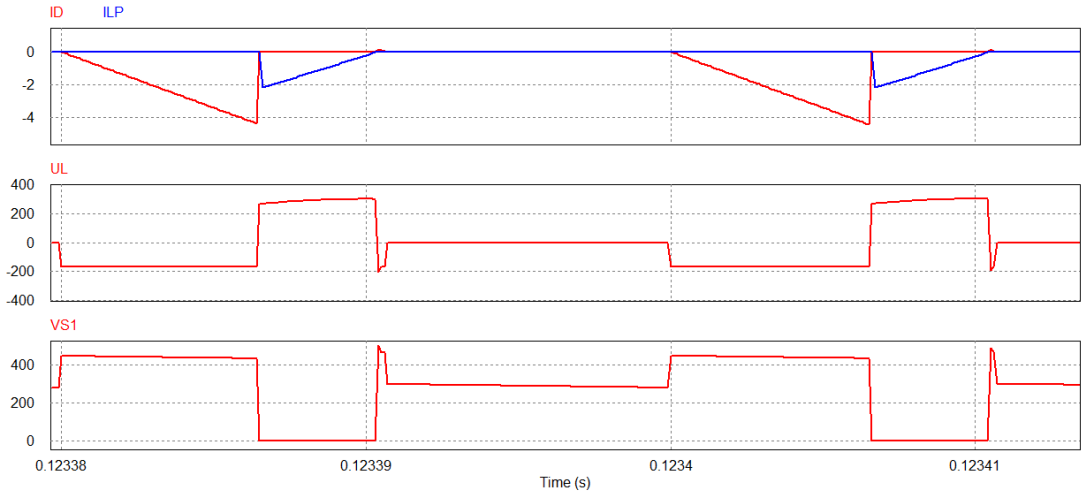

Fig. 8.20. Inverter mode simulation waveforms with the proposed switching pattern

Complete simulation

The simulation that mixes rectifier and inverter modes is explained ahead. The converter is initialised in rectifier mode with a fixed duty d_1 and then d_2 is calculated with a current reference of +0.5 A. In

t=0.08 s the WT starts-up and then the bus voltage increases. In t = 0.15 s the current reference changes and it begins to decrease lineally from + 0.5 A to -0.5 A. During this period, the duties change their sign and the converter passes from rectifier mode to inverter mode. As it can be seen in Fig. 8.21, at the beginning, in rectifier mode, the current i_g is in phase with the grid voltage because the converter is operating as a PFC. On the other hand, during inverter mode, this same current is 180º phase-shifted respect to the grid voltage. Notice that the order of the currents i_{LP} and i_D change depending on the operation mode.

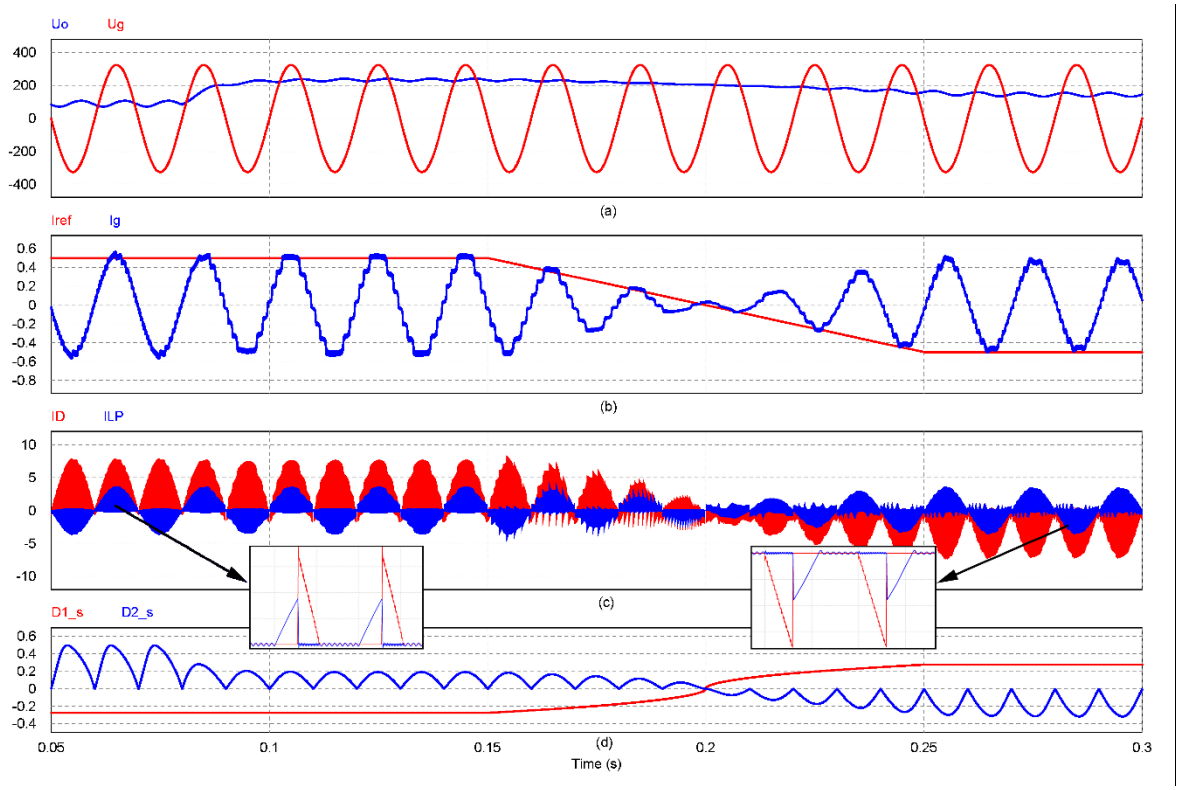

Fig. 8.21. Simulation results in open loop (variables from Fig. 8.18)

8.3.3 Experimental results

Before testing the proposed idea in the lab bench, both the rectifier and inverter modes were tested individually in current control closed loop, in order to assess the DCM operation of the system in all cases. This means that a current reference was given to the power and then, both duty cycles were calculated by the DSP.

Hence, Fig. 8.22 depicts the scheme of the experimental setup that was built in the laboratory. The RES unit was emulated with a variable voltage source and a series resistor in order to inject current into the bus with a certain ripple as it was done in the simulation. However, in order to perform a more realistic experiment, a load was placed between the grid and the converter. In such way, the grid supplies this load until the power converter enters in inverter mode. Then, the utility grid can reduce its power contribution to the line.

Thus, two experimental results will be shown. The first one will emulate the rectifier mode and the second one, the inverter mode. In both experiments, a current control loop is implemented in the microcontroller. The only changed parameter is the current reference. In rectifier mode it is positive and in inverter mode it is negative, just as explained before.

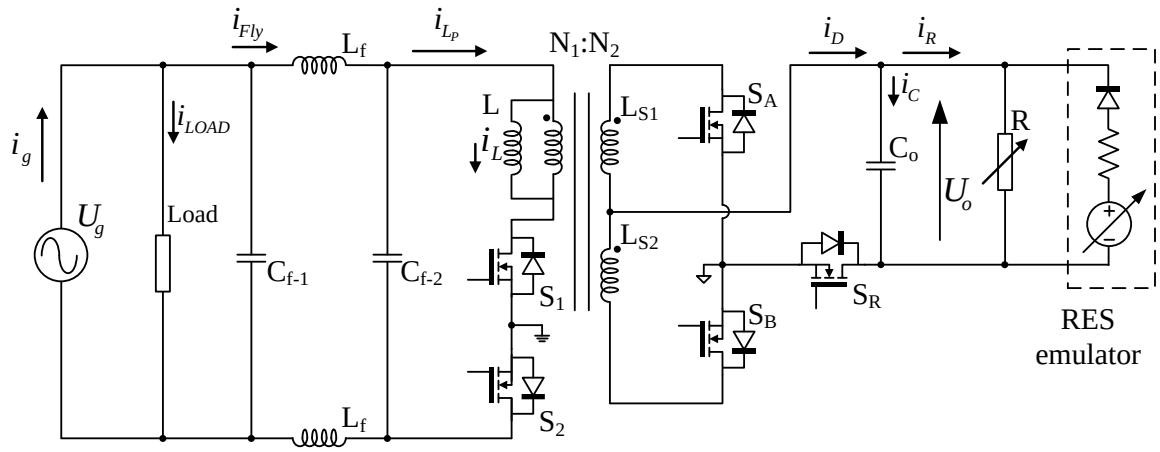

Fig. 8.22. Laboratory setup scheme

Rectifier mode experiment

Before closing the loop, the common switching pattern was tested for the rectifier mode. Fig. 8.23 shows the main waveforms of the DCM Flyback converter in rectifier mode: inductor voltage, S_1 switch voltage, and currents through the grid and DC bus side inductors.

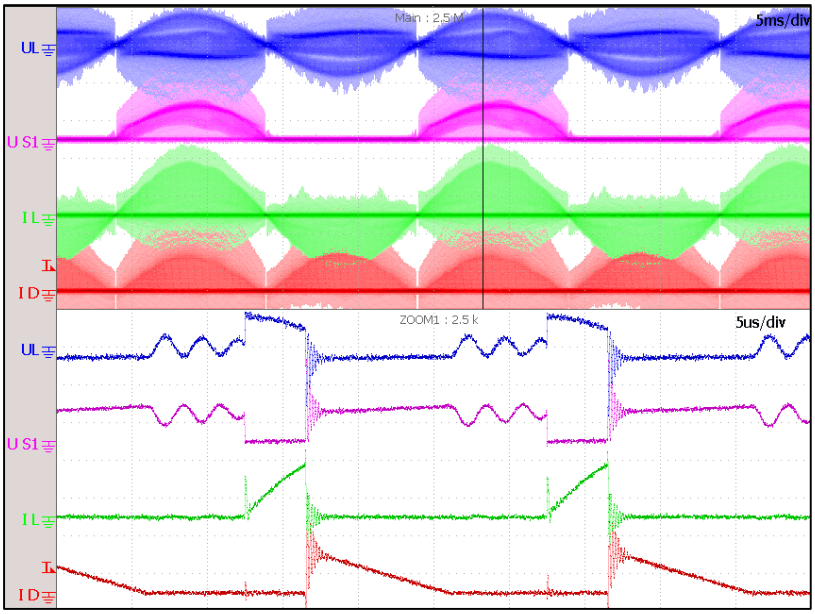

Fig. 8.23. Rectifier mode experimental waveforms with the proposed switching pattern. CH1: inductor voltage (blue, 500 V/div). CH2: mosfet S_1 voltage (purple, 500 V/div). CH3: grid side input current (green, 10 A/div). CH4: bus side output current (red, 10 A/div)

After checking that the Flyback converter operates in DCM, as expected, a new experiment for the rectifier mode was performed. In this case, both the RES emulator and the grid side load are disconnected. The current reference value is fixed to 0.25 A, and in steady state, this value forces a constant voltage level in the DC bus. At a certain moment, the load *R* of the DC bus is changed to a higher ohmic value, therefore decreasing the absorbed power. As the current reference keeps constant, the DC bus will increase. Take into account that in this experiment, the RES emulator is not working and neither is connected the load of the grid side. In Fig. 8.24, the obtained results in rectifier mode are shown. The red shadow indicates the moment when the load is decreased. Notice that the bus voltage increases (purple waveform) but the grid current remains at the reference (green waveform), as expected.

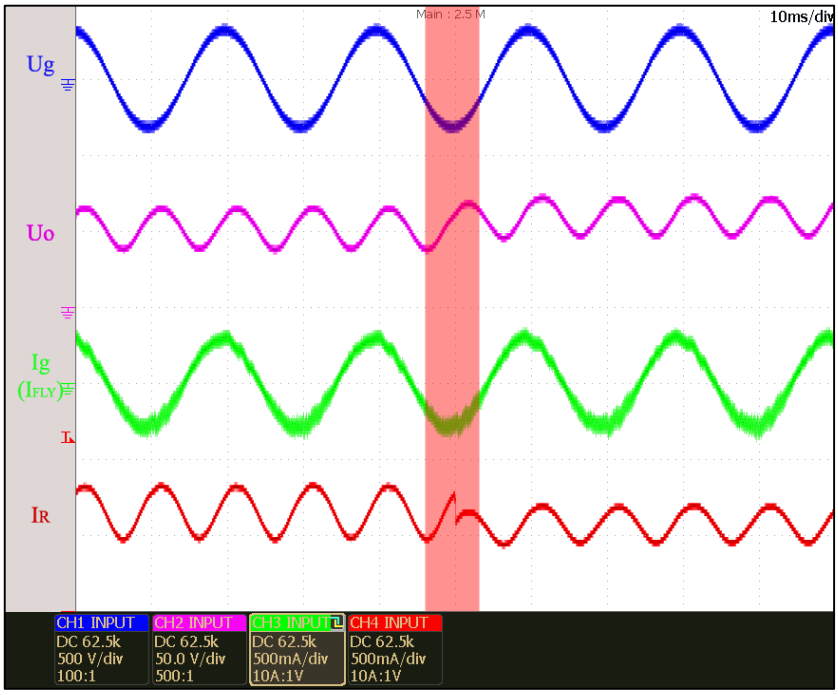

Fig. 8.24. Rectifier mode experimental results

Inverter mode experiment

The same initial test for the inverter mode was performed. The main waveforms of the converter are depicted in Fig. 8.25: inductor voltage, S_1 switch voltage, and currents through the grid and DC bus side inductors. It can be notice that the converter stays in DCM in steady-state operation.

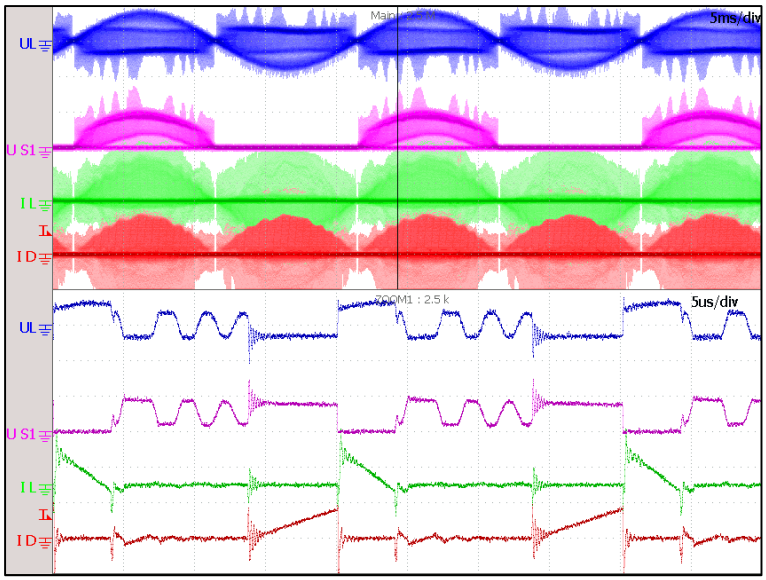

Fig. 8.25. Inverter mode experimental waveforms with the proposed switching pattern. CH1: inductor voltage (blue, 500 V/div). CH2: mosfet S_1 voltage (purple, 500 V/div). CH3: grid side output current (green, 2 A/div). CH4: bus side input current (red, 5 A/div)

Therefore, the inverter mode can be tested closing the loop and its experimental results can be seen in Fig. 8.27. This time, the load of the grid side is connected and therefore it is draining current from the utility mains until the Flyback begins to inject current into the load. At this moment, the grid reduces its power contribution without disturbing the load consumption. Notice that this time, the converter current and grid voltage are 180º phase-shifted, as expected.

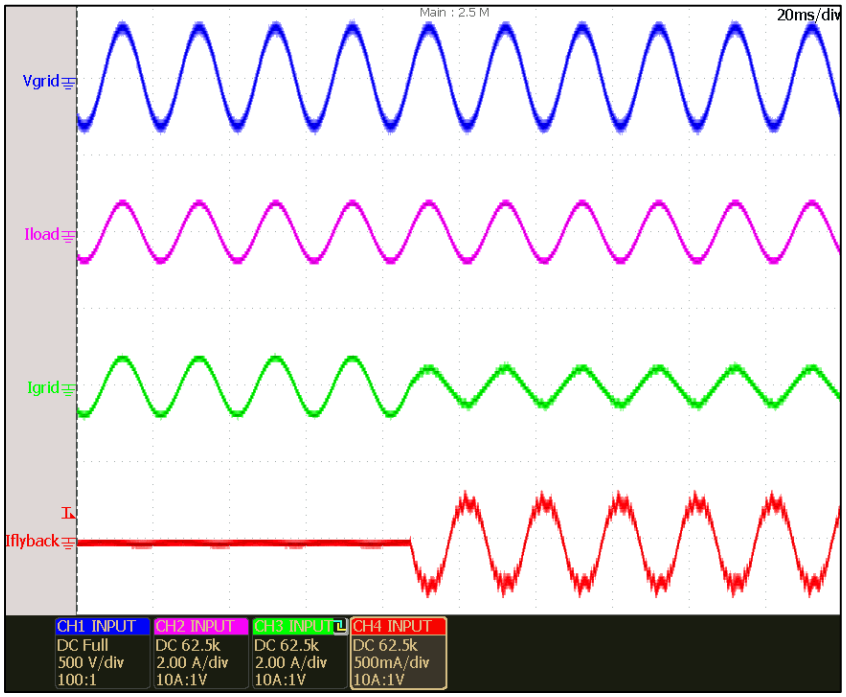

Fig. 8.26. Inverter mode experimental results without snubber

The power inverter, even whether it operates as a perfect current source, produces harmonics due to switching, dead-times, semiconductor voltage drops, parasitic reactive components, etc. These harmonics must not prevent the input current to comply with standard regulations (e.g. IEEE 1574 THD <5%). However, in this experiment, the measured THD of the injected current equals to 9.4% and it exceeds the allowed limits. Therefore, a snubber can be placed in order to improve this THD, since the high frequency input filter was not able to eliminate all the harmonic content. The same experiment was done with a RC snubber in the DC bus side and the results are shown in Fig. 8.27. Now, the measured THD is of 6.1%. Although the result is close to the standard regulations, further studies are needed in order to reduce this THD to the minimum 5%.

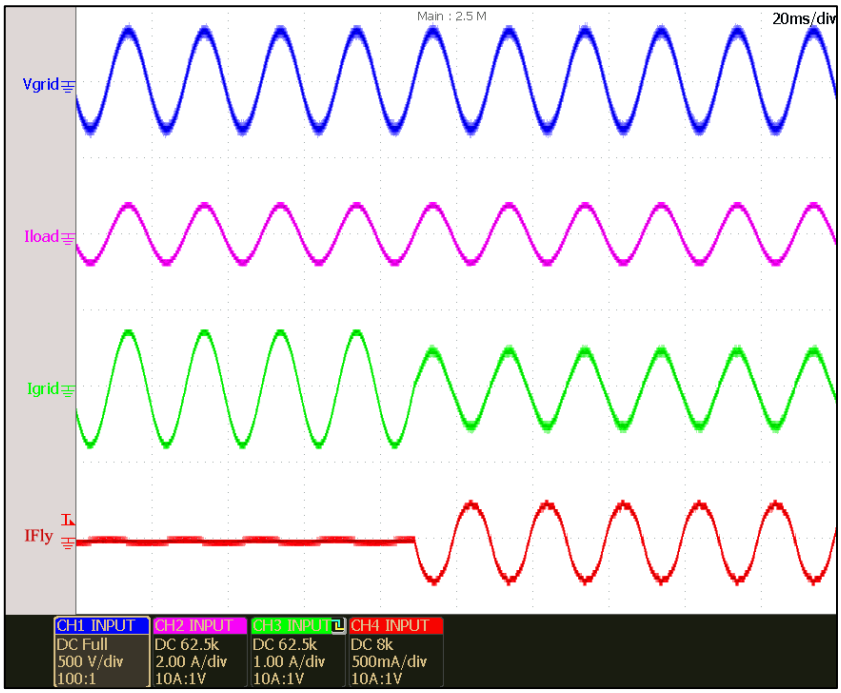

Fig. 8.27. Inverter mode experimental results with a snubber connected

Additionally, the comparison between both results is shown in Fig. 8.28. The high frequency noise is almost neglected with a simple RC net. It would be interesting the use of energy regenerative snubber instead a dissipative one, in order to improve the efficiency of the converter.

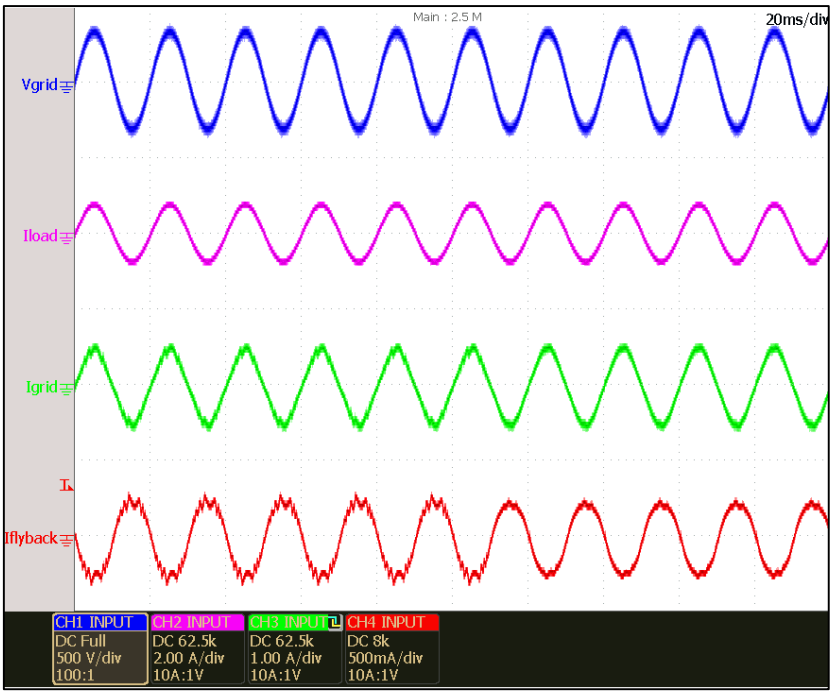

Fig. 8.28. Comparison between having or not the snubber

Fig. 8.29 depicts a comparative of the harmonic content between having or not the snubber switched on. As it may be appreciated, the most harmful harmonic is the 3rd.

Fig. 8.29. Harmonic content of the injected current with and without a snubber

Transition between modes

The transition between both modes, from rectifier to inverter and vice versa has been tested in several laboratory experiments. Fig. 8.30 depicts the behaviour of the whole system when the power converter is demanding +0.25 A to supply the lamp, thus it is rectifier mode, and then, it changes to inverter mode gradually due to the extra power available in the DC bus because of the WT. Notice how the current I_{fly}, which represents the current in the filter (as shown in Fig. 8.22) is in phase with the grid voltage at the beginning since the converter is in rectifier mode (Fig. 8.30 top-left). When it changes to inverter mode, the same current phase-shiftes 180º the grid voltage (Fig. 8.30 top-right).

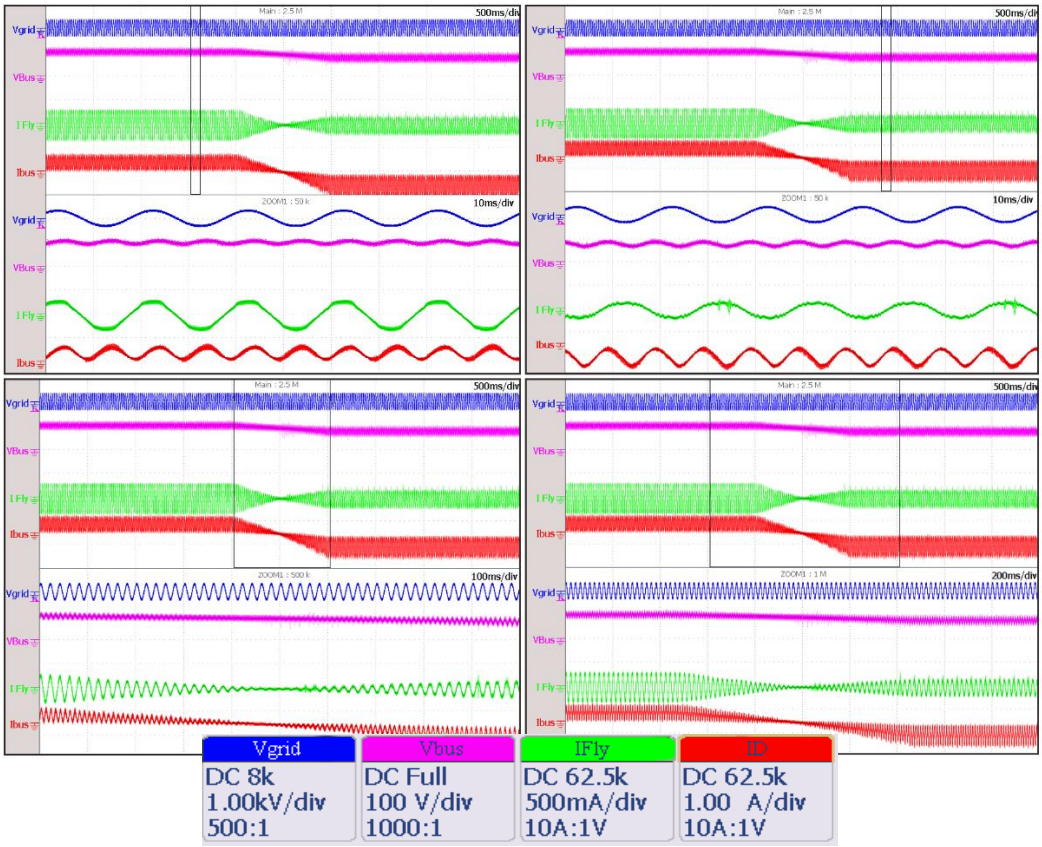

Fig. 8.30. Transition from rectifier mode to inverter mode and a current reference of 0.25 A.

On the other hand, Fig. 8.31 shows this very same change from rectifier to inverter mode plus the variation in the grid current. The contribution of the grid in order to supply all the loads is reduced when the bidirectional power converter begins to support it with the power obtained from the renewable energy sources.

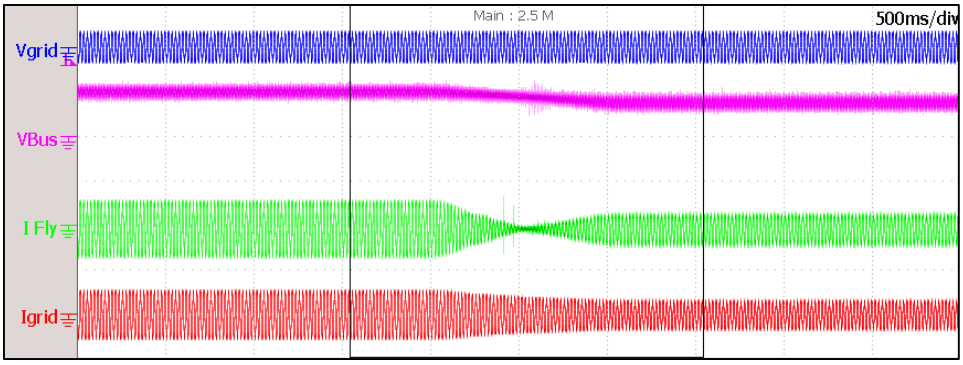

Fig. 8.31. Grid current contribution under different converter operation modes

Fig. 8.32 depicts a different experiment. In this case, the bidirectional Flyback converter is operating in inverter mode at the beginning and suddenly the WT stops injecting power in the DC bus. Therefore, in order to supply the load, the control decides to absorb this power from the grid. Notice that this time the current reference is bigger than in the previous experiment.

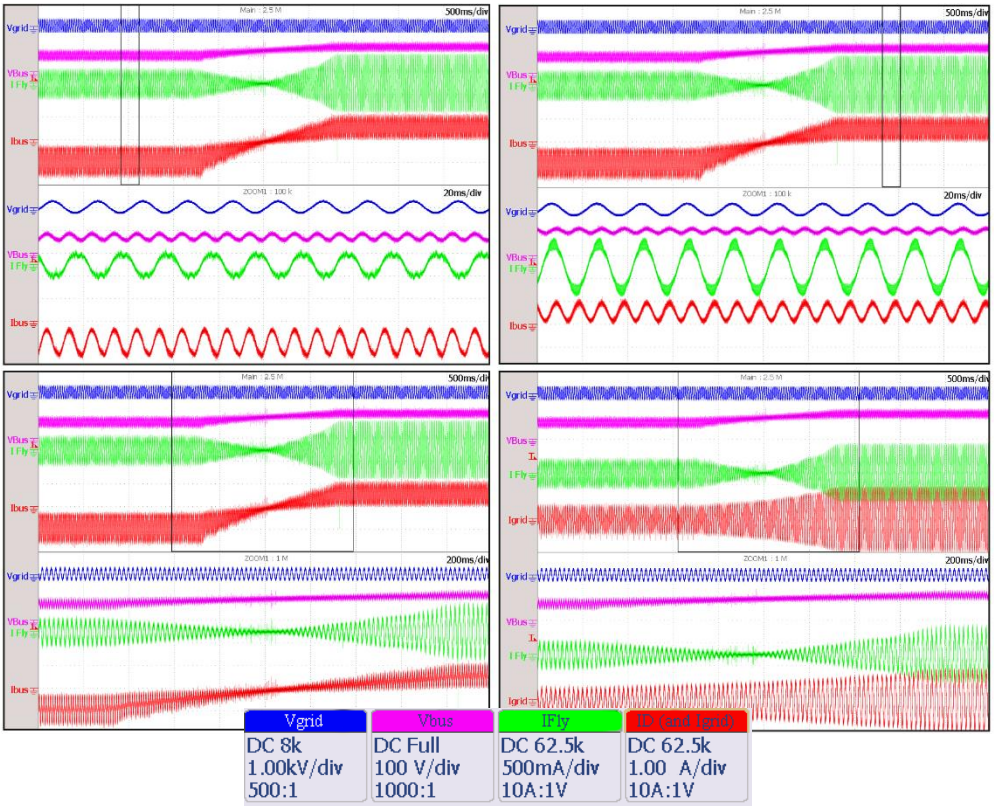

Fig. 8.32. Transition from inverter mode to rectifier mode. Current reference of 0.4 A in rectifier mode. Grid current contribution depicted in bottom-right

8.4 Summary and conclusions

This chapter has defined and demonstrated the implementation of a unified switching pattern for every switch in a bidirectional DCM Flyback converter for the grid interface of a street lighting system with power generation capability. It was proved that it is possible to change from rectifier mode to inverter mode automatically with the same switching pattern scheme, therefore allowing for an easy implementation of the stage control at the PWM modules of existing Digital Controllers. It was studied how to trigger the transistors by analysing mathematically the equations of the converter and the duties for the grid and bus sides. A simulation was performed in order to test this idea and an experimental setup has being built in order to prove it physically.

As a future development, the idea of trying to phase-shift the converter current and inject or absorb certain amount of reactive power is interesting. However, it is a fact that there will be conflicts when the grid voltage zero-crossing points.

Chapter 9

Conclusions and future developments

This final chapter summarises the main conclusions obtained through the development of this PhD thesis work, stating its importance and relating these achievements with the publications in conferences and journals. Finally, a discussion on future developments is as well carried out.

9.1 Conclusions and main contributions

This PhD Thesis entitled "Power Electronic Supplies For Public Lighting Systems With Distributed Generation Capability: Solution Proposals For Power And Control Stages, Characterization And Minimization Of The Impact In Grid Quality" was developed as a part of the research activities of the Efficient Energy Conversion, Industrial Electronics and Lighting Engineering group (CE^3I^2) of University of Oviedo.

Many topics have been studied through this PhD Thesis. First of all, a brief introduction to lighting systems has been included. The most important technologies of lamps have been exposed, defined and characterized, focusing then on the LED-based solid state lamps. These lamps need a dedicated electronic driver in order to achieve an optimal behaviour. This work deals with the proposal for solutions to the electronic stage that interfaces the single-phase mains facility with the lighting system of the solid state lamp.

One of the constraint of such interfacing system is the standards fulfilment. The IEC 61000-3-2 regulation was briefly commented in order to define power factor and harmonic content limits of the interfacing power converter for lighting applications. The presented work studies the constraints in a system imposed by the coexistence of the proposed power converters with electromagnetic ballasts, which are non-linear loads used in the past to drive discharge lamps (as the high-pressure sodium lamps considered). Within this scope, it has been proposed a methodology to improve the THD of a distribution line configuration with multiple non-linear loads. This proposal measures only the voltage at the PCC, thus avoiding the use of current measurement. This contribution is intended for a low-cost solution that avoids the use of current sensors, therefore:

- It is possible to decrease the harmonic content of a distribution network by measuring just the voltage at the point of common coupling.
- However, the amount of correction of this harmonic content depends on a variable we have called k_1 that is quite difficult to calculate.
- The tuning of the regulators in the control loop depends on that variable; however, a simplification has been proposed in order to substitute such expression by a gain. This approach changes consequently the effect over the harmonics.
- Finding an optimal value for that gain is a complex task, as that the injected current aimed to correct the harmonic content generated by the non-linear loads must be kept within reasonable values.
- This work was published in the conference IECON 2013 with the following title "Minimization of current harmonics content in conventional lighting distribution lines without current sensing" [7].

The next study carried out involved the effect of such dedicated lighting systems (with mixed non-linear loads and electronic interfacing stages) on microgrids and minigrids, including the normal grid-tied operation and islanding mode. Two different control strategies were evaluated in order to find a good solution for THD and harmonics improvement in microgrids. The resonant controller and the stationary reference frame were introduced and they were compared with the single-phase synchronous reference frame in terms of efficiency and computational cost. The contributions of this work can be summarised as:

- A theoretical comparative of the most common harmonics minimisation techniques was studied, comparing control schemes and computational costs.

- A practical implementation to verify this comparative was performed. The stationary control (αβ) has been proved to need less calculations to reduce the harmonic content of the power line. On the other hand, the final THD and harmonic content is slightly higher than using a synchronous (*dq*) control.
- In addition, it has been studied two kind of controllers: PI for DC signals and PR for AC signals. It was observed how the PR controllers are more sensitive to perturbations and difficult to tune, thus the system could go unstable more easily.
- Therefore, in order to choose a technique for harmonics content reduction, there is no universal solution. A compromise choice has to be done, thinking in the computational power available and the desirable results.

The next chapter was dedicated to the study of the most suitable renewable energy sources to be installed in street lampposts. After this survey, photovoltaic and micro wind turbines were chosen as the most appealing solutions.

After a brief state of the art of power factor correctors, including topics such as main control techniques, operation modes and architectures, a high bandwidth control technique for a PFC Flyback converter was proposed:

- The original contribution of this work was the proposed control with high bandwidth that improved the THD and the harmonic content of the input current when compared to classic control, validated through simulations and experimental results.
- The dynamics involved in the whole system (control and power converter) avoid reaching higher bandwidths experimentally. Further studies in this issue can be done in order to detect the exact reason why the converter trips at bandwidths beyond 250 Hz.
- This work was presented in the conference IAS 2015 with the following title “Fast Dynamics Current Control of DCM Flyback as PFC Front Converter for Lighting Applications”.

Then, the bidirectional Flyback converter operating in DCM, that allows full power flow control was considered. The previous works were optimised by defining a unified switching strategy for the converter.

- A smooth transition between rectifier and inverter modes is now feasible without turning off the converter.
- The control strategy is the same for both modes, thus there is no incompatibilities or different switching pattern.
- The implementation is easy in a DSP.
- The employ of snubbers is desirable since they allow to smooth the output current when the converter is injecting into the utility grid.
- This work was also published in the conference IAS 2015 with the following title “A Unified Switching Strategy in Bidirectional Grid Interface DCM Flyback Stages for Public Street Lighting Systems with Microgeneration Capability”.

Then, this Ph.D. thesis defines a proper single-phase interface stage in a distributed generation lighting system. The grid impact issue was addressed from a top-bottom approximation, beginning by studying the consequences of the harmonics in a microgrid (grid-tied or islanded) and evaluating solutions to improve the harmonic content with and without current sensors; after that, a topology to fulfil the constraints imposed by the current waveforms defined from the aforementioned impact study has been studied. The power topology based on a DCM Flyback converter was proposed together with several needed modifications which allow to use it as a bidirectional converter, from the

point of view of the control as well as the power topology. Finally, a unified switching strategy was developed in order to implement physically the studied control for two operation modes: rectifier and inverter. All the grid interface stages were tested experimentally by means of built prototypes of nominal power.

In this way, a final design for grid harmonics reduction in lighting systems with distributed generation capability was developed. This solution provides a much more versatile control of the system, allowing the use of design technical tools, control and management of power flows in high performance systems (e.g. controlled three-phase rectifiers, active filters, etc.). In addition, this solution is low-cost and provides galvanic isolation.

9.2 Future developments

As the last contribution of this work, several future development topics have been identified:

Regarding the control strategy for the correction of the harmonic content generated by electromagnetic ballasts of chapter 3, a laboratory experimentation would be adequate to check the simulation results. Furthermore, an algorithm that estimates the load consumption and makes a decision of how much current it takes to correct the harmonic content should be the next step.

In chapter 4, two control techniques, in stationary and synchronous reference frame were validated with the dSPACE machine. However, this study lacks of experimental results, thus a laboratory prototype needs to be built in order to finally test both control techniques.

In addition, there are two published papers where the idea of communicating several single-phase RES units by means of small power line signalling in a microgrid was started. These works were presented in the conferences SmartMILE 2014 with the title “Control of single-phase islanded PV/battery streetlight cluster based on power-line signaling” ([66]) and SSD 2015 under the title “Control of single-phase islanded PV/battery minigrids based on power-line signaling” ([67]).

There is much room for improvement here due to the fact that it combines almost all the concepts this Thesis has dealt with. It would be interesting to create a small-scale microgrid with several RES units that would adapt the power they are injecting depending on the connected loads. This concept was already done with a dSPACE but it was not in the laboratory.

The PFC and the control strategy proposed could see a further progress if active harmonics cancellation techniques were included. This means that, instead of calculating only a duty cycle, look for the higher frequency duties, like d_3, d_5, d_7, corresponding to each odd harmonic. This would need current sensing and obviously, it would complicate the control and likely, the behaviour of the converter in terms of efficiency and reliability.

Finally, testing the unified switching strategy in the laboratory, changing from one operating mode to the other and vice versa is mandatory. In addition, trying to phase-shift the converter current with respect to the grid voltage and inject or absorb a certain amount of reactive power could be a promising work. However, this is a bit tricky since the bidirectional Flyback does not operate as an H-bridge. It has inductors that would react to sudden changes in the current that is flowing through them. Thus, when there is no voltage but the converter is trying to demand or inject current, there would be conflicts.

Capítulo 10
Conclusiones y desarrollos futuros

Este capítulo recopila las principales conclusiones que se han obtenido a través del desarrollo de la tesis. Después se expondrán los futuros desarrollos para mejorar más este trabajo.

10.1 Conclusiones y principales contribuciones

Este trabajo de Tesis Doctoral titulado "Equipos Electrónicos De Alimentación En Sistemas De Alumbrado Público Con Capacidad De Microgeneración Distribuida: Propuesta De Soluciones Para Etapas De Potencia Y Control, Caracterización Y Minimización Del Impacto En La Red Eléctrica" fue desarrollado dentro del grupo de investigación Conversión Eficiente de Energía, Electrónica Industrial e Iluminación (CE^3I^2) de la Universidad de Oviedo.

Diferentes temas se han ido tratando a lo largo de este trabajo. Primeramente se hizo una introducción a los sistemas de iluminación y los tipos de lámparas más comunes, centrándose en las que más atención atraen en estos tiempos, las de tipo LED.

Después se buscó información sobre la normativa IEC 61000-3-2, que define conceptos como el factor de potencia y la limitación del contenido armónico de los convertidores de potencia cuando hay sistemas de iluminación involucrados. Este estudio se relacionó con los balastos electromagnéticos, que son un tipo de cargas no lineales que se emplearon hace años para controlar las lámparas de descarga, como las de alta presión de sodio. Se estudió una metodología para mejorar el THD de una línea de distribución con múltiples cargas no lineales conectadas a ella, midiendo únicamente la tensión de red en el punto de acoplamiento. Con esto se consigue evitar la medida de la corriente, cosa que influye en el coste final y en la fiabilidad de la solución propuesta. Por lo tanto:

- Es posible reducir el contenido armónico de una línea de distribución midiendo solo la tensión en el punto de acoplamiento.
- Sin embargo, existe una variable k_1 que es difícil de calcular y que afecta claramente en cuánto este contenido armónico puede ser reducido.
- La calibración de los controladores en el lazo de control depende de esta variable; sin embargo, se puede utilizar una simplificación. Esta aproximación cambia el efecto sobre los armónicos pero mantiene el sistema estable.
- Encontrar un valor óptimo para esta ganancia es una ardua tarea porque debe mantener la referencia de corriente que corrige los armónicos dentro de unos valores razonables.
- Este trabajo fue publicado en la conferencia IECON 2013 con el siguiente título: "Minimization of current harmonics content in conventional lighting distribution lines without current sensing" [7].

El siguiente estudio se relaciona con las microrredes monofásicas en isla y conectadas a la red y el efecto que tienen las cargas no lineales. Se evaluaron dos estrategias de control diferentes para buscar una buena solución para la corrección del THD y del contenido armónico en este tipo de redes. Los controladores resonantes y el consiguiente marco de referencia estacionario fueron estudiados y comparados con el marco de referencia síncrono monofásico en términos de eficiencia y coste computacional. En conclusión:

- Una comparativa teórica de las más comunes técnicas de minimización de armónicos fue estudiada, comparando esquemas de control y costes computacionales.
- Una implementación práctica para verificar esta comparativa fue realizada. El control estacionario (αβ) necesita menos cálculos para reducir el contenido armónico de la red eléctrica. Por otra parte, el THD final y el contenido armónico es ligeramente mayor que si se usara un control síncrono (*dq*).

- Además de esto, se estudiaron dos tipos de controladores: los PI para señales de DC y los PR para señales de alterna. Se observó cómo los controladores resonantes PR eran más sensibles a perturbaciones y difíciles de ajustar, por lo que el sistema se puede volver inestable con más facilidad.
- Por lo tanto, se debe buscar una solución de compromiso pensando en el coste computacional que ambos sistemas de control implican y en cuánto se quiere reducir el THD y los armónicos de la red.

Después de un estado del arte sobre correctores de factor de potencia, principales técnicas de control, modos de operación y arquitecturas más comunes, se propuso una técnica de control con un ancho de banda grande para un Flyback operando como corrector de factor de potencia:

- La contribución de este trabajo fue la propuesta de un control con un alto ancho de banda que mejora el THD y el contenido armónico de la corriente de entrada en comparación con el control clásico, validado a través de simulaciones y resultados experimentales.
- Las dinámicas que envuelven el sistema al completo (control y convertidor) evitaron alcanzar mayores anchos de banda experimentalmente. Se realizarán más estudios sobre este tema para detectar la razón exacta de por qué el convertidor dejaba de funcionar a anchos de banda mayores de 250 Hz.
- Este trabajo fue presentado en la conferencia IAS 2015 bajo el título “Fast Dynamics Current Control of DCM Flyback as PFC Front Converter for Lighting Applications”.

Finalmente, se estudió más en profundidad cómo mejorar el convertidor bidireccional tipo Flyback que permite el flujo de energía desde la red a la carga o viceversa y en modo discontinuo.

- Sin apagar el convertidor, ahora es posible una transición suave entre modo rectificador e inversor.
- La estrategia de control es la misma para ambos modos, por lo que no se verán incompatibilidades o diferencias en el patrón de disparo de los semiconductores. Es común para los dos modos.
- La implementación es sencilla en un DSP.
- El empleo de snubbers es una buena opción en modo inversor para suavizar la corriente inyectada a la red y cumplir así con las regulaciones que establecen límites al THD.
- Este trabajo fue presentado también en la conferencia IAS 2015 con el siguiente título: “A Unified Switching Strategy in Bidirectional Grid Interface DCM Flyback Stages for Public Street Lighting Systems with Microgeneration Capability”.

En esta tesis se ha definido la etapa de interface necesaria con la red monofásica, en un sistema de iluminación con generación distribuida. El problema del impacto en la red se ha considerado desde una aproximación top-bottom, comenzando en estudiar las consecuencias en los armónicos en la microrred (funcionamiento normal/islanding), y en estudiar soluciones para mejorar el contenido armónico, tanto con o sin sensores de corriente. Una vez hecho esto, se considera el convertidor de interface desde el punto de vista de la forma de onda instantánea, cumpliendo la normativa de armónico, u estudiando la etapa electrónica como PFC activo. Tras esto, se propone la topología, basada en Flyback DCM, y se proponen las modificaciones que es necesario realizar para poder utilizarlo como convertidor bidireccional, tanto desde el punto de vista del control como de la topología de potencia. Finalmente, se establece la secuencia de pulsos de gobiernos necesarios para implementar físicamente el control estudiado. Todos los diseños de las etapas de interface con la red han sido verificados experimentalmente mediante demostradores y prototipos de la potencia nominal.

De esta forma, se concluye el diseño total de una solución al problema de los armónicos en red de sistemas de iluminación distribuida con capacidad de generación. Esto abre la posibilidad de un control mucho más versátil del sistema, permitiendo el uso de herramientas técnicas de diseño, control y gestión del flujo de potencia típicas de los sistemas de altas prestaciones (por ejemplo, rectificador trifásico controlado, filtros activos, etc.), pero con una solución ajustada a la aplicación, a un coste bajo, y permitiendo aislamiento galvánico.

10.2 Desarrollos futuros

Y como última contribución a este trabajo, diferentes trabajos futuros han sido identificados:

Respecto a la estrategia de control desarrollada para corregir el contenido armónico generado por los balastos electromagnéticos en el capítulo 3. Sería una buena idea el testar experimentalmente en el laboratorio esta idea y ver cómo reaccionaría un convertidor real. Además sería necesario desarrollar un algoritmo que estime el consumo de potencia de la carga y tome una decisión de cuánta corriente tiene que inyectar para corregir el contenido armónico.

En el capítulo 4 se validaron con la dSPACE dos técnicas de control diferentes, en marcos de referencia estacionario y síncrono. Sin embargo, sería necesaria una prueba de laboratorio aunque los resultados en dSPACE se podrían parecer bastante a los reales. Construir un pequeño convertidor de potencia y comprobar el efecto de los dos tipos de controladores así como el coste computacional en un DSP es siempre una buena idea.

Además de esto, hay dos artículos publicados ([66], [67]) donde se investiga la idea de comunicar diferentes fuentes de energía renovables y sus correspondientes convertidores en una microrred monofásica mediante el empleo de pequeñas señales a través de la red eléctrica. Hay margen de mejora en estos trabajos debido al hecho de que se están combinando casi todos los conceptos mencionados en esta tesis. Sería muy interesante crear una microrred a pequeña escala y conectar diferentes fuentes renovables que adapten la potencia inyectada en función de las cargas conectadas. Esta idea fue desarrollada en entorno de dSPACE pero aún no en el laboratorio.

Con respecto al capítulo 7, se podrían hacer progresos en la estrategia de control propuesta si se incluyeran técnicas de cancelación de armónicos. Esto significaría que, en vez de calcular un ciclo de trabajo, se deberían buscar también los relacionados con las altas frecuencias, como serían los ciclos de trabajo d_3, d_5, d_7, que corresponderían a los armónicos impares. Esto necesitaría de una medida de corriente y, obviamente, complicaría el control y probablemente el comportamiento del convertidor en términos de eficiencia y fiabilidad.

Finalmente, hay un trabajo pendiente en el capítulo 8 que se corresponde con probar en el laboratorio la estrategia de disparo unificada de los interruptores, cambiando entre ambos modos. Además de esto, sería una buena idea el tratar de desfasar la corriente del convertidor y conseguir así inyectar o absorber cierta cantidad de potencia reactiva. Sin embargo, este concepto es delicado porque un Flyback bidireccional no opera exactamente como un puente completo en H. Al tener un transformador de alta frecuencia, habrá reacciones a los cambios repentinos en la corriente que esté circulando por las bobinas. Por lo tanto, si se desea un desfase entre tensión y corriente, cuando esta primera esté pasando por cero, la segunda estará en un valor distinto de cero, por lo que se tiene un conflicto asegurado en ese punto.

Appendix A: Flyback parameters calculation

In this appendix, all the steps followed in order to calculate the parameters of the Flyback bidirectional converter are gathered.

As it was presented in [26], so as to define all the components of the proposed converter, both operation modes must be analysed mathematically. The semiconductor stresses, the switching frequency, the power the high frequency transformer would handle as well as the peak voltage of the grid shall define the value of the magnetising inductor.

Rectifier mode parameters

In Fig. A.1 the inductor *L* voltage during a switching period, *T* is represented. The maximum duty cycle d_{max} is defined when there is no dead time, d_3T.

$$U_g\, d_{max}\, T = U_o \frac{N_1}{N_2}(1 - d_{max})T \rightarrow d_{max} = \frac{U_o N_1}{U_{g\,pk}\, N_2 + U_o N_1} \qquad (A.1)$$

Where $U_{g\,pk}$ is the peak voltage of the grid, N_1 the turns of the grid side inductor and N_2 the turns number of the bus side inductors.

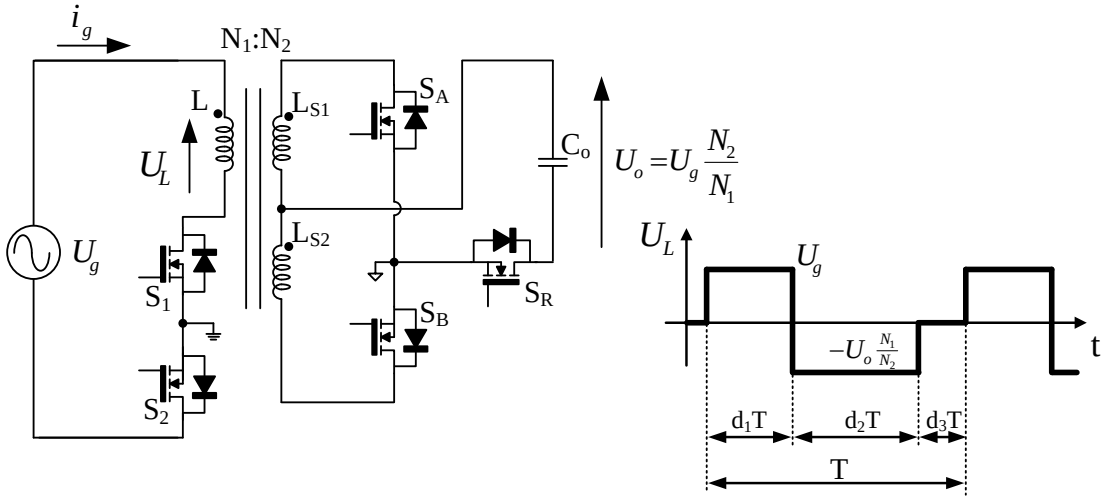

Fig. A.1. Bidirectional Flyback simplified scheme

In order to define the expression of the magnetising inductor, *L*, the definition of the average power during a grid period, T_g can be stated.

$$P_{in} = \frac{1}{T_g}\left(\int_0^{T_g/2} p(t)dt + \int_{T_g/2}^{T_g} p(t)dt\right) = \frac{2}{T_g}\int_0^{T_g/2} p(t)dt = \frac{2}{T_g}\int_0^{T_g/2} U_g(t)\, i_g(t)dt \qquad (A.2)$$

$U_g(t)$ is the grid voltage and thus is easy to define:

$$U_g = U_{g\,pk}\sin(t) \qquad (A.3)$$

The expression for $i_g(t)$ can be obtained from the already depicted current waveforms (Fig. 7.2).

$$\langle i_g \rangle = \frac{1}{T}\int_0^{d_{max}T} \frac{U_g}{L} t\, dt = \frac{U_g\, T\, {d_{max}}^2}{2\, L} \qquad (A.4)$$

And since the current would have a sinusoidal shape:

$$i_g = \frac{U_g\, T\, {d_{max}}^2}{2\, L}\sin(t) \qquad (A.5)$$

Then, combining (A.2),(A.3) and (A.5):

$$\begin{aligned} P_{in} &= \frac{2}{T_g}\int_0^{T_g/2} \left(U_{g\,pk}\sin(\omega t)\right)\left(\frac{U_g\, T\, {d_{max}}^2}{2\, L}\sin(t)\right) dt \\ &= \frac{2}{T_g}\int_0^{T_g/2} \left(U_{g\,pk}\right)\left(\frac{U_g\, T\, {d_{max}}^2}{2\, L}\right)(\sin(t))^2 dt \\ &= \frac{2}{T_g}\int_0^{T_g/2} \left(U_{g\,pk}\right)\left(\frac{U_g\, T\, {d_{max}}^2}{2\, L}\right)\left(\frac{1-\cos(2t)}{2}\right) dt \\ &= \frac{{U_{g\,pk}}^2 T\, {d_{max}}^2}{4\, L} \end{aligned} \qquad (A.6)$$

And from, (A.6), the magnetising inductance can be defined as:

$$L = \frac{{U_{g\,pk}}^2 T\, {d_{max}}^2}{4\, P_{in}} \qquad (A.7)$$

The maximum currents in the secondary side can be calculated as follows. First of all, the maximum current in the grid side is defined as:

$$i_{g\,max} = \frac{U_g}{L}\, d_{max}\, T \qquad (A.8)$$

Combining (A.7) and (A.8), it can be obtained:

$$i_{g\,max} = \frac{4\, P_{in}}{d_{max} U_{g\,pk}} \qquad (A.9)$$

And this current, seen from the bus side:

$$i_{Ls\,max} = \frac{4\, P_{in}}{d_{max} U_{g\,pk}}\frac{N_1}{N_2} \qquad (A.10)$$

Inverter mode parameters

The same analyses can be done for the inverter mode. The expressions that shall be obtained are the following:

The maximum duty ratio is defined as:

$$d_{max} = \frac{U_{g\,pk}\, N_2}{U_o\, N_1 + U_{g\,pk}\, N_2} \qquad (A.11)$$

In order to obtain the expression of the magnetising inductor, the same procedure as in rectifier mode shall be applied. This time, the results are:

$$P_{in} = \frac{{U_o}^2 {U_{g\,pk}}^2 {N_1}^2\, T\, {d_{max}}^2}{4\, L \left(U_o\, N_1 + U_{g\,pk}\, N_2\right)^2} \qquad (A.12)$$

$$L = \frac{{U_o}^2 {U_{g\,pk}}^2 {N_1}^2\, T\, {d_{max}}^2}{4\, P_{in} \left(U_o\, N_1 + U_{g\,pk}\, N_2\right)^2} \qquad (A.13)$$

The expression of the maximum current in the secondary side is:

$$i_{Ls\,max} = \frac{4\, P_{in}\left(U_o\, N_1 + U_{g\,pk}\, N_2\right)}{U_o\, U_{g\,pk}} \frac{N_2}{N_1} \qquad (A.14)$$

Semiconductor maximum voltage stresses

On the other hand, the maximum voltage semiconductor stresses are gathered together in TABLE A.I:

TABLE A.I

SWITCHES VOLTAGE STRESS EQUATIONS

	S_A, S_B	S_1, S_2	S_R
Rectifier mode	$2U_g \frac{N_1}{N_2}$	$U_g + U_O \frac{N_1}{N_2}$	$U_g \frac{N_1}{N_2} - U_O$
Inverter mode	$U_g + U_O \frac{N_1}{N_2}$	$U_g + U_O \frac{N_1}{N_2}$	$U_g \frac{N_1}{N_2} - U_O$

Thus, after having all this information, several diagrams can be depicted in order to choose the optimum values for the power converter.

DC bus voltage

The DC bus voltage influences the maximum currents that the secondary side will handle. Thus, the diagram of Fig. A.2 represents this statement taking into account also the turns ratio of the high frequency transformer. It was chosen 100 V as a proper value.

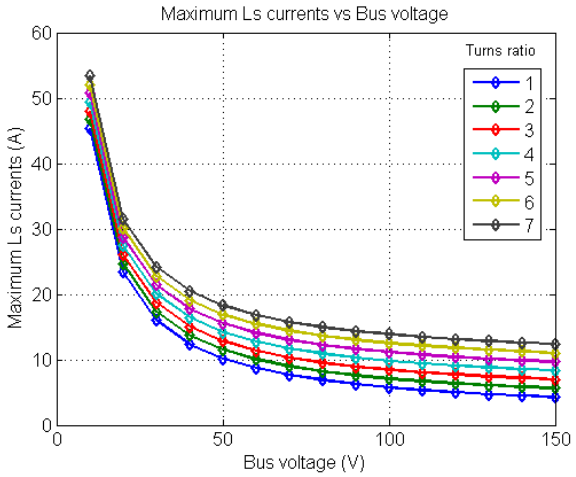

Fig. A.2. L_s currents depending on the DC bus voltage and turns ratio

Turns ratio

Based on (A.10), (A.14) and on TABLE A.I, the turns ratio of the high frequency transformer can be defined. Fig. A.3 depicts the maximum voltage stresses of the semiconductors in both modes vs the turns ratio.

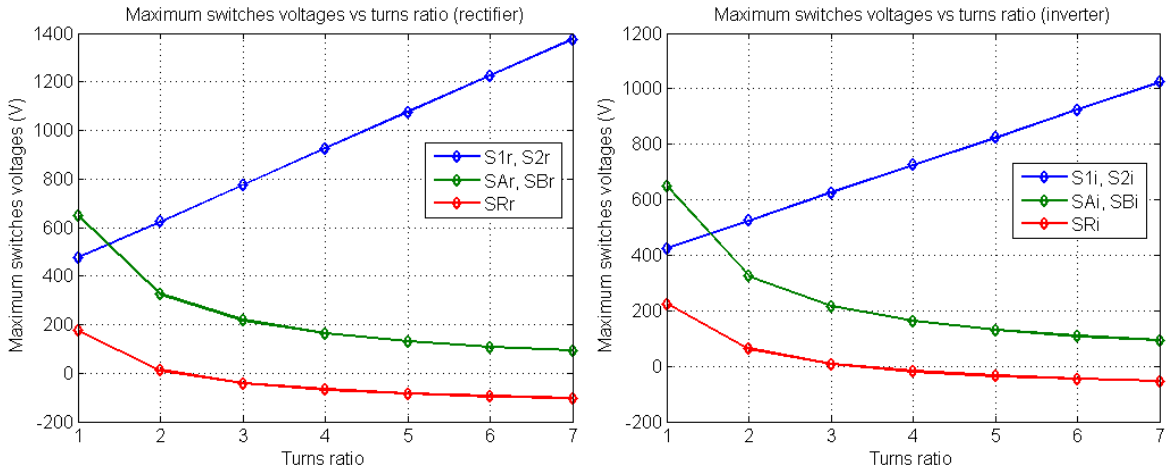

Fig. A.3. Maximum switches voltages vs turns ratio in (right) rectifier mode and (left) inverter mode

On the other hand, Fig. A.4 gathers the maximum currents depending also on the turns ratio.

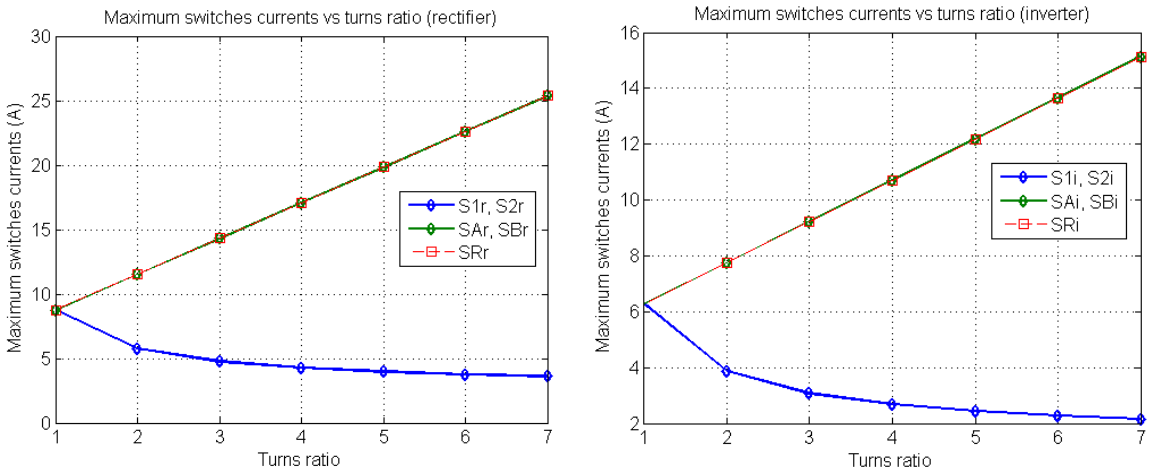

Fig. A.4. Maximum currents vs turns ratio in (right) rectifier mode and (left) inverter mode

Hence, after plotting this information, a decision can be made. Since the secondary side currents and also the grid side voltage that the semiconductors must bear increase lineally, a turns ratio of 2 can be a good choice since it is a compromise solution.

Magnetising inductor

The magnetising inductor was defined for both operation modes in (A.7) and (A.13). As it can be seen in those equations, after defining the turns ratio and the power the Flyback is going to handle, the magnetising inductor only depends on one variable: the switching frequency. Fig. A.5 represents the way this variable influences in the final inductor value. It was chosen a value of 50 kHz for the switching frequency which defines a value of 500 µH for the magnetising inductor of the transformer, ensuring DCM operation mode for both operation modes: rectifier and inverter.

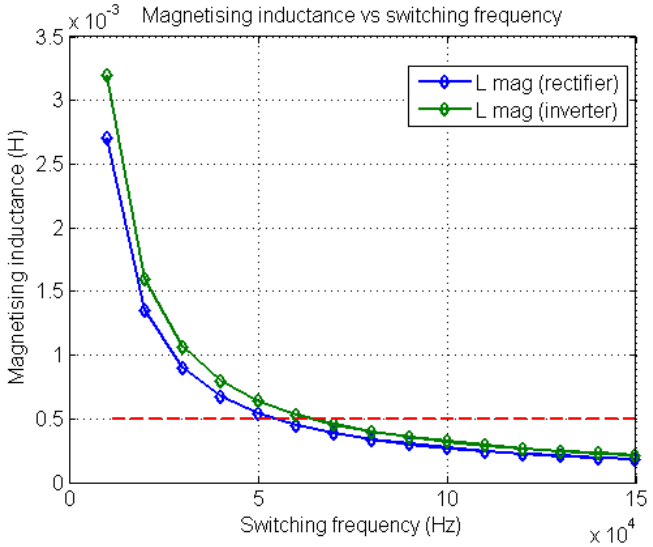

Fig. A.5. Magnetising inductance vs switching frequency

REFERENCES

[1] David Gacio, "Off-line suppy of solid-state lamps. Lamp modelling, application of the integrated Buck-Flyback converter, and proposal of a new optimised dimming scheme," *Ph.D dissertation, University of Oviedo*, 2013.

[2] I.L. Azevedo, M.G. Morgan, and F. Morgan, "The Transition to Solid-State Lighting," *Proceedings of the IEEE*, vol. 97, no. 3, pp. 481-510, March 2009.

[3] Yen Kheng Tan, Truc Phuong Huynh, and Zizhen Wang, "Smart Personal Sensor Network Control for Energy Saving in DC Grid Powered LED Lighting System," *Smart Grid, IEEE Transactions on*, vol. 4, no. 2, pp. 669-676, June 2013.

[4] Comité Español de Iluminación, "Guía Técnica de Eficiencia Energética en Iluminación," 2001.

[5] "Climate TechBook: Residential and Commercial Sectors Overview, 2009,".

[6] M.F. da Silva et al., "Analysis and Design of a Single-Stage High-Power-Factor Dimmable Electronic Ballast for Electrodeless Fluorescent Lamp," *Industrial Electronics, IEEE Transactions on*, vol. 60, no. 8, pp. 3081-3091, Aug 2013.

[7] P. Quintana, J. Garcia, E.L. Corominas, A.J. Calleja, and P. Garcia, "Minimization of current harmonics content in conventional lighting distribution lines without current sensing," in *Industrial Electronics Society, IECON 2013 - 39th Annual Conference of the IEEE*, Nov 2013, pp. 6093-6098.

[8] C. Branas, F.J. Azcondo, and S. Bracho, "Evaluation of an electronic ballast circuit for HID lamps with passive power factor correction," in *IECON 02 [Industrial Electronics Society, IEEE 2002 28th Annual Conference of the]*, vol. 1, Nov 2002, pp. 371-376 vol.1.

[9] E.L. Corominas et al., "A novel low cost two-stage electronic ballast for 250 W high pressure mercury vapor lamps based on current-mode-controlled buck-boost inverter," in *Applied Power Electronics Conference and Exposition, 2001. APEC 2001. Sixteenth Annual IEEE*, vol. 2, 2001, pp. 676-682 vol.2.

[10] M. Rico-Secades et al., "Complete low-cost two-stage electronic ballast for 70-W high-pressure sodium vapor lamp based on current-mode-controlled buck-boost inverter," *Industry Applications, IEEE Transactions on*, vol. 41, no. 3, pp. 728-734, May 2005.

[11] M.A. Dalla Costa, J.M. Alonso, J. Garcia-Garcia, J. Cardesin, and J. Ribas, "Analysis, Design and Experimentation of a Closed-Loop Metal Halide Lamp Electronic Ballast," in *Industry Applications Conference, 2006. 41st IAS Annual Meeting. Conference Record of the 2006 IEEE*, vol. 3, Oct 2006, pp. 1384-1390.

[12] E. F. Schubert, *Light-emitting diodes*, 2nd ed. Cambridge, 2003.

[13] J. D. Bullough, "Lighting answers: LED lighting systems," Rensselaer polytechnic Institute, National Lighting Product Information Program 2003.

[14] S. Dietrich, S. Strache, R. Wunderlich, and S. Heinen, "Get the LED Out: Experimental Validation of a Capacitor-Free Single-Inductor, Multiple-Output LED Driver Topology," *Industrial Electronics Magazine, IEEE*, vol. 9, no. 2, pp. 24-35, June 2015.

[15] P. Santos Almeida, D. Camponogara, M. Dalla Costa, H. Braga, and J.M. Alonso, "Matching LED and Driver Life Spans: A Review of Different Techniques," *Industrial Electronics Magazine, IEEE*, vol. 9, no. 2, pp. 36-47, June 2015.

[16] Regina Mueller-Mach, Gerd O. Mueller, M.R. Krames, and T. Trottier, "High-power phosphor-converted light-emitting diodes based on III-Nitrides," *Selected Topics in Quantum Electronics, IEEE Journal of*, vol. 8, no. 2, pp. 339-345, Mar 2002.

[17] Shuji Nakamura, "GaN-based blue/green semiconductor laser," *Selected Topics in Quantum Electronics, IEEE Journal of*, vol. 3, no. 2, pp. 435-442, Apr 1997.

[18] M.R. Krames et al., "Status and Future of High-Power Light-Emitting Diodes for Solid-State Lighting," *Display Technology, Journal of*, vol. 3, no. 2, pp. 160-175, June 2007.

[19] J.K. Sheu et al., "White-light emission from near UV InGaN-GaN LED chip precoated with blue/green/red phosphors," *Photonics Technology Letters, IEEE*, vol. 15, no. 1, pp. 18-20, Jan 2003.

[20] M.S. Shur and A. Zukauskas, "Solid-State Lighting: Toward Superior Illumination," *Proceedings of the IEEE*, vol. 93, no. 10, pp. 1691-1703, Oct 2005.

[21] D.A. Steigerwald et al., "Illumination with solid state lighting technology," *Selected Topics in Quantum Electronics, IEEE Journal of*, vol. 8, no. 2, pp. 310-320, Mar 2002.

[22] Peter Baureis, "Compact modeling of electrical, thermal and optical LED behavior," in *Solid-State Device Research Conference, 2005. ESSDERC 2005. Proceedings of 35th European*, Sept 2005, pp. 145-148.

[23] E.C. Lennox, "Street lighting," *Electrical Engineers - Part II: Power Engineering, Journal of the Institution of*, vol. 93, no. 32, pp. 170-183, April 1946.

[24] M. Shahidehpour et al., "Streetlights Are Getting Smarter: Integrating an Intelligent Communications and Control System to the Current Infrastructure," *Power and Energy Magazine, IEEE*, vol. 13, no. 3, pp. 67-80, May 2015.

[25] Intelligent Energy Europe. Guide for energy efficient street lighting installations. Competitiveness and Innovation Program. [Online]. http://www.e-streetlight.com/Documents/Homepage/0_3%20Guide_For%20EE%20Street%20Lighting.pdf

[26] M.F. de Melo, A.L. Kirsten, M.A. Dalla Costa, J. Garcia, and P.J. Quintana, "Bidirectional Flyback converter connected to the grid and applied to a distributed microgeneration and street lighting system," in *Industry Applications Society Annual Meeting, 2014 IEEE*, Oct 2014, pp. 1-6.

[27] R.A. Pinto et al., "Street lighting system based on integrated buck-flyback converter to supply LEDs without energy consumption during the peak load time," in *Power Electronics Conference (COBEP), 2011 Brazilian*, Sept 2011, pp. 891-897.

[28] R. Barraza Garcia, G. Velazquez Angulo, J. Romero Gonzalez, E. Flores Tavizon, and J.I. Huertas Cardozo, "LED street lighting as a strategy for climate change mitigation at local government level," in *Global Humanitarian Technology Conference (GHTC), 2014 IEEE*, Oct 2014, pp. 345-349.

[29] X. Long, R. Liao, and J. Zhou, "Development of street lighting system-based novel high-brightness LED modules," *Optoelectronics, IET*, vol. 3, no. 1, pp. 40-46, February 2009.

[30] N. Huerta-Medina and E.L. Corominas, "A set of software tools for management and simulation of a Lighting Smart Grid," in *New Concepts in Smart Cities: Fostering Public and Private Alliances (SmartMILE), 2013 International Conference on*, Dec 2013, pp. 1-6.

[31] M. Martin-Arias, N. Huerta-Medina, and M. Rico-Secades, "Using wireless technologies in Lighting Smart Grids," in *New Concepts in Smart Cities: Fostering Public and Private Alliances (SmartMILE), 2013 International Conference on*, Dec 2013, pp. 1-6.

[32] H. Van der Broeck, Georg Sauerlander, and M. Wendt, "Power driver topologies and control schemes for LEDs," in *Applied Power Electronics Conference, APEC 2007 - Twenty Second Annual IEEE*, Feb 2007, pp. 1319-1325.

[33] Huang-Jen Chiu et al., "A High-Efficiency Dimmable LED Driver for Low-Power Lighting Applications," *Industrial Electronics, IEEE Transactions on*, vol. 57, no. 2, pp. 735-743, Feb 2010.

[34] S.Y.R. Hui, Si Nan Li, Xue Hui Tao, Wu Chen, and W.M. Ng, "A Novel Passive Offline LED Driver With Long Lifetime," *Power Electronics, IEEE Transactions on*, vol. 25, no. 10, pp. 2665-2672, Oct 2010.

[35] International, IEC 61000-3-2:2005 “Electromagnetic compatibility (EMC)- Part 3-2: Limits - Limits for harmonic current emissions (equipment input current ≤ 16 A per phase).

[36] B. Keogh, "Power Factor Correction Using the Buck Topology – Efficiency Benefits and Practical Design Considerations," in *Texas Instruments Power Supply Design Seminar*, 2010-2011.

[37] F. Nyland, L.C.M. Schlichting, M.B. Liz, and A. Raizer, "Analysis of harmonic distortion and electromagnetic interference due to and electromagnetic ballasts," in *Harmonics and Quality of Power, 2002. 10th International Conference on*, vol. 2, Oct 2002, pp. 765-769 vol.2.

[38] Bhim Singh, K. Al-Haddad, and A. Chandra, "A review of active filters for power quality improvement," *Industrial Electronics, IEEE Transactions on*, vol. 46, no. 5, pp. 960-971, Oct 1999.

[39] A. Rodriguez et al., "Analysis of repetitive-based controllers for selective harmonic compensation in active power filters," in *IECON 2010 - 36th Annual Conference on IEEE Industrial Electronics Society*, Nov 2010, pp. 2013-2018.

[40] M.J. Newman and D.G. Holmes, "A universal custom power conditioner (UCPC) with selective harmonic voltage compensation," in *IECON 02 [Industrial Electronics Society, IEEE 2002 28th Annual Conference of the]*, vol. 2, Nov 2002, pp. 1261-1266 vol.2.

[41] M. Savaghebi, A. Jalilian, J.C. Vasquez, and J.M. Guerrero, "Selective compensation of voltage harmonics in an islanded microgrid," in *Power Electronics, Drive Systems and Technologies Conference (PEDSTC), 2011 2nd*, Feb 2011, pp. 279-285.

[42] A. Micallef, M. Apap, C. Spiteri-Staines, and J.M. Guerrero, "Cooperative control with virtual selective harmonic capacitance for harmonic voltage compensation in islanded microgrids," in *IECON 2012 - 38th Annual Conference on IEEE Industrial Electronics Society*, Oct 2012, pp. 5619-5624.

[43] F. Briz, P. Garcia, M.W. Degner, D. Diaz-Reigosa, and J.M. Guerrero, "Dynamic Behavior of Current Controllers for Selective Harmonic Compensation in Three-Phase Active Power Filters," *Industry Applications, IEEE Transactions on*, vol. 49, no. 3, pp. 1411-1420, May 2013.

[44] D. Wojciechowski, "Grid voltages sensorless control system of the PWM rectifier with active filtering function," in *Compatibility in Power Electronics, 2005. IEEE*, June 2005, pp. 238-246.

[45] D.A. Torrey and A.M.A.M. Al-Zamel, "Single-phase active power filters for multiple nonlinear loads," *Power Electronics, IEEE Transactions on*, vol. 10, no. 3, pp. 263-272, May 1995.

[46] H. Fujita, T. Yamasaki, and H. Akagi, "A hybrid active filter for damping of harmonic resonance in industrial power systems," *Power Electronics, IEEE Transactions on*, vol. 15, no. 2, pp. 215-222, Mar 2000.

[47] N.F.A. Rahman, M.K. Hamzah, S.Z.M. Noor, and A.S.A. Hasim, "Single-phase hybrid active power filter using single switch parallel active filter and simple passive filter," in *Power Electronics and Drive Systems, 2009. PEDS 2009. International Conference on*, Nov 2009, pp. 40-45.

[48] E. Lavopa, P. Zanchetta, M. Sumner, and P. Bolognesi, "Improved voltage harmonic control for sensorless shunt active power filters," in *Power Electronics Electrical Drives Automation and Motion (SPEEDAM), 2010 International Symposium on*, June 2010, pp. 221-226.

[49] P.N. Enjeti, W. Shireen, P. Packebush, and I.J. Pitel, "Analysis and Design of a New Active Power Filter to Cancel Neutral Current Harmonics in Three-Phase Four-Wire Electric Distribution Systems," *Industry Applications, IEEE Transactions on*, vol. 30, no. 6, pp. 1565-, Nov 1994.

[50] S. Buso, L. Malesani, and P. Mattavelli, "Comparison of current control techniques for active filter applications," *Industrial Electronics, IEEE Transactions on*, vol. 45, no. 5, pp. 722-729, Oct 1998.

[51] ELT Ballast, Model VSI 15/22-3T-A.

[52] OSRAM HPS lamp. Model: VIALOX NAV-E SON-E 150. [Online]. http://goo.gl/jxDBqp

[53] Wei Yan and S.Y.R. Hui, "A universal PSpice model for HID lamps," *Industry Applications, IEEE Transactions on*, vol. 41, no. 6, pp. 1594-1602, Nov 2005.

[54] R.O. Sanchez et al., "Electric Dynamic Modeling of HID Lamps for Electronic Ballast Design," *Industrial Electronics, IEEE Transactions on*, vol. 57, no. 5, pp. 1655-1662, May 2010.

[55] Wang Wei, Zhu Guo dong, and Xu Dian-Guo, "A physics-based model for HID lamps with rectifying effect," in *Vehicle Power and Propulsion Conference, 2008. VPPC '08. IEEE*, Sept 2008, pp. 1-5.

[56] J. Cardesin, P. Quintana, J. Garcia, and E.L. Corominas, "Simple HPS lamp circuital model for both line-frequency and high-frequency operations," *Electronics Letters*, vol. 50, no. 9, pp. 699-701, April 2014.

[57] Woei-Luen Chen and Yuan-Yih Hsu, "Direct output voltage control of a static synchronous compensator using current sensorless d-q vector-based power balancing scheme," in *Transmission and Distribution Conference and Exposition, 2003 IEEE PES*, vol. 2, Sept 2003, pp. 545-549 vol.2.

[58] Remus Teodorescu, Marco Liserre, and Pedro Rodríguez, *Grid converters for photovoltaic and wind power systems*.: John Wiley & Sons, 2011.

[59] Xiongfei Wang, F. Blaabjerg, and Zhe Chen, "Autonomous control of inverter-interfaced Distributed Generation units for harmonic current filtering and resonance damping in an islanded microgrid," in *Energy Conversion Congress and Exposition (ECCE), 2012 IEEE*, Sept 2012, pp. 211-218.

[60] S. Anwar, A. Elrayyah, and Y. Sozer, "Efficient Single-Phase Harmonics Elimination Method for Microgrid Operations," *Industry Applications, IEEE Transactions on*, vol. 51, no. 4, pp. 3394-3403, July 2015.

[61] M. Savaghebi, J.M. Guerrero, A. Jalilian, J.C. Vasquez, and Tzung-Lin Lee, "Hierarchical control scheme for voltage Harmonics Compensation in an islanded droop-controlled microgrid," in *Power Electronics and Drive Systems (PEDS), 2011 IEEE Ninth International Conference on*, Dec 2011, pp. 89-94.

[62] Xiongfei Wang, J.M. Guerrero, F. Blaabjerg, and Zhe Chen, "Secondary voltage control for harmonics suppression in islanded microgrids," in *Power and Energy Society General Meeting, 2011 IEEE*, July 2011, pp. 1-8.

[63] F. Blaabjerg, R. Teodorescu, M. Liserre, and A.V. Timbus, "Overview of Control and Grid Synchronization for Distributed Power Generation Systems," *Industrial Electronics, IEEE Transactions on*, vol. 53, no. 5, pp. 1398-1409, Oct 2006.

[64] J.C. Vasquez, J.M. Guerrero, J. Miret, M. Castilla, and L.G. de Vicuña, "Hierarchical Control of Intelligent Microgrids," *Industrial Electronics Magazine, IEEE*, vol. 4, no. 4, pp. 23-29, Dec 2010.

[65] P.J. Quintana, J. Garcia, J.M. Guerrero, T. Dragicevic, and J.C. Vasquez, "Control of single-phase islanded PV/battery streetlight cluster based on power-line signaling," in *New Concepts in Smart Cities: Fostering Public and Private Alliances (SmartMILE), 2013 International Conference on*, Dec 2013, pp. 1-6.

[66] P.J. Quintana, J.M. Guerrero, T. Dragicevic, and J.C. Vasquez, "Control of single-phase islanded PV/battery minigrids based on power-line signaling," in *Multi-Conference on Systems, Signals Devices (SSD), 2014 11th International*, Feb 2014, pp. 1-6.

[67] A. Micallef, M. Apap, C. Spiteri-Staines, J.M. Guerrero, and J.C. Vasquez, "Reactive Power Sharing and Voltage Harmonic Distortion Compensation of Droop Controlled Single Phase Islanded Microgrids," *Smart Grid, IEEE Transactions on*, vol. 5, no. 3, pp. 1149-1158, May 2014.

[68] M. Savaghebi, J.C. Vasquez, A. Jalilian, J.M. Guerrero, and Tzung-Lin Lee, "Selective harmonic virtual impedance for voltage source inverters with LCL filter in microgrids," in *Energy Conversion Congress and Exposition (ECCE), 2012 IEEE*, Sept 2012, pp. 1960-1965.

[69] U.A. Miranda, L.G.B. Rolim, and M. Aredes, "A DQ Synchronous Reference Frame Current Control for Single-Phase Converters," in *Power Electronics Specialists Conference, 2005. PESC '05. IEEE 36th*, June 2005, pp. 1377-1381.

[70] M.J. Ryan and R.D. Lorenz, "A synchronous-frame controller for a single-phase sine wave inverter," in *Applied Power Electronics Conference and Exposition, 1997. APEC '97 Conference Proceedings 1997., Twelfth Annual*, vol. 2, Feb 1997, pp. 813-819 vol.2.

[71] J. Salaet, S. Alepuz, Gilabert A, and J. Bordonau, "Comparison between two methods of DQ transformation for single phase converters control. Application to a 3-level boost rectifier," in *Power Electronics Specialists Conference, 2004. PESC 04. 2004 IEEE 35th Annual*, vol. 1, June 2004, pp. 214-220 Vol.1.

[72] R. Zhang, M. Cardinal, P. Szczesny, and M. Dame, "A grid simulator with control of single-phase power converters in D-Q rotating frame," in *Power Electronics Specialists Conference, 2002. pesc 02. 2002 IEEE 33rd Annual*, vol. 3, 2002, pp. 1431-1436 vol.3.

[73] Louis Bell, "Discussion," *American Institute of Electrical Engineers, Transactions of the*, vol. XVI, pp. 297-301, Jan 1899.

[74] R. Costa-Castelló, R. Grino, and E. Fossas, "Odd-harmonic digital repetitive control of a single-phase current active filter," *Power Electronics, IEEE Transactions on*, vol. 19, no. 4, pp. 1060-1068, July 2004.

[75] J.R. Espinoza, G. Joos, J.I. Guzman, L.A. Moran, and R.P. Burgos, "Selective harmonic elimination and current/voltage control in current/voltage-source topologies: a unified approach," *Industrial Electronics, IEEE Transactions on*, vol. 48, no. 1, pp. 71-81, Feb 2001.

[76] A. V. Oppenheim, R. W. Schafer, and J. R. Buck, *Discrete-time signal processing*, 2nd ed., NJ: Prentice Hall, Ed.: Upper Saddle River, 1999.

[77] M.A. De Jesus, M. Teixeira, L. Vicente, and Y. Rodriguez, "Nonuniform Discrete Short-Time Fourier Transform A Goertzel Filter Bank versus a FIR Filtering Approach," in *Circuits and Systems, 2006. MWSCAS '06. 49th IEEE International Midwest Symposium on*, vol. 2, Aug 2006, pp. 188-192.

[78] F. Zaplata and M. Kasal, "Using the Goertzel algorithm as a filter," in *Radioelektronika (RADIOELEKTRONIKA), 2014 24th International Conference*, April 2014, pp. 1-3.

[79] MathWorks, "abc to Alpha-Beta-Zero, Alpha-Beta-Zero to abc,". [Online]. http://es.mathworks.com/help/physmod/sps/powersys/ref/abctoalphabetazeroalphabetazerotoabc.html

[80] A. Khamis, M. Armstrong, and M. Sulaiman, "The Impact of Embedded Generation Due to Harmonic Performance," in *Modelling Simulation, 2009. AMS '09. Third Asia International Conference on*, May 2009, pp. 514-519.

[81] Jun Wei Chuah, A. Raghunathan, and N.K. Jha, "An evaluation of energy-saving technologies for residential purposes," in *Power and Energy Society General Meeting, 2010 IEEE*, July 2010, pp. 1-8.

[82] M. Burgos-Payan, F. Correa-Moreno, and J. Riquelme-Santos, "Improving the energy efficiency of street lighting. A case in the South of Spain," in *European Energy Market (EEM), 2012 9th International Conference on the*, May 2012, pp. 1-8.

[83] "Renewables Directive: 2009/28/EC," European Union, Tech. rep. 2009.

[84] "Directive 2010/31/EU," European Parliament, Tech. rep. 2010.

[85] Joshua David Bollinger, "Application of Solar Energy to Power Stand-Alone Area and Street Lighting," University of Mossouri-Rolla, Master's thesis 2007.

[86] J. Garcia, M.A. Dalla-Costa, A. Kirsten, D. Gacio, and P. Quintana, "Study of a flyback-based stage as grid interface topology for micro-generation applications," in *Power Electronics and Motion Control Conference (EPE/PEMC), 2012 15th International*, Sept 2012, pp. LS7a.2-1-LS7a.2-6.

[87] F. Edwin, Weidong Xiao, and V. Khadkikar, "Topology review of single phase grid-connected module integrated converters for PV applications," in *IECON 2012 - 38th Annual Conference on IEEE Industrial Electronics Society*, Oct 2012, pp. 821-827.

[88] M. Jaureguizar, D. Garcia-Llera, M. Rico-Secades, A.J. Calleja, and E.L. Corominas, "Enerlight project: Walking from electronic lighting systems to Lighting Smart Grid," in *New Concepts in Smart Cities: Fostering Public and Private Alliances (SmartMILE), 2013 International Conference on*, Dec 2013, pp. 1-6.

[89] S.B. Kjaer, J.K. Pedersen, and F. Blaabjerg, "A review of single-phase grid-connected inverters for photovoltaic modules," *Industry Applications, IEEE Transactions on*, vol. 41, no. 5, pp. 1292-1306, Sept 2005.

[90] Dong-Jo Won, Yong-Su Noh, Moo-Young Ryu, Chung-Yuen Won, and Hong woo Lim, "A study of grid-connected PV-AC module with active power decoupling and ESS," in *Industrial Technology (ICIT), 2014 IEEE International Conference on*, Feb 2014, pp. 491-496.

[91] S.R. Harrington and T.D. Hund, "Photovoltaic lighting system performance," in *Photovoltaic Specialists Conference, 1996., Conference Record of the Twenty Fifth IEEE*, May 1996, pp. 1307-1310.

[92] Francesca Jane Born, "Aiding Renewable Energy Integration through Complimentary Demand-Supply Matching," University of Strathclyde. Energy Systems Research Unit, Ph.D. dissertation 2001.

[93] Tamás Kerekes, "Analysis and Modeling of Transformerless Photovoltaic Inverter Systems," Aalborg University. Institute of Energy Technology, Ph.D. dissertation 2009.

[94] Wu Libo, Zhao Zhengming, Liu Jianzheng, and Wang Jian, "Implementation of a stand-alone photovoltaic lighting system with maximum power point tracking and high pressure sodium lamp," in *Power Electronics and Drive Systems, 2003. PEDS 2003. The Fifth International Conference on*, vol. 2, Nov 2003, pp. 1570-1573 Vol.2.

[95] V. Salas, M.J. Manzanas, A.M. Roldan, A. Barrado, and E. Olias, "The control strategies for photovoltaic regulators applied to stand-alone systems," in *IECON 02 [Industrial Electronics Society, IEEE 2002 28th Annual Conference of the]*, vol. 4, Nov 2002, pp. 3274-3279 vol.4.

[96] Global Energy Wind Council (GEWC), "Global wind report. Annual market update," Tech. rep. 2013. [Online]. http://www.gwec.net/wp-content/uploads/2014/04/GWEC-Global-Wind-Report_9-April-2014.pdf

[97] Global Energy Wind Council (GEWC), "Global wind stadistics," Tech. rep. 2014. [Online]. http://www.gwec.net/wp-content/uploads/2015/02/GWEC_GlobalWindStats2014_FINAL_10.2.2015.pdf

[98] Siegfried Heier, *Grid Integration of Wind Energy: Onshore and Offshore Conversion Systems*, 3rd ed., June 2014.

[99] Dr. David Wood, *Small Wind Turbines Analysis, Design, and Application*.: University of Calgary, 2011.

[100] Michael Rhodes, "Assessing the Potential Wind Resource Available for Standalone Renewable Street Lighting in the Urban Environment - Cardiff a Case Study," Cardiff University, Ph.D. dissertation.

[101] Dong Li, Shujie Wang, and Peng Yuan, "A Review of Micro Wind Turbines in the Built Environment," in *Power and Energy Engineering Conference (APPEEC), 2010 Asia-Pacific*, March 2010, pp. 1-4.

[102] Centurion Energy, http://centurionenergy.net/types-of-wind-turbines.

[103] N. Stannard and J.R. Bumby, "Performance aspects of mains connected small-scale wind turbines," *Generation, Transmission Distribution, IET*, vol. 1, no. 2, pp. 348-356, March 2007.

[104] A. K. Wright and D. H. Wood, "The starting and low wind speed behaviour of a small horizontal axis wind turbine," *Journal of Wind Engineering and Industrial Aerodynamics*, vol. 92, pp. 1265–1279, 2004.

[105] S.O. Ani, H. Polinder, and J.A. Ferreira, "Comparison of Energy Yield of Small Wind Turbines in Low Wind Speed Areas," *Sustainable Energy, IEEE Transactions on*, vol. 4, no. 1, pp. 42-49, Jan 2013.

[106] S.O. Ani, H. Polinder, and J.A. Ferreira, "Energy yield of two generator systems for small wind turbine application," in *Electric Machines Drives Conference (IEMDC), 2011 IEEE International*, May 2011, pp. 735-740.

[107] P.R. Ebert and D.H. Wood, "Observations of the starting behaviour of a small horizontalaxis wind turbine," *Renewable Energy*, vol. 12, pp. 245–257, 1997.

[108] A.M. De Broe, S. Drouilhet, and V. Gevorgian, "A peak power tracker for small wind turbines in battery charging applications," *Energy Conversion, IEEE Transactions on*, vol. 14, no. 4, pp. 1630-1635, Dec 1999.

[109] Kuo-Yuan Lo, Yaw-Ming Chen, and Yung-Ruei Chang, "MPPT Battery Charger for Stand-Alone Wind Power System," *Power Electronics, IEEE Transactions on*, vol. 26, no. 6, pp. 1631-1638, June 2011.

[110] Hsuang-Chang Chiang and Hsuan-Yu Tsai, "Design and implementation of a grid-tied wind power micro-inverter," *Renewable Power Generation, IET*, vol. 7, no. 5, pp. 493-503, Sept 2013.

[111] M.A. Khan, S. Zorlu, R. Guan, P. Pillay, and K.D. Visser, "An Integrated Design Approach for Small Grid-tied Permanent Magnet Wind Generators," in *Power Engineering Society Conference and Exposition in Africa, 2007. PowerAfrica '07. IEEE*, July 2007, pp. 1-6.

[112] Hong-Geuk Park, Seok-Ho Jang, Dong-Choon Lee, and Heung-Geun Kim, "Low-cost converters for micro wind turbine systems using PMSG," in *Power Electronics, 2007. ICPE '07. 7th Internatonal Conference on*, Oct 2007, pp. 483-487.

[113] Gaëtan Masson and Manoël Rekinger Sinead Orlandi, "Global market outlook for photovoltaics," European Photovoltaic Industri Association, Tech. rep. 2014-2018.

[114] European Photovoltaic Industry Association, "Global Market Outlook for Photovoltaics," 2014.

[115] T. Penick and B. Louk, "Photovoltaic Power Generation," TEI Controls, Tech. rep. March 2007.

[116] R. Messenger and J. Ventre, *Photovoltaic Systems Engineering*.: New York: CRC Press, 2000.

[117] Bo Yang, Wuhua Li, Yi Zhao, and Xiangning He, "Design and Analysis of a Grid-Connected Photovoltaic Power System," *Power Electronics, IEEE Transactions on*, vol. 25, no. 4, pp. 992-1000, April 2010.

[118] J.H.R. Enslin and D.B. Snyman, "Combined low-cost, high-efficient inverter, peak power tracker and regulator for PV applications," *Power Electronics, IEEE Transactions on*, vol. 6, no. 1, pp. 73-82, Jan 1991.

[119] Tsai-Fu Wu, Chien-Hsuan Chang, and Yong-Jing Wu, "Single-stage converters for PV lighting systems with MPPT and energy backup," *Aerospace and Electronic Systems, IEEE Transactions on*, vol. 35, no. 4, pp. 1306-1317, Oct 1999.

[120] J.H.R. Enslin, M.S. Wolf, D.B. Snyman, and W. Swiegers, "Integrated photovoltaic maximum power point tracking converter," *Industrial Electronics, IEEE Transactions on*, vol. 44, no. 6, pp. 769-773, Dec 1997.

[121] M.A.S. Masoum, H. Dehbonei, and E.F. Fuchs, "Theoretical and experimental analyses of photovoltaic systems with voltageand current-based maximum power-point tracking," *Energy Conversion, IEEE Transactions on*, vol. 17, no. 4, pp. 514-522, Dec 2002.

[122] Daniel A. Pritchard, "Sun tracking by peak power positioning for photovoltaic concentrator arrays," *Control Systems Magazine, IEEE*, vol. 3, no. 3, pp. 2-8, August 1983.

[123] Quan Li and P. Wolfs, "A Review of the Single Phase Photovoltaic Module Integrated Converter Topologies With Three Different DC Link Configurations," *Power Electronics, IEEE Transactions on*, vol. 23, no. 3, pp. 1320-1333, May 2008.

[124] Maicol Flores de Melo, "Sistema de geração distribuída de energia fotovoltaica integrado a um sistema de iluminação pública à base de leds," Universidade Federal de Santa Maria, Master's thesis 2014.

[125] Haibing Hu, S. Harb, N. Kutkut, I. Batarseh, and Z.J. Shen, "Power decoupling techniques for micro-inverters in PV systems-a review," in *Energy Conversion Congress and Exposition (ECCE), 2010 IEEE*, Sept 2010, pp. 3235-3240.

[126] D. Meneses, F. Blaabjerg, O. García, and J.A. Cobos, "Review and Comparison of Step-Up Transformerless Topologies for Photovoltaic AC-Module Application," *Power Electronics, IEEE Transactions on*, vol. 28, no. 6, pp. 2649-2663, June 2013.

[127] S.Z. Mohammad Noor, A.M. Omar, N.N. Mahzan, and I.R. Ibrahim, "A review of single-phase single stage inverter topologies for photovoltaic system," in *Control and System Graduate Research Colloquium (ICSGRC), 2013 IEEE 4th*, Aug 2013, pp. 69-74.

[128] J.M.A. Myrzik and M. Calais, "String and module integrated inverters for single-phase grid connected photovoltaic systems - a review," in *Power Tech Conference Proceedings, 2003 IEEE Bologna*, vol. 2, June 2003, pp. 8 pp. Vol.2-.

[129] R. Erickson, M. Madigan, and S. Singer, "Design of a simple high-power-factor rectifier based on the flyback converter," in *Applied Power Electronics Conference and Exposition, 1990. APEC '90, Conference Proceedings 1990., Fifth Annual*, March 1990, pp. 792-801.

[130] J. Garcia, M.A. Dalla-Costa, A.L. Kirsten, D. Gacio, and A.J. Calleja, "A Novel Flyback-Based Input PFC Stage for Electronic Ballasts in Lighting Applications," *Industry Applications, IEEE Transactions on*, vol. 49, no. 2, pp. 769-777, March 2013.

[131] Lee Jong-Jae, Jung-Min Kwon, Kim Eung-Ho, Woo-Young Choi, and Bong-Hwan Kwon, "Single-Stage Single-Switch PFC Flyback Converter Using a Synchronous Rectifier," *Industrial Electronics, IEEE Transactions on*, vol. 55, no. 3, pp. 1352-1365, March 2008.

[132] W. Tang, Y. Jiang, G.C. Hua, F.C. Lee, and I. Cohen, "Power factor correction with flyback converter employing charge control," in *Applied Power Electronics Conference and*

Exposition, 1993. APEC '93. Conference Proceedings 1993., Eighth Annual, Mar 1993, pp. 293-298.

[133] H. Wei and I. Batarseh, "Comparison of basic converter topologies for power factor correction," in *Southeastcon '98. Proceedings. IEEE*, Apr 1998, pp. 348-353.

[134] European Power Supply Manufacturers Association, "Harmonic Current Emissions. Guidelines to the Standard EN 61000-3-2," EPMSA, Tech. rep. 2010. [Online]. http://www.epsma.org/pdf/PFC%20Guide_November%202010.pdf

[135] O. Garcia, J.A. Cobos, R. Prieto, P. Alou, and J. Uceda, "Single phase power factor correction: a survey," *Power Electronics, IEEE Transactions on*, vol. 18, no. 3, pp. 749-755, May 2003.

[136] J.C.W. Lam and P.K. Jain, "A Modified Valley Fill Electronic Ballast Having a Current Source Resonant Inverter With Improved Line-Current Total Harmonic Distortion (THD), High Power Factor, and Low Lamp Crest Factor," *Industrial Electronics, IEEE Transactions on*, vol. 55, no. 3, pp. 1147-1159, March 2008.

[137] Yong-Sik Youn, Gyun Chae, and Gyu-Hyeong Cho, "A unity power factor electronic ballast for fluorescent lamp having improved valley fill and valley boost converter," in *Power Electronics Specialists Conference, 1997. PESC '97 Record., 28th Annual IEEE*, vol. 1, Jun 1997, pp. 53-59 vol.1.

[138] A.R. Seidel, F.E. Bisogno, D. Pappis, M.A. Dalla Costa, and R.N. do Prado, "Simple valley-fill self-oscillating electronic ballast with low crest factor using pulse-frequency modulation," in *Industry Applications Conference, 2003. 38th IAS Annual Meeting. Conference Record of the*, vol. 2, Oct 2003, pp. 779-784 vol.2.

[139] Hongbo Ma et al., "A Novel Valley-Fill SEPIC-Derived Power Supply Without Electrolytic Capacitor for LED Lighting Application," *Power Electronics, IEEE Transactions on*, vol. 27, no. 6, pp. 3057-3071, June 2012.

[140] L. Huber, B.T. Irving, and M.M. Jovanovic, "Effect of Valley Switching and Switching-Frequency Limitation on Line-Current Distortions of DCM/CCM Boundary Boost PFC Converters," *Power Electronics, IEEE Transactions on*, vol. 24, no. 2, pp. 339-347, Feb 2009.

[141] Ye-Then Chang and Yen-Shin Lai, "Online Parameter Tuning Technique for Predictive Current-Mode Control Operating in Boundary Conduction Mode," *Industrial Electronics, IEEE Transactions on*, vol. 56, no. 8, pp. 3214-3221, Aug 2009.

[142] J.M. Alonso, M.A. Dalla Costa, and C. Ordiz, "Integrated Buck-Flyback Converter as a High-Power-Factor Off-Line Power Supply," *Industrial Electronics, IEEE Transactions on*, vol. 55, no. 3, pp. 1090-1100, March 2008.

[143] M.A. Dalla Costa, J.M. Alonso, J.C. Miranda, J. Garcia, and D.G. Lamar, "A Single-Stage High-Power-Factor Electronic Ballast Based on Integrated Buck Flyback Converter to Supply Metal

Halide Lamps," *Industrial Electronics, IEEE Transactions on*, vol. 55, no. 3, pp. 1112-1122, March 2008.

[144] A.J. Calleja et al., "Analysis and experimental results of a single-stage high-power-factor electronic ballast based on flyback converter," *Power Electronics, IEEE Transactions on*, vol. 14, no. 6, pp. 998-1006, Nov 1999.

[145] Chin Sien Moo, Kuo Hsing Lee, Hung Liang Cheng, and Wei Ming Chen, "A Single-Stage High-Power-Factor Electronic Ballast With ZVS Buck–Boost Conversion," *Industrial Electronics, IEEE Transactions on*, vol. 56, no. 4, pp. 1136-1146, April 2009.

[146] R. Redl, "Power-factor correction in single-phase switching-mode power supplies – an overview," *International Journal of Electronics*, vol. 77, pp. 555-582, 1994.

[147] G. Spiazzi and S. Buso, "Power factor preregulators based on combined buck-flyback topologies," *Power Electronics, IEEE Transactions on*, vol. 15, no. 2, pp. 197-204, Mar 2000.

[148] J.M. Alonso et al., "Investigation of a novel high-power-factor electronic ballast based on the input current shaper," in *Power Electronics Specialists Conference, 1999. PESC 99. 30th Annual IEEE*, vol. 2, 1999, pp. 1109-1114 vol.2.

[149] D.G. Lamar, J.S. Zuniga, A.R. Alonso, M.R. Gonzalez, and M.M.H. Alvarez, "A Very Simple Control Strategy for Power Factor Correctors Driving High-Brightness LEDs," *Power Electronics, IEEE Transactions on*, vol. 24, no. 8, pp. 2032-2042, Aug 2009.

[150] O. Garcia, J.A. Cobos, R. Prieto, P. Alou, and J. Uceda, "An alternative to supply DC voltages with high power factor," *Industrial Electronics, IEEE Transactions on*, vol. 46, no. 4, pp. 703-709, Aug 1999.

[151] D. Gacio, J.M. Alonso, A.J. Calleja, J. Garcia, and M. Rico-Secades, "A Universal-Input Single-Stag2e High-Power-Factor Power Supply for HB-LEDs Based on Integrated Buck-Flyback Converter," *Industrial Electronics, IEEE Transactions on*, vol. 58, no. 2, pp. 589-599, Feb 2011.

[152] M.A. Dalla Costa, J.M. Alonso, T.B. Marchesan, M. Cervi, and R.N. Prado, "Generalized Analysis and Comparison of High-Power-Factor Integrated Topologies to Supply Metal Halide Lamps with Low Frequency Square Waveform," in *Industry Applications Conference, 2007. 42nd IAS Annual Meeting. Conference Record of the 2007 IEEE*, Sept 2007, pp. 484-489.

[153] S.-K. Ki, D.K.W. Cheng, and D.D.C. Lu, "Analysis and design of a single-phase hybrid mode power factor correction converter," *Power Electronics, IET*, vol. 1, no. 1, pp. 72-83, March 2008.

[154] P.S. Almeida, H.A.C. Braga, M.A. Dalla Costa, and J.M. Alonso, "Offline Soft-Switched LED Driver Based on an Integrated Bridgeless Boost-Half-Bridge Converter," *Industry Applications, IEEE Transactions on*, vol. 51, no. 1, pp. 761-769, Jan 2015.

[155] D. Gacio, J.M. Alonso, J. Garcia, D. Garcia-Llera, and J. Cardesin, "Optimization of a Front-End DCM Buck PFP for an HPF Integrated Single-Stage LED Driver," *Emerging and Selected Topics in Power Electronics, IEEE Journal of*, vol. 3, no. 3, pp. 666-678, Sept 2015.

[156] Jae-Kuk Kim, Jae-Bum Lee, and Gun-Woo Moon, "Isolated Switch-Mode Current Regulator With Integrated Two Boost LED Drivers," *Industrial Electronics, IEEE Transactions on*, vol. 61, no. 9, pp. 4649-4653, Sept 2014.

[157] I. Barbi, J.C. Fagundes, and E.V. Kassick, "A compact AC/AC voltage regulator based on an AC/AC high frequency flyback converter," in *Power Electronics Specialists Conference, 1991. PESC '91 Record., 22nd Annual IEEE*, Jun 1991, pp. 846-852.

[158] A. Fernandez, J. Sebastian, M.M. Hernando, M. Arias, and G. Perez, "Single Stage Inverter for a Direct AC Connection of a Photovoltaic Cell Module," in *Power Electronics Specialists Conference, 2006. PESC '06. 37th IEEE*, June 2006, pp. 1-6.

[159] M.R. Sahid and A.H.M. Yatim, "An isolated bridgeless AC-DC converter with high power factor," in *Power and Energy (PECon), 2010 IEEE International Conference on*, Nov 2010, pp. 791-796.

[160] Woo-Young Choi, Wen-Song Yu, and Jih-Sheng Lai, "A novel bridgeless single-stage half-bridge AC/DC converter," in *Applied Power Electronics Conference and Exposition (APEC), 2010 Twenty-Fifth Annual IEEE*, Feb 2010, pp. 42-46.

[161] A.L. Kirsten, T.B. Marchesan, M.A. Dalla Costa, and R.N. do Prado, "Resonant technique for bidirectional flyback converter," *Electronics Letters*, vol. 45, no. 25, pp. 1345-1346, December 2009.

[162] Jong-Won Shin, Jong bok Baek, and Bo-Hyung Cho, "Bridgeless isolated PFC rectifier using bidirectional switch and dual output windings," in *Energy Conversion Congress and Exposition (ECCE), 2011 IEEE*, Sept 2011, pp. 2879-2884.

[163] J. Beristain et al., "An integrated flyback rectifier with fast response using the Tibuck converter," in *Telecommunications Energy Conference, 1998. INTELEC. Twentieth International*, 1998, pp. 588-594.

[164] V. Vorperian, "Simplified analysis of PWM converters using model of PWM switch. II. Discontinuous conduction mode," *Aerospace and Electronic Systems, IEEE Transactions on*, vol. 26, no. 3, pp. 497-505, May 1990.

[165] D.S.L. Simonetti, J. Sebastian, and J. Uceda, "A small-signal model for SEPIC, Cuk and flyback converters as power factor preregulators in discontinuous conduction mode," in *Power Electronics Specialists Conference, 1993. PESC '93 Record., 24th Annual IEEE*, Jun 1993, pp. 735-741.

[166] Robert W. Erickson and Dragan Maksimovic, *Fundamentals of Power Electronics*, 2nd ed.: Springer US, 2001.

[167] Ned Mohan, Tore M. Underland, and William P. Robbins, *Power Electronics: Converters, Applications, and Design*, 3rd ed., 2002.

[168] G.H. Tan, J.Z. Wang, and Y.C. Ji, "Soft-switching flyback inverter with enhanced power decoupling for photovoltaic applications," *Electric Power Applications, IET*, vol. 1, no. 2, pp. 264-274, March 2007.

[169] T. Shimizu, K. Wada, and N. Nakamura, "Flyback-Type Single-Phase Utility Interactive Inverter With Power Pulsation Decoupling on the DC Input for an AC Photovoltaic Module System," *Power Electronics, IEEE Transactions on*, vol. 21, no. 5, pp. 1264-1272, Sept 2006.

[170] N. Pragallapati and V. Agarwal, "Single phase solar PV module integrated flyback based micro-inverter with novel active power decoupling," in *Power Electronics, Machines and Drives (PEMD 2014), 7th IET International Conference on*, April 2014, pp. 1-6.

[171] B. Tamyurek and B. Kirimer, "An Interleaved High-Power Flyback Inverter for Photovoltaic Applications," *Power Electronics, IEEE Transactions on*, vol. 30, no. 6, pp. 3228-3241, June 2015.